Laboratori per a la Innovació Tecnològica d'Estructures i Materials
UNIVERSITAT POLITÈCNICA DE CATALUNYA

Ph.D. Thesis

# *Analysis of unreinforced and TRM-strengthened brick masonry walls subjected to eccentric axial load*

*by*

Ernest Bernat-Maso

Directed by:

Lluís Gil Espert
Pere Roca Fabregat

Tesi presentada per obtenir el títol de Doctor per la Universitat Politècnica de Catalunya

Programa de doctorat d'Anàlisis Estructural, Departament de Resistència de Materials i Estructures a l'Enginyeria

Escola Tècnica Superior d'Enginyeria Industrial i Aeronàutica de Terrassa. Universitat Politècnica de Catalunya, *BarcelonaTECH*

Terrassa, octubre de 2013

# A2

# Finite Element Analysis data annex

## A2.1 Introduction

Finite element analyses of the buckling problem of unreinforced masonry walls and TRM strengthened masonry walls have been carried out. The definition of the model is fully explained in Chapter 4. Details of the simulation of each experimental case presented in Chapter 3 and Annex 1 are summarised in this Annex which includes all the particular input data and the obtained results for these cases and also for theoretical ones in order to extend the knowledge about the application of TRM.

## A2.2 FEA of Unreinforced Masonry Walls

Three models were run for each experimentally tested wall. The first and most important model considered a deterministic set of values for the main variables of the problem. The average values for compressive and flexural strength and Young's modulus of masonry were taken into account to carry out the calculus and the obtained data is the one analysed in more detail. Two extra simulations, one corresponding with the "lowest" values of the materials properties (the combination of which leaded to the minimum load-bearing capacity) according with the experimental research, and other corresponding with the "highest" values. This is a very simplified way to analyse how the scattering in the input data affects the calculated result of the load-bearing capacity in the current finite element model. The only result of these simulations analysed herein is the maximum load.

## A2.2.1. Wall W#1

### *A2.2.1.1 Input parameters*

This wall corresponded with the H series. All defining variables which varied for the three simulations of this case are summarised in Table A2. 1. Poisson's coefficient and the mesh size were maintained constant to 0.35 and 20mm respectively.

| ***Variable*** | ***Average values*** | ***Lowest values*** | ***Highest values*** |
|---|---|---|---|
| $f_{cm}$ *(MPa)* | 18.20 | 7.00 | 15.00 |
| $f_{xt}$ *(MPa)* | 0.23 | 0.10 | 0.70 |
| $G_f^I$ *(N/m)* | 8.4 | 4 | 26 |
| *E (MPa)* | 780 | 400 | 1100 |

Table A2. 1 Input data for the FEA of wall W#1

### *A2.2.1.2 Results*

The maximum load-bearing capacity of the wall W#1 ranged from 44.9kN to 144.1kN depending on the values of the input variables. However, for the most representative set of values, the maximum calculated applied load at the failure point was 91.8kN. Thus, the numeric result is highly dependent on the selected input variables.

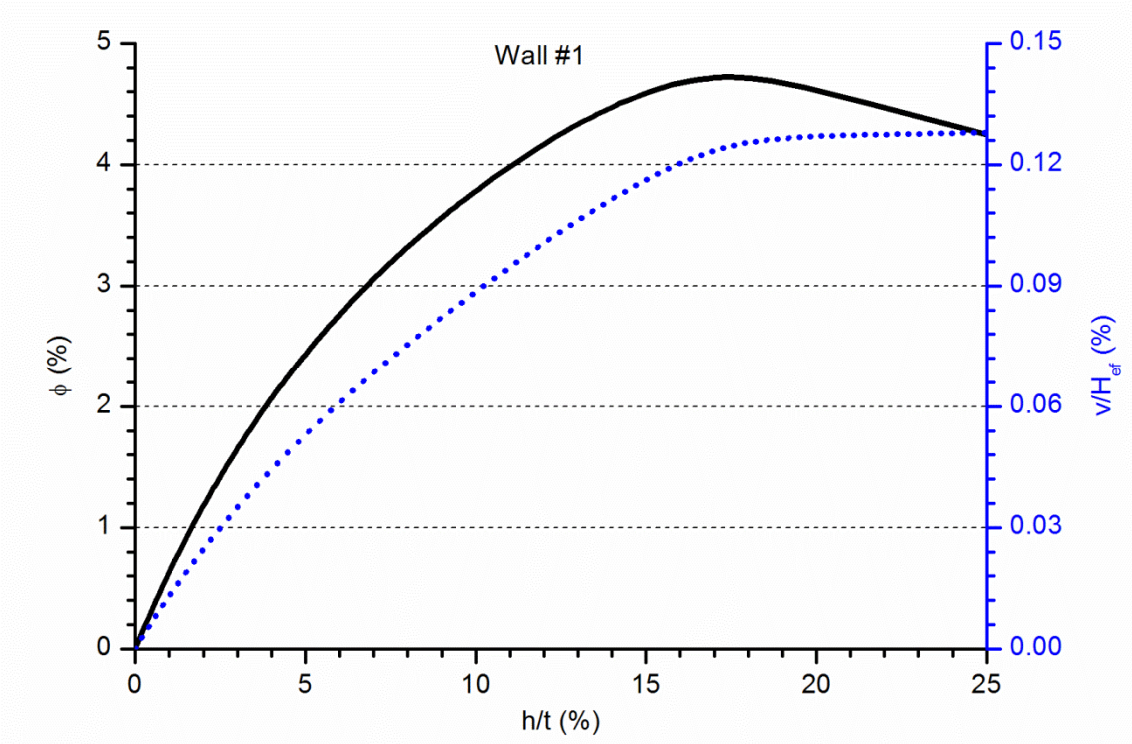


Figure A2. 1 Vertical and lateral calculated response of the wall W#1

Figure A2. 1 represents the wall's response relating the applied load ($\phi$) with the vertical displacement at the top of the wall ($v/H_{ef}$) and the lateral displacement at mid-height ($h/t$). All the calculated variables which are represented are dimensionless. The load coefficient, $\phi$, is a ratio of the applied load over the masonry section compressive capacity under a uniform stress distribution (see Chapter 4), the vertical displacement was related with the effective height of the wall, and the lateral displacement with the thickness of the wall.

The graph in Figure A2. 1 shows a clearly non-linear response of the lateral displacement when applying the load (black continuous line) what makes it evident that the numerical model represents the second order effects. The response after the maximum load is also represented for a few calculation steps. The relationship between vertical and lateral displacements (blue dotted line) is non-linear too. Moreover, a clear change in the response is observed from the maximum load in this case. The lateral movement increases far quicker than the vertical displacement from the maximum load and on.

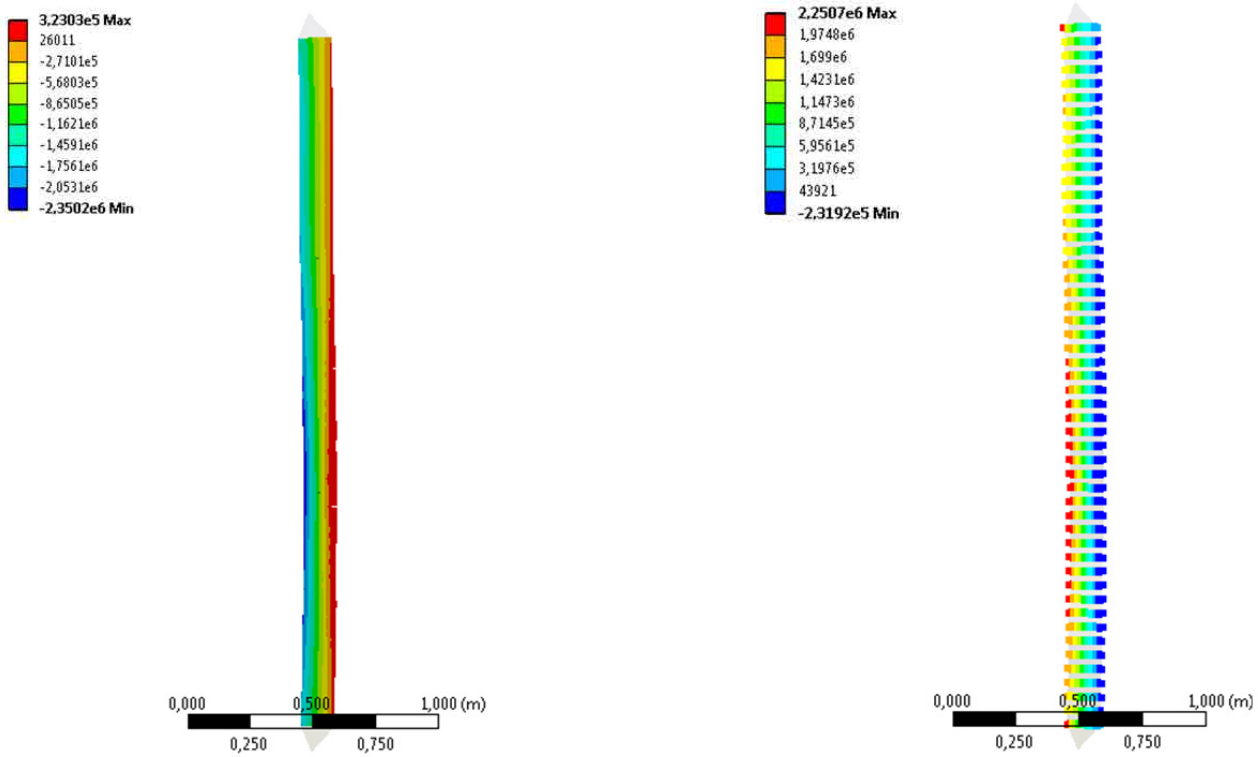


Figure A2. 2 Vertical stress distribution (left) and contact pressure (right) corresponding to the maximum calculated load for wall W#1. Values in Pa

Figure A2. 2 represents the vertical stress distribution and the contact pressure calculated at the step corresponding with the maximum applied load. Regarding the first one, it is worth noticing that the maximum tensile stress is not placed at the mid-height but at a lower position. The same pattern is shown in the contacts' pressure distribution for which the maximum tensile and compressive contact stresses are located below the mid-height position. In none of the two representations the maximum compressive

strength of masonry is reached but the contact maximum tensile stress is reached. This indicates that in the real case, the failure would be due to the opening of a mortar joint.

From the simulation results it is observed that the failure is due to a buckling effect facilitated by the second order bending deformations caused by the eccentricity of the load.

## A2.2.2. Wall W#2

### *A2.2.2.1 Input parameters*

This was the second wall of the H series. Table A2. 2 summarises the values of the input variables for the average set of values and the maximum and minimum experimental possibilities. Poisson's coefficient and the mesh size were maintained constant to 0.35 and 20mm respectively.

| ***Variable*** | ***Average values*** | ***Lowest values*** | ***Highest values*** |
|---|---|---|---|
| $f_{cm}$ *(MPa)* | 12.90 | 7.00 | 15.00 |
| $f_{xt}$ *(MPa)* | 0.36 | 0.10 | 0.70 |
| $G_f^I$ *(N/m)* | 13 | 4 | 26 |
| *E (MPa)* | 780 | 400 | 1100 |

Table A2. 2 Input data for the FEA of wall W#2 to W#5

### *A2.2.2.2 Results*

The maximum load-bearing capacity of the wall W#2 ranged from 43.6kN to 143.1kN for the extreme values of the input variables. However, for the most representative set of values and the real geometry, the load-bearing capacity was 95.0kN. Like in most of the carried out simulations, the high dependence on the input variables is evident.

Figure A2. 3 shows the calculated response for wall W#2. The non-linear response of the lateral displacement is represented with the black continuous line, whereas the relationship between the vertical displacement and the lateral movement (blue dotted line) might be modelled as a tri-linear response. Regarding the representation of the vertical movements, there is an almost straight line for lateral displacements from 3% to 15% of the wall's thickness.

The vertical stress distribution is similar to the one obtained for wall W#1 except for the fact that at the maximum calculated load one of the contacts between masonry rows had begun to open. It is observed in Figure A2. 4 (left). Below the mid-height there is a stress discontinuity in the tensile side corresponding with a pressure discontinuity (right image of Figure A2. 4). It indicates the first joint failure which leaded to the wall's collapse according with the finite element analysis. The maximum compressive stress is far from the compressive strength of the masonry and the maximum tensile stress at the contacts is slightly higher the corresponding strength.

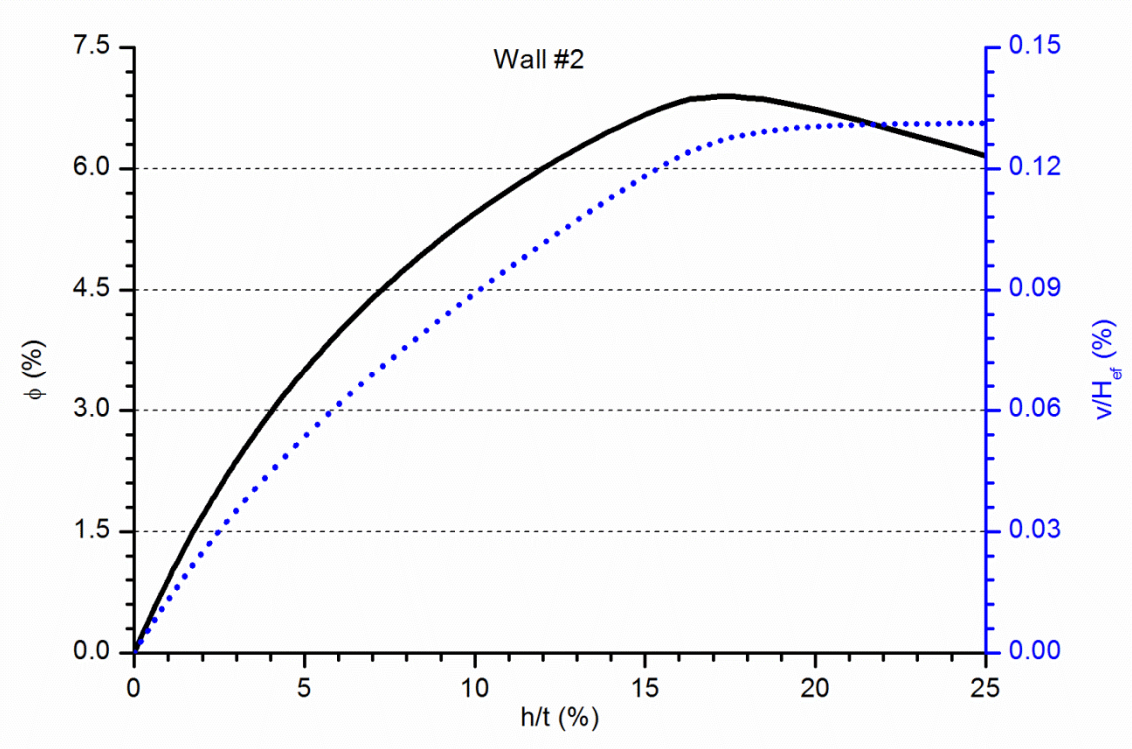


Figure A2. 3 Vertical and lateral calculated response of the wall W#2

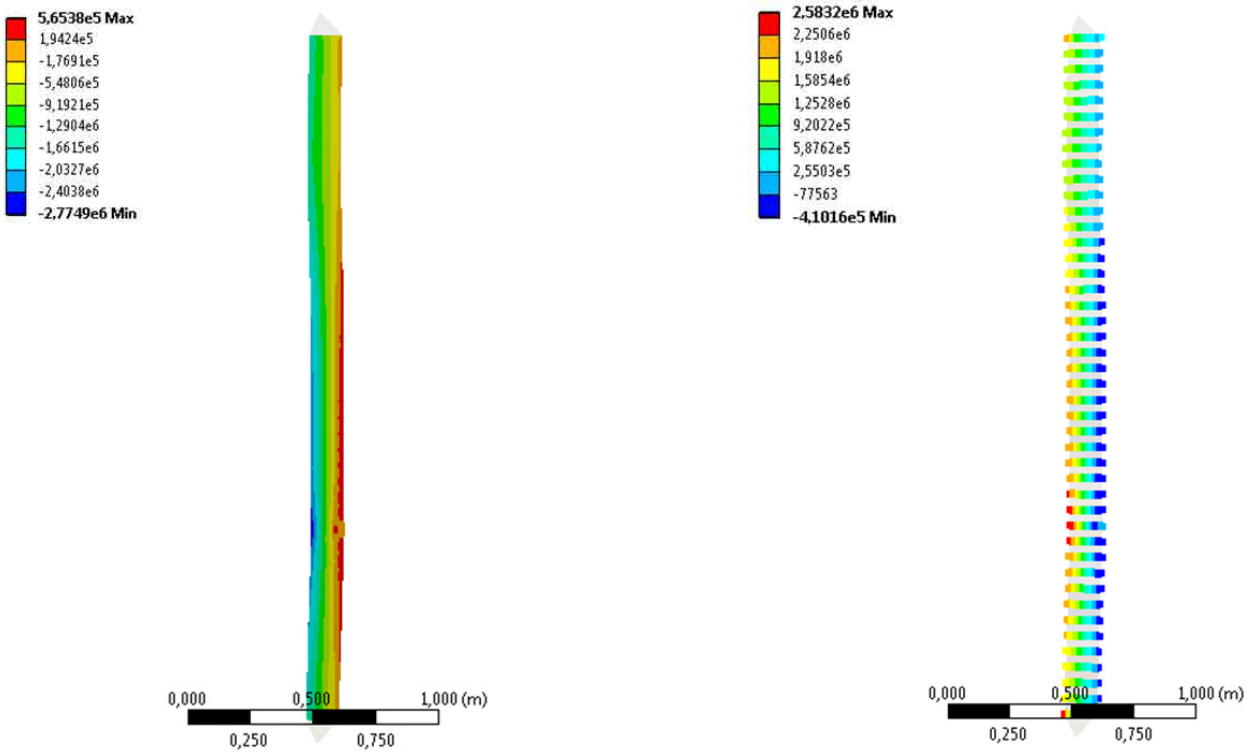


Figure A2. 4 Vertical stress distribution (left) and contact pressure (right) corresponding to the maximum calculated load for wall W#2. Values in Pa

The simulation indicates that the failure is due to a buckling process which caused the opening of a mortar joint for wall W#2.

## A2.2.3. Wall W#3

### *A2.2.3.1 Input parameters*

This was the third wall of the H series. Table A2. 2 summarises the values of the input variables for the average set of values and the maximum and minimum experimental possibilities. These are the same for walls W#2 to W#5. Poisson's coefficient and the mesh size were maintained constant to 0.35 and 20mm respectively.

### *A2.2.3.2 Results*

The maximum load-bearing capacity of the wall W#3 ranged from 64.4kN to 192.1kN for the extreme values of the input variables. For the most representative set of values and the real geometry, the load-bearing capacity was 132.7kN. The high dependence on the input variables is evidenced.

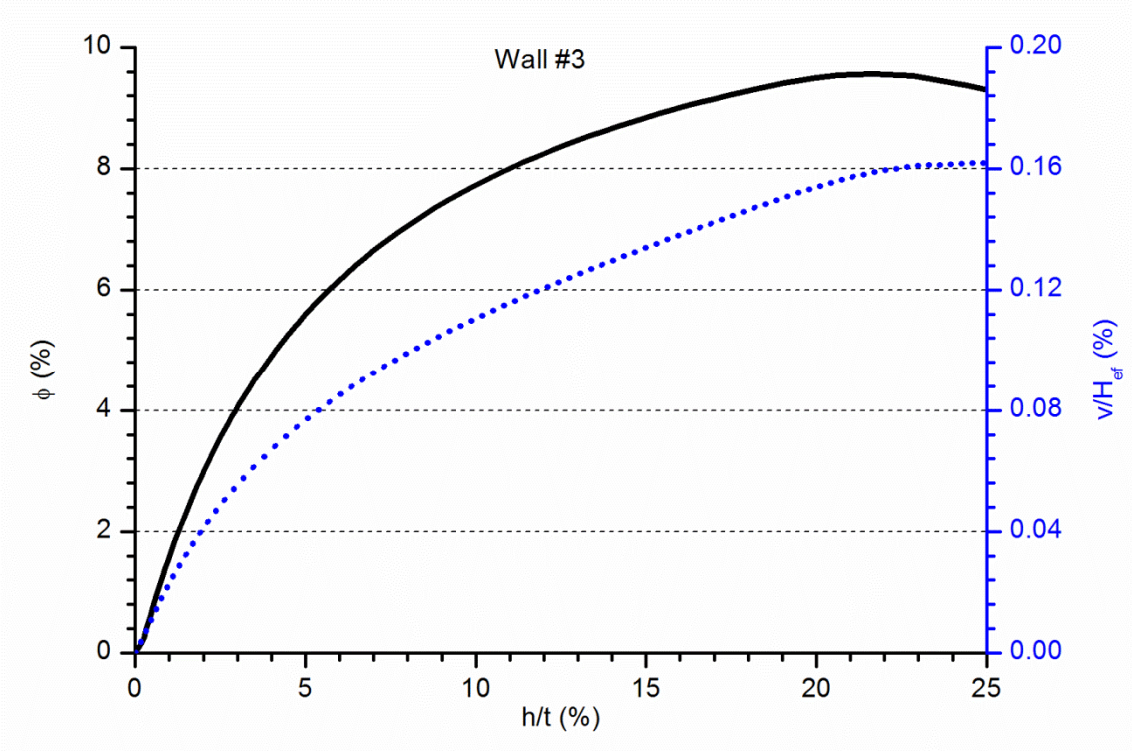


Figure A2. 5 Vertical and lateral calculated response of the wall W#3

Figure A2. 5 shows the response obtained from the finite element analysis of wall W#3. The behaviour is similar to the previous analysed cases with a non-linear relationship between the applied load and the lateral displacement at mid-height (black continuous line). The maximum load and the corresponding lateral displacement are greater than for the previous two cases and the calculated response after the maximum load indicates a softer collapse with a slow decrease in the load. The relationship vertical displacement versus the lateral movement has a non-linear shape with an almost linear range from 7% to 22% of lateral displacement out of wall's thickness.

The vertical stress contour (Figure A2. 6) shows a symmetric distribution which is also observable in the contact's pressure distribution. It has to be outlined that the maximum compressive stress for the maximum applied load is far from the compressive strength of the masonry. The value of the maximum tensile stress in the contacts is close to the flexural strength of the masonry but slightly higher what indicates that the simulated failure happened because of the opening of a horizontal mortar joint.

Thus, the finite element resulting collapse mode is associated with a buckling process accentuated by the second order effects observable in Figure A2. 5. The adherence between bricks and mortar is the parameter that controls the failure point.

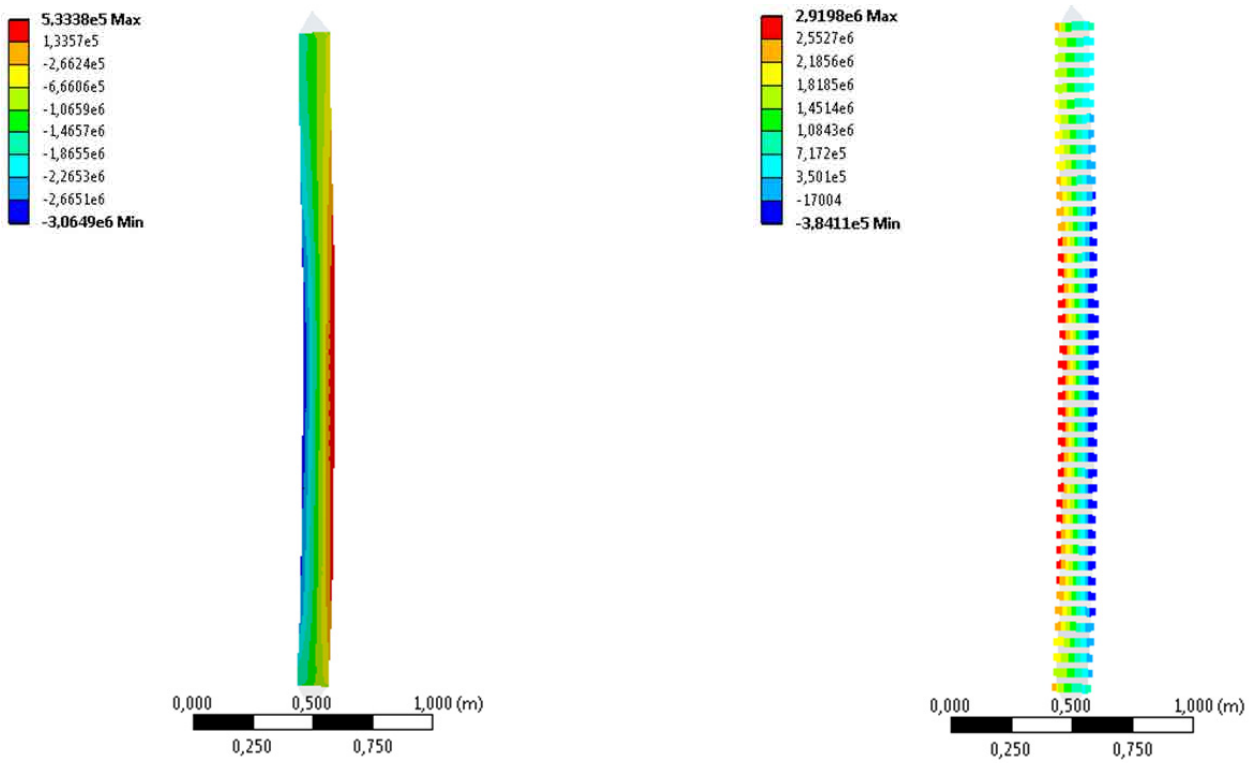


Figure A2. 6 Vertical stress distribution (left) and contact pressure (right) corresponding to the maximum calculated load for wall W#3. Values in Pa

## A2.2.4. Wall W#4

### *A2.2.4.1 Input parameters*

This was the only wall of the F series (with the base of the wall fixed instead of pinned). Table A2. 2 summarises the values of the input variables. These are the same for walls W#2 to W#5. Poisson's coefficient and the mesh size were 0.35 and 20mm respectively.

#### *A2.2.4.2 Results*

The maximum load-bearing capacity of the wall W#4 ranged from 153.6kN to 432.3kN for the extreme values of the input variables. For the most representative set of values and the real geometry, the load-bearing capacity was 303.9kN.

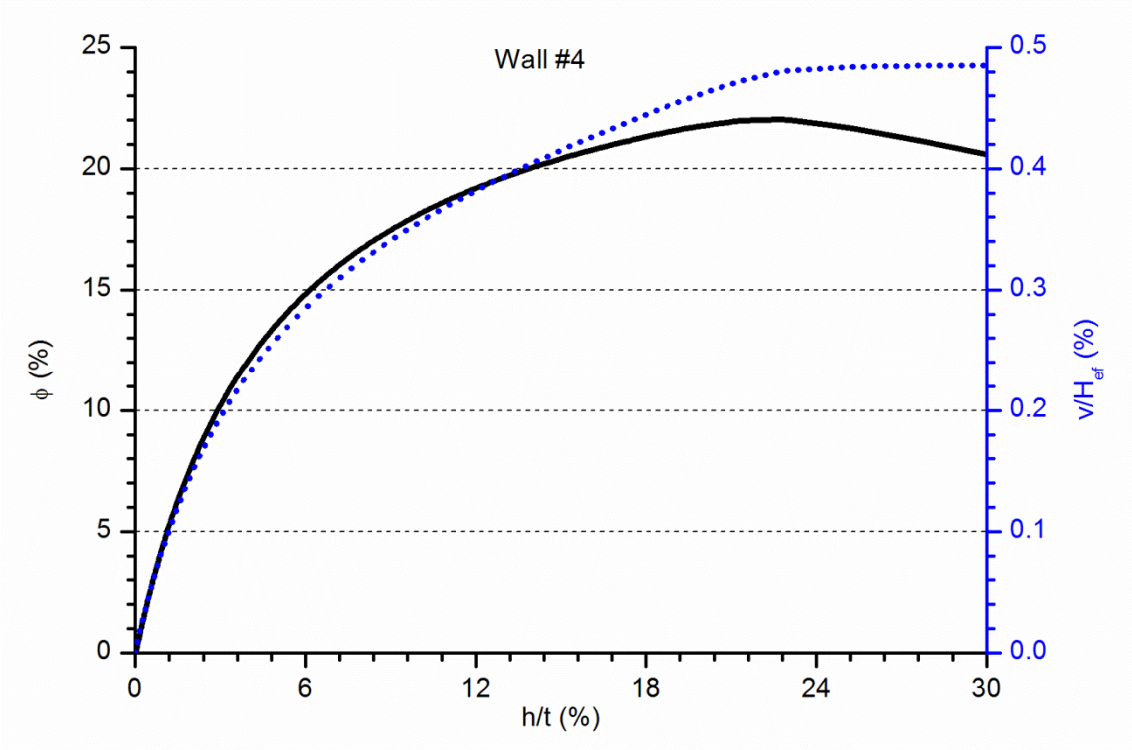


Figure A2. 7 Vertical and lateral calculated response of the wall W#4

Regarding the calculated response of this wall (see Figure A2. 7), which had different boundary conditions, it has to be said that the behaviour was similar to previous analysis of walls with both extremes pinned. However, observing the plotted values it is noticed that the non-linear relationship between force and lateral displacement becomes evident for larger loads but similar lateral-displacements (black continuous line). The non-linear relationship between vertical and lateral displacement is noticed from very low loads. In contrast with previous tests, there is no a linear range in this representation (blue dotted line).

The distribution of the vertical component of stresses in masonry and the pressure in contacts (Figure A2. 8) is quite different from previous cases. The typical distribution with the compressive stresses in on side and the tensile in the other one is inverted near the bottom of the wall because of the different boundary conditions. The response is absolutely asymmetric. The maximum compressive stress in far lower than the masonry compressive strength. Thus, once again, the wall's collapse is caused for the failure of the contact corresponding with one horizontal mortar joint. In this case, the breaking point would be over the mid-height. For the maximum load the maximum tensile stress in the contacts was

almost the flexural strength of masonry so the collapse happened due to a buckling process influenced for the second order bending deformations.

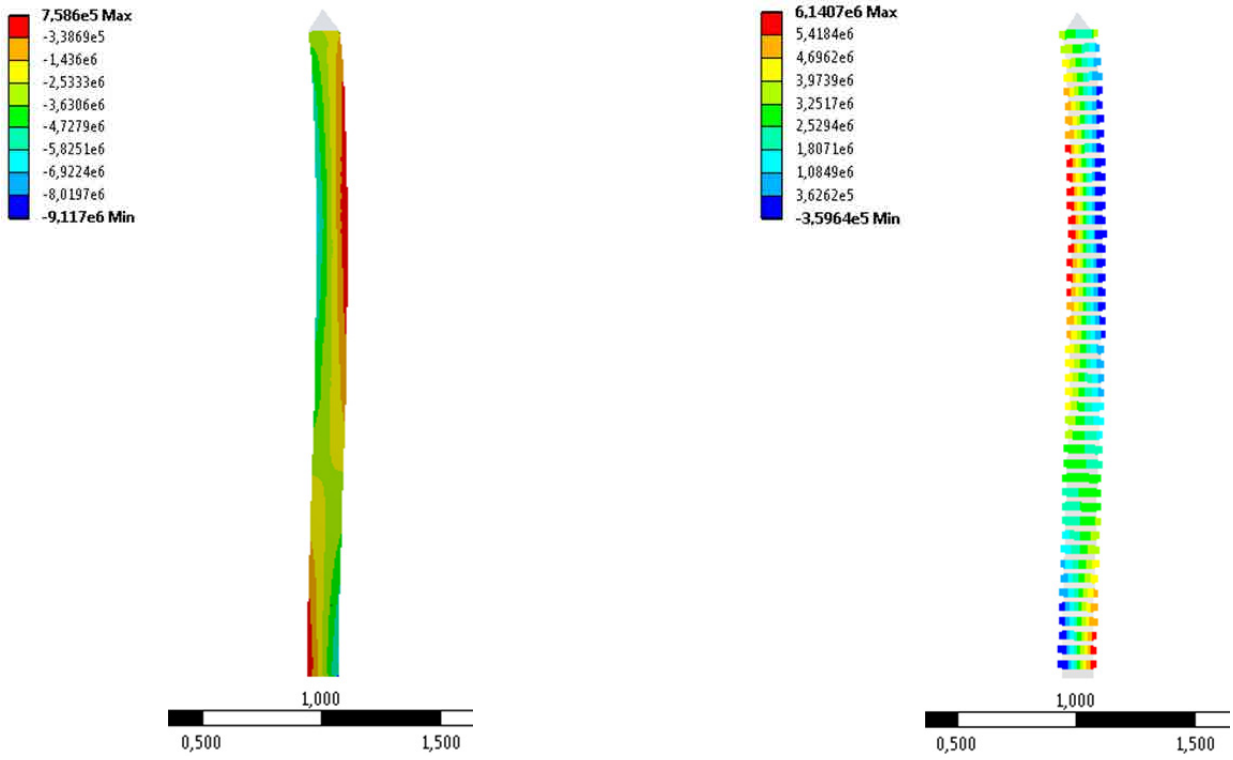


Figure A2. 8 Vertical stress distribution (left) and contact pressure (right) corresponding to the maximum calculated load for wall W#4. Values in Pa

## A2.2.5. Wall W#5

### *A2.2.5.1 Input parameters*

This was another wall of the H series and the last one of the construction batch which included walls W#2 to W#5, so the properties are showed in Table A2. 2. Poisson's coefficient and the mesh size were 0.35 and 20mm respectively.

### *A2.2.5.2 Results*

The maximum load-bearing capacity of the wall W#5 ranged from 55.4kN to 169.6kN for the extreme values of the input variables. For the most representative set of values and the real geometry, the load-bearing capacity was 116.0kN.

Regarding the simulated response of this wall (see Figure A2. 9), it has to be highlighted that the sudden change in the behaviour corresponding with the maximum load was not so evident in comparison with previous cases. The relationship between the vertical movement of the top of the wall and lateral displacement at mid-height (blue dotted line) is non-linear and the three ranges identified for previous

walls are no clear in this case. The second order effects are influencing the response from the very first beginning of the loading history (black continuous line).

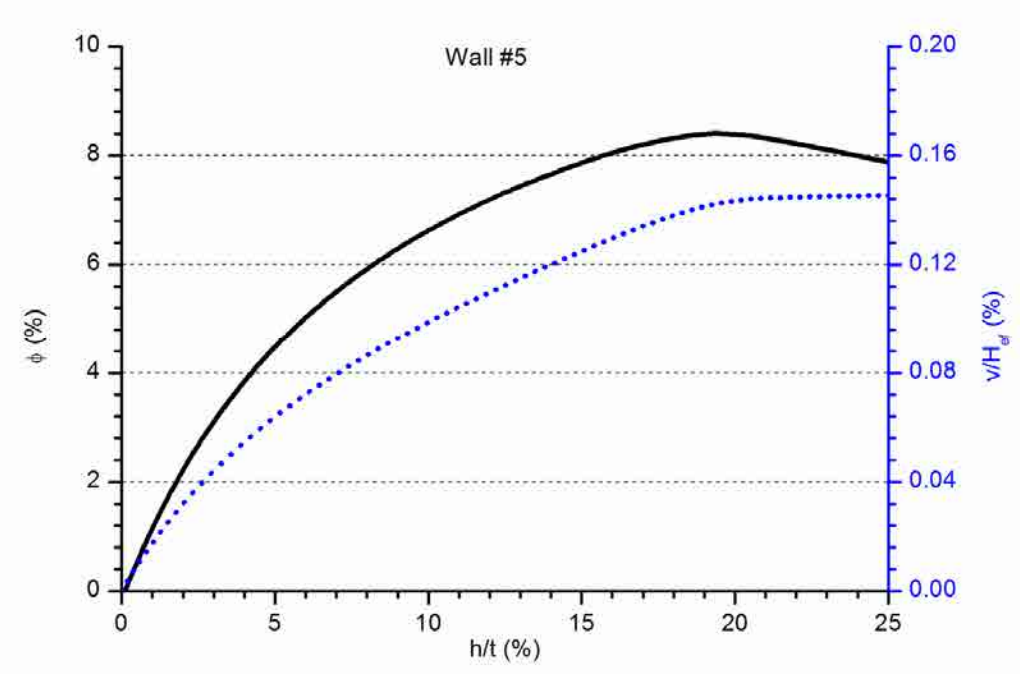


Figure A2. 9 Vertical and lateral calculated response of the wall W#5

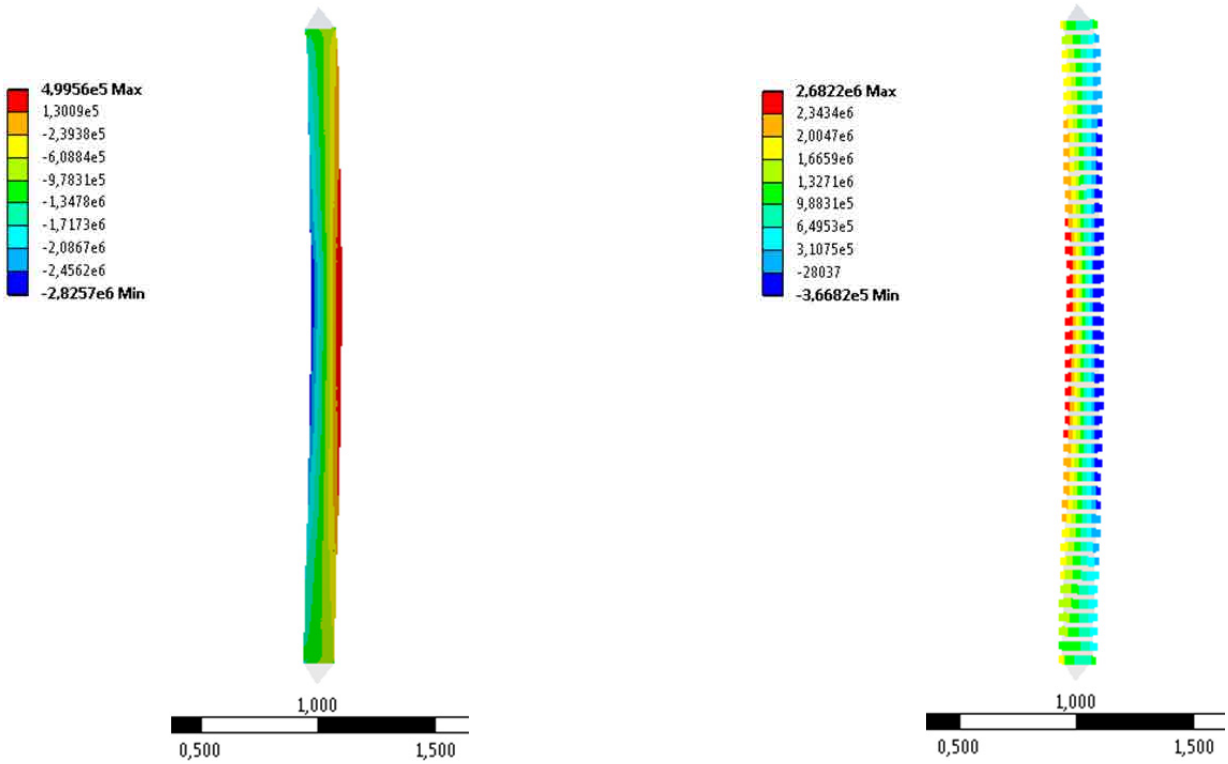


Figure A2. 10 Vertical stress distribution (left) and contact pressure (right) corresponding to the maximum calculated load for wall W#5. Values in Pa

Observing the vertical stress distribution (left side of Figure A2. 10) the symmetry of the wall's response is evident. The maximum compressive stress is far from the compressive strength of masonry and the results indicate, once again, that the collapse is caused by the tensile failure in one of the contacts between masonry rows (see right side of Figure A2. 10). The maximum tensile pressure is slightly over the flexural strength of the masonry.

## A2.2.6. Wall W#6

### *A2.2.6.1 Input parameters*

This is the first wall of the construction batch which included walls W#6 to W#9. Thus, the values of the properties included in Table A2. 3 are slightly different from the previous ones. Poisson's coefficient and the mesh size were 0.35 and 20mm respectively as in all simulations.

| ***Variable*** | ***Average values*** | ***Lowest values*** | ***Highest values*** |
|---|---|---|---|
| $f_{cm}$ *(MPa)* | 13.70 | 7.00 | 15.00 |
| $f_{xt}$ *(MPa)* | 0.36 | 0.10 | 0.70 |
| $G_f^I$ *(N/m)* | 13 | 4 | 26 |
| *E (MPa)* | 780 | 400 | 1100 |

Table A2. 3 Input data for the FEA of walls W#6 to W#9

### *A2.2.6.2 Results*

The maximum load-bearing capacity of the wall W#6 ranged from 24.4kN to 93.6kN for the extreme values of the input variables. For the most representative set of values and the real geometry, the load-bearing capacity was 58.6kN.

For the most representative set of values the calculated response of the wall W#6 is plotted in Figure A2. 11. The behaviour is more proportional to the applied load than in previous cases. In fact, the force vs. lateral displacement at mid-height might be modelled as a bilinear curve (black continuous line). In the same way, the relationship between the vertical displacement at the top of the wall and the lateral movement at mid-height (blue dotted line) is represented by an almost straight line up to the collapse load.

In this case the collapse was calculated to happen for a quite low load (compared with previous simulations), and according with the stresses in the contacts represented in the right image of Figure A2. 12, the tensile failure of a mortar joint at the wall's mid-height is the cause of the loss of equilibrium and the collapse of the structure. The maximum tensile stress in the contacts between masonry rows is slightly higher than the tensile strength. In contrast, the maximum compressive stress in the masonry (left image of Figure A2. 12) is far from the compressive strength (around 10%).

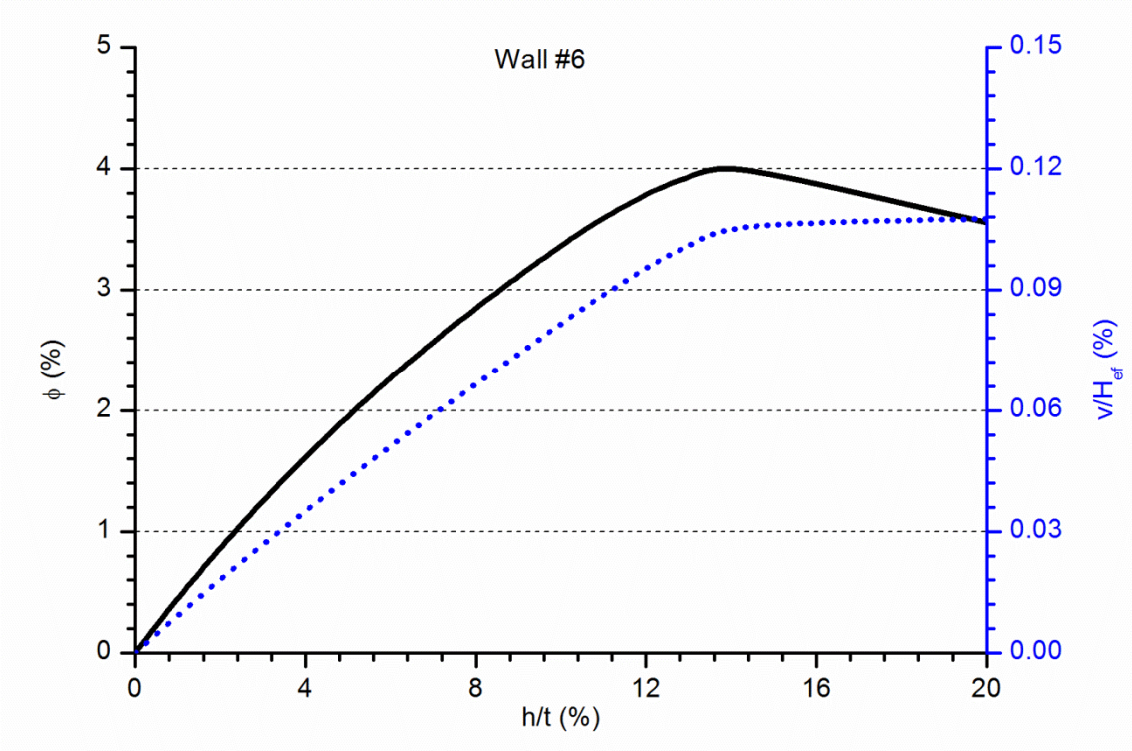


Figure A2. 11 Vertical and lateral calculated response of the wall W#6

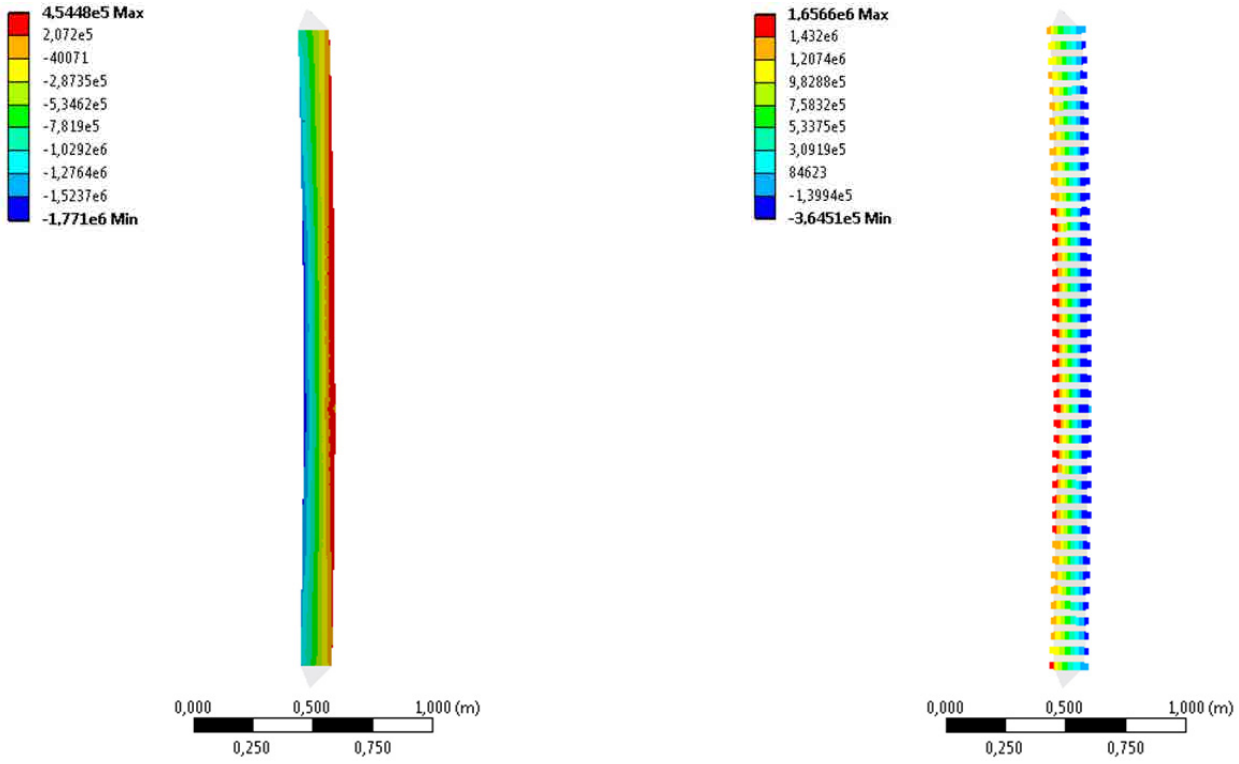


Figure A2. 12 Vertical stress distribution (left) and contact pressure (right) corresponding to the maximum calculated load for wall W#6. Values in Pa

## A2.2.7. Wall W#7

### *A2.2.7.1 Input parameters*

This is the second wall of the construction batch which included walls W#6 to W#9. Thus, the values of the properties are the ones included in Table A2. 3. Poisson's coefficient and the mesh size were 0.35 and 20mm respectively as in all simulations.

### *A2.2.7.2 Results*

The maximum load-bearing capacity of the wall W#7 ranged from 55.7kN to 170.6kN for the extreme values of the input variables. For the most representative set of values and the real geometry, the load-bearing capacity was 116.5kN.

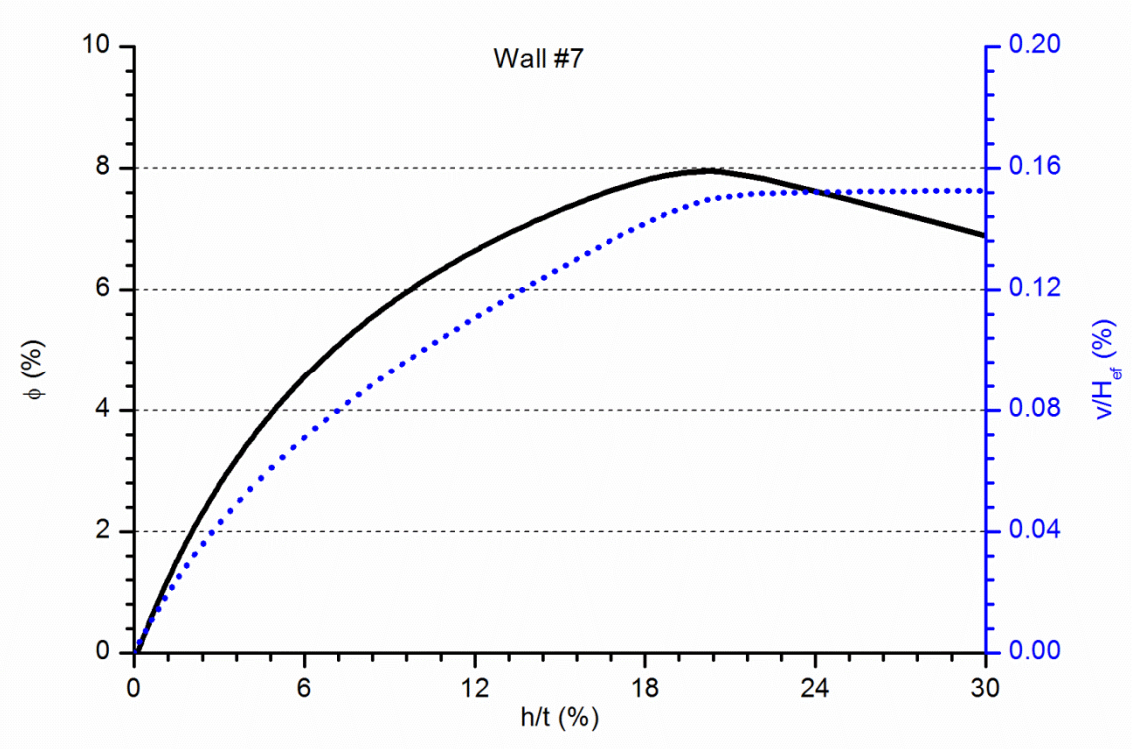


Figure A2. 13 Vertical and lateral calculated response of the wall W#7

Figure A2. 13 shows the calculated response from the finite element analysis of wall W#7. The relationship between force and lateral displacement at mid-height (black continuous line) is analogue to previous cases like W#5, with a remarkable non-linear relation associated with the second order bending effects. Once again, the relationship between vertical and lateral displacements (blue dotted line) presents two noticeable changes, one at the beginning (around 5% of lateral displacement) and the other one corresponding with the maximum load.

Observing the Figure A2. 14, it is noticed that the resulting collapse cause is the opening of a horizontal masonry joint. The maximum tensile stress in the contacts is slightly higher than the flexural strength of

masonry so one joint fails. In contrast, the maximum compressive stress in the masonry (2.8MPa) is far from the compressive strength (13.7MPa)

For comparison purposes the same simulation of W#7 has been carried out with a littler mesh with the following result:

Using a mesh size of 20mm the maximum load was 116.5kN, whereas using a mesh size of 10mm the load bearing capacity was 117.1kN.

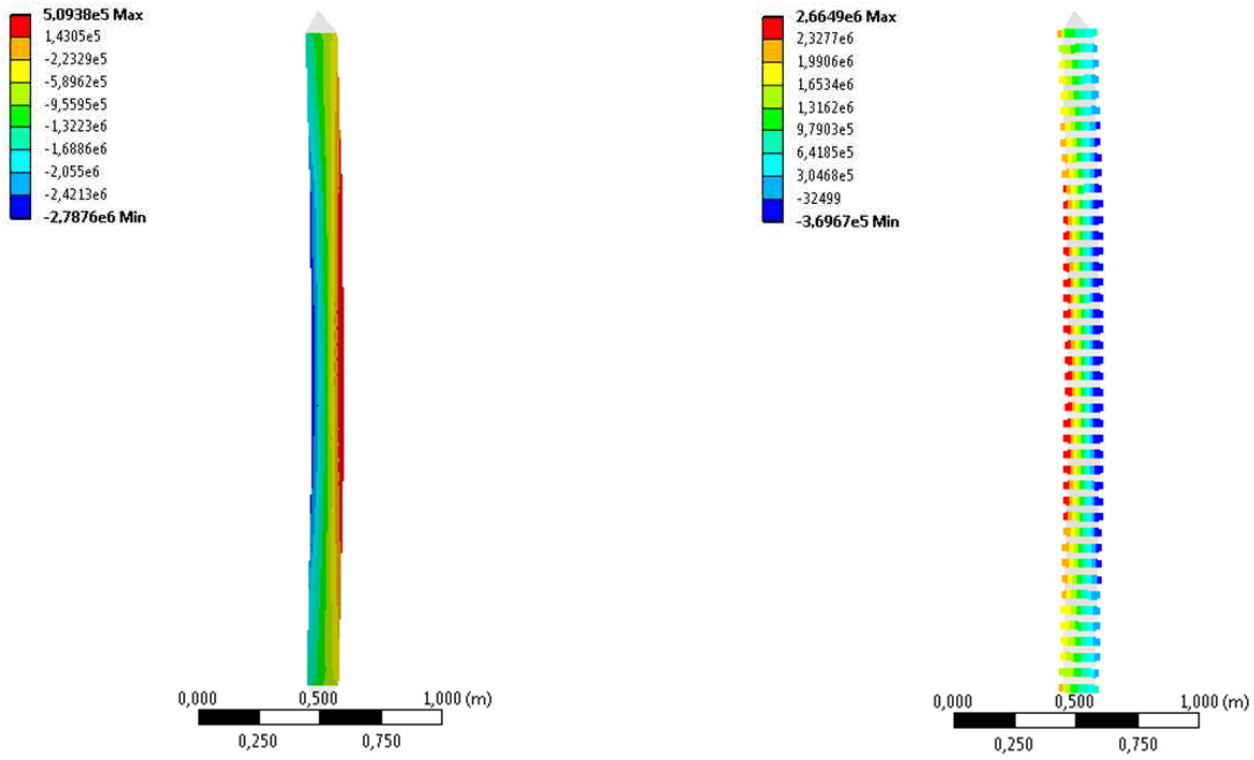


Figure A2. 14 Vertical stress distribution (left) and contact pressure (right) corresponding to the maximum calculated load for wall W#7. Values in Pa

## A2.2.8. Wall W#8

### *A2.2.8.1 Input parameters*

This is the third wall of the construction batch which included walls W#6 to W#9. Thus, the values of the properties are the ones included in Table A2. 3. Poisson's coefficient and the mesh size were 0.35 and 20mm respectively as in all simulations.

#### *A2.2.8.2 Results*

It is worth noticing that wall W#8 showed an abnormal behaviour caused by its initial eccentricity at mid-height which was opposite to the eccentricity at the extremes of the wall. The consequence is that the wall moved backwards at the beginning of the simulation. The maximum load-bearing capacity of the wall W#8 ranged from 80.9kN to 229.2kN for the extreme values of the input variables. For the most representative set of values and the real geometry, the load-bearing capacity was 181.0kN.

Observing the simulation results plotted in Figure A2. 15, it is noticed that the initial tendency was to bend in the opposite direction from the forced by the initial eccentricity at wall's extremes. The second order effect increases the speed of this backward deformation up to a point close to the maximum force (see the black continuous line) when the wall changes its deformation direction and with almost constant vertical displacement moves laterally a 40% of its thickness (see the blue dotted line) increasing the applied load up to the load-bearing capacity. This behaviour evidences the high dependency the simulation has on the initial geometry.

In Figure A2. 16 it is shown that the collapse mode is associated with the flexural failure of a horizontal joint of the masonry placed below the mid-height. The maximum tensile stress corresponds with the flexural strength of masonry whilst the maximum compressive stress is far from the masonry strength.

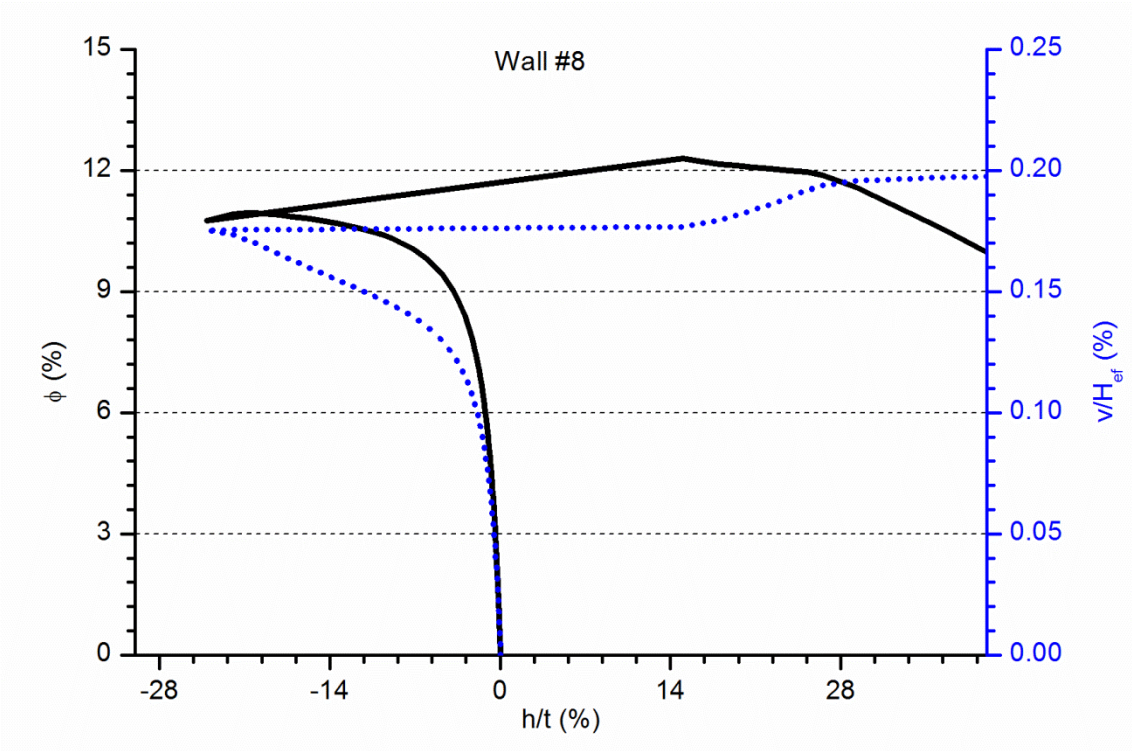


Figure A2. 15 Vertical and lateral calculated response of the wall W#8

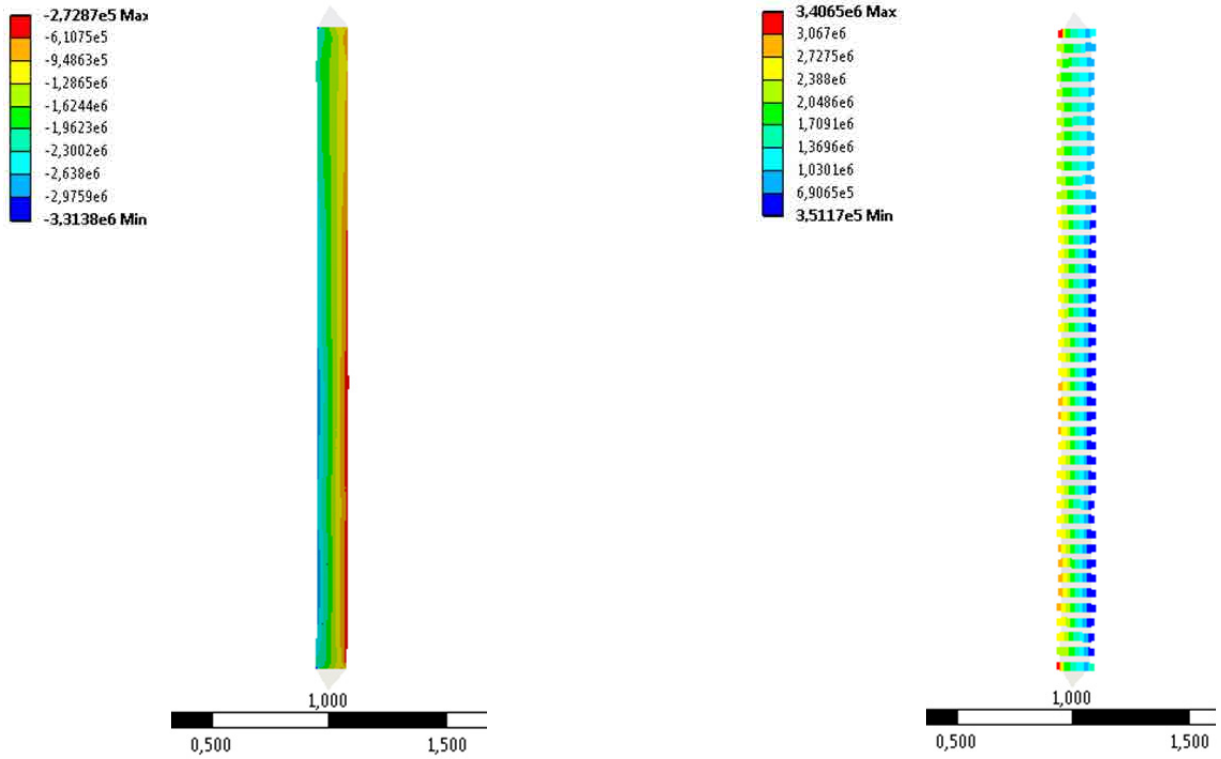


Figure A2. 16 Vertical stress distribution (left) and contact pressure (right) corresponding to the maximum calculated load for wall W#8. Values in Pa

## A2.2.9. Wall W#9

### *A2.2.9.1 Input parameters*

This is the last wall of the construction batch whose material characteristics are summarised in Table A2. 3. Poisson's coefficient and the mesh size are the same than in the previous simulations.

### *A2.2.9.2 Results*

The whole response of wall W#9 is in accordance with all previous walls except for W#8. The maximum load-bearing capacity of the wall W#9 ranged from 42.6kN to 139.1kN for the extreme values of the input variables. For the most representative set of values and the real geometry, the load-bearing capacity was 92.7kN.

Figure A2. 17 shows the vertical (blue dotted line) response of wall W#9 in relation with the lateral movement at mid-height. It is a non-linear relationship at the beginning and the final steps of the simulation but it is represented with an almost straight line at the central part. In contrast, the relationship between the lateral displacement at mid-height and the applied force (black continuous line) is non-linear because of the second order effects. This out-of-plane deformation accelerates with the load up to the collapse.

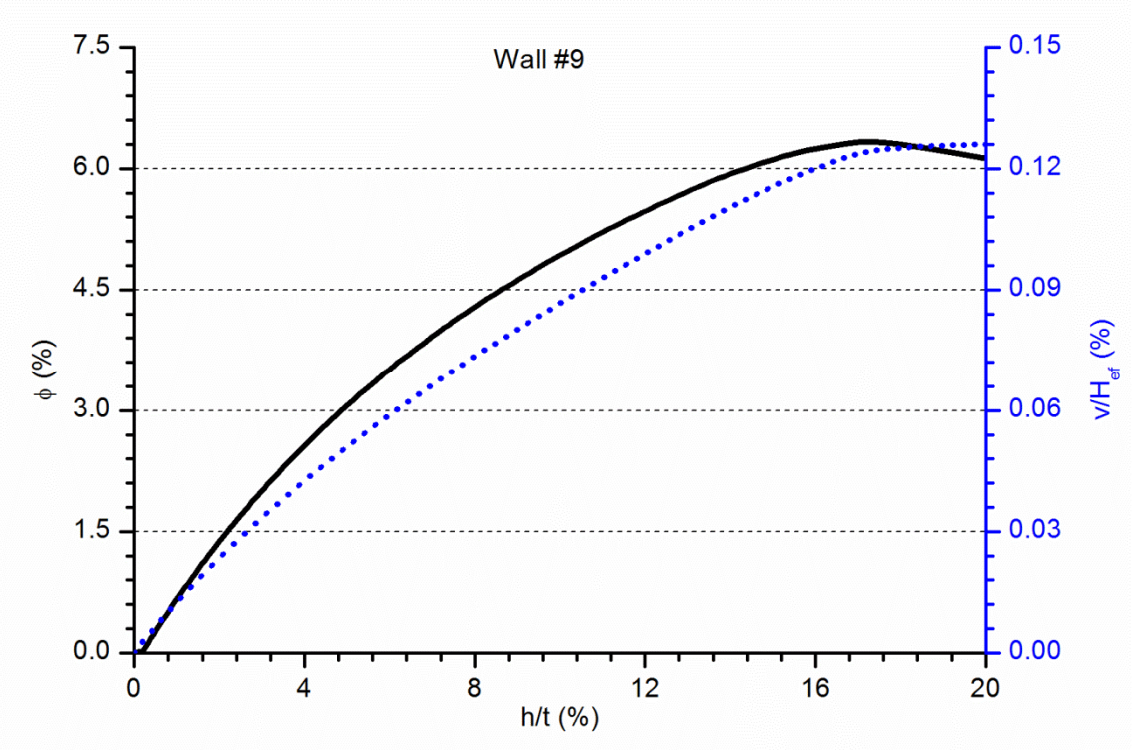


Figure A2. 17 Vertical and lateral calculated response of the wall W#9

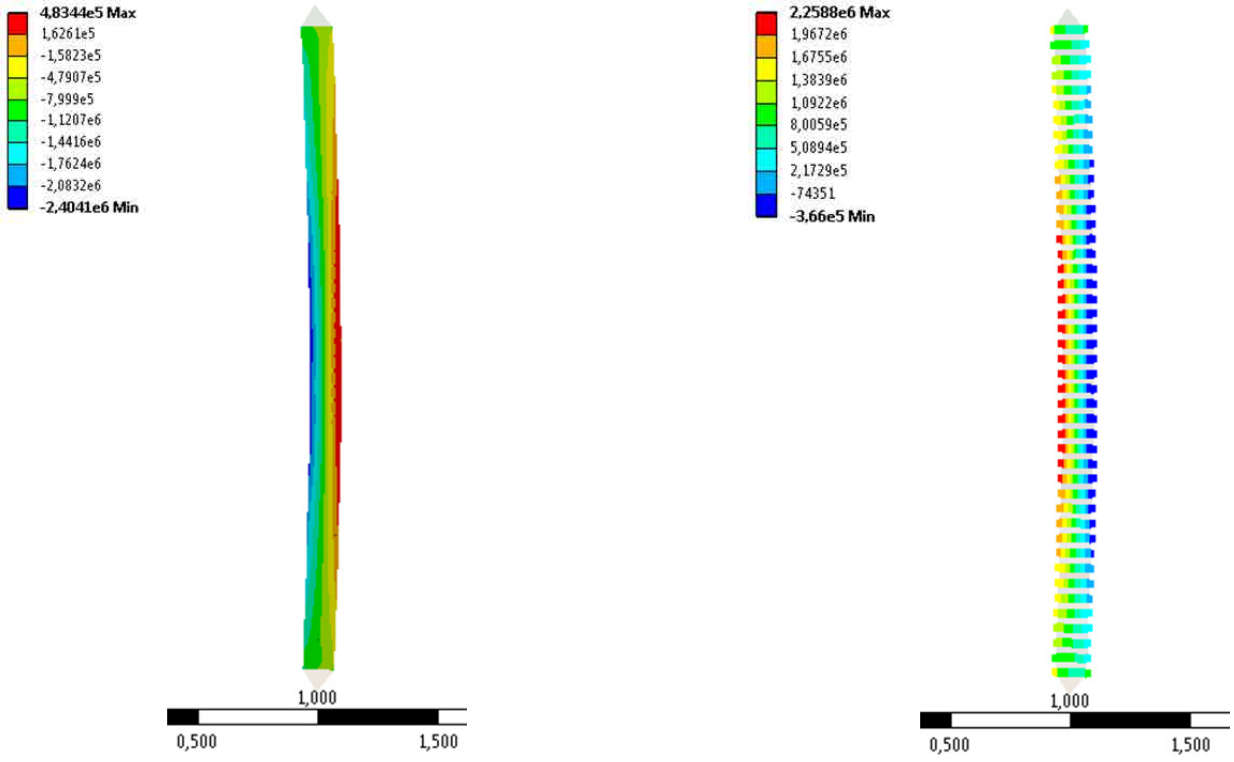


Figure A2. 18 Vertical stress distribution (left) and contact pressure (right) corresponding to the maximum calculated load for wall W#9. Values in Pa

For the maximum simulated load the compressive stresses are far from the masonry compressive strength (see left side of Figure A2. 18) whereas the maximum developed tensile stresses in the contacts between masonry rows are coincident with the maximum flexural strength of masonry (see right side of Figure A2. 18). This indicates that the cause of the collapse is the opening of a horizontal mortar joint at mid-height position, according with the FEA.

## A2.2.10. Wall W#10

### *A2.2.10.1 Input parameters*

Wall W#10 is the first one of the M series and it belongs to a construction batch which includes walls W#10 to W#17. The material properties for the three simulations of this case are summarised in Table A2. 4. Poisson's coefficient is 0.35, the same than in previous simulations, but the mesh size is reduced to 5mm in this and all the following cases.

| ***Variable*** | ***Average values*** | ***Lowest values*** | ***Highest values*** |
|---|---|---|---|
| $f_{cm}$ *(MPa)* | 10.8 | 7.00 | 15.00 |
| $f_{xt}$ *(MPa)* | 0.36 | 0.10 | 0.70 |
| $G_f^I$ *(N/m)* | 13 | 4 | 26 |
| *E (MPa)* | 780 | 400 | 1100 |

Table A2. 4 Input data for the FEA of walls W#10 to W#29

### *A2.2.10.2 Results*

The maximum load-bearing capacity of the wall W#10 ranged from 167.8kN to 475.2kN for the extreme values of the input variables. For the most representative set of values and the real geometry, the load-bearing capacity was 333.2kN.

Observing Figure A2. 19 it is noticed that the relationship between applied force and lateral displacement at mid-height (black continuous line) is almost the same than the relationship between vertical and lateral displacements (blue dotted line). This implies that the applied force and the vertical displacement are almost proportional indicating the lower influence of the second order effects in comparison with H series walls. However, the second order bending is noticed with the curvature of the two curves plotted in Figure A2. 19 which represent that the lateral displacement increases at a growing ratio when raising the load or descending the top of the wall. The point corresponding with the maximum force is an inflection point of the graphs.

The failure mode in this case is associated with the opening of a horizontal joint between masonry rows. Looking at Figure A2. 20 it is noticed that the maximum compressive stress is close to the maximum compressive strength of the masonry but still below the value whereas the maximum tensile stress of the horizontal joints is slightly over the flexural strength of masonry (because of stress concentration in a

singular punt when the contacts open). Thus, according with the simulation wall W#10 collapsed by opening a masonry joint below the mid-height position.

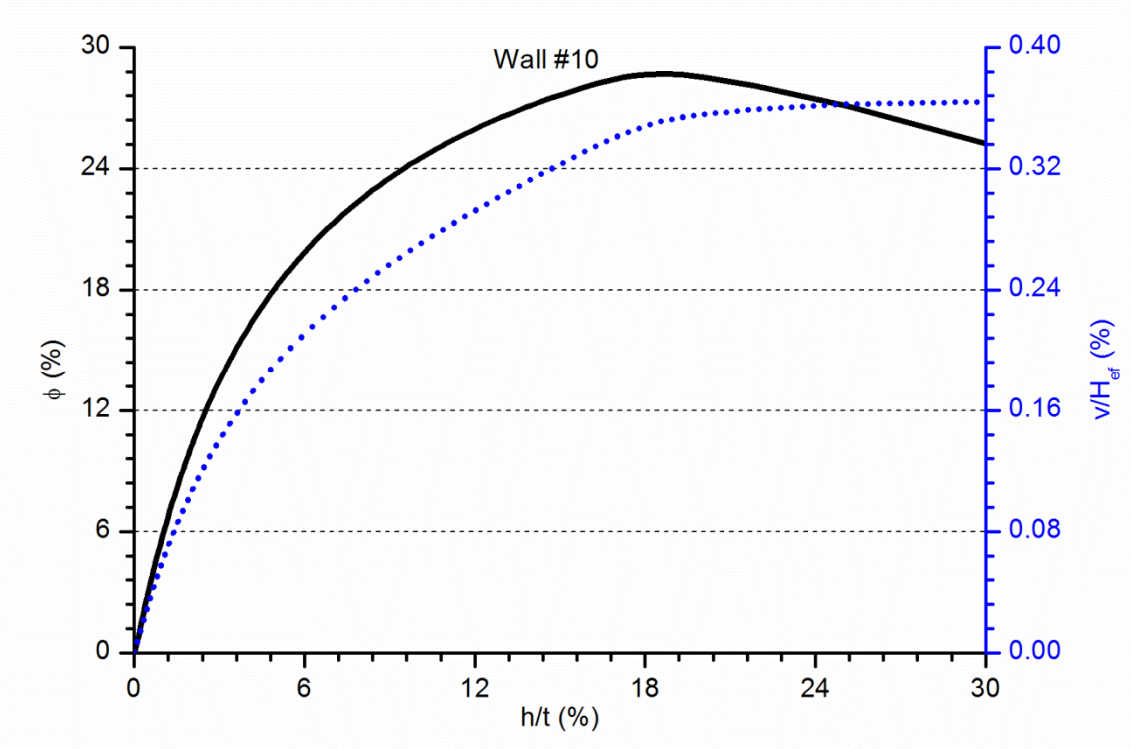


Figure A2. 19 Vertical and lateral calculated response of the wall W#10

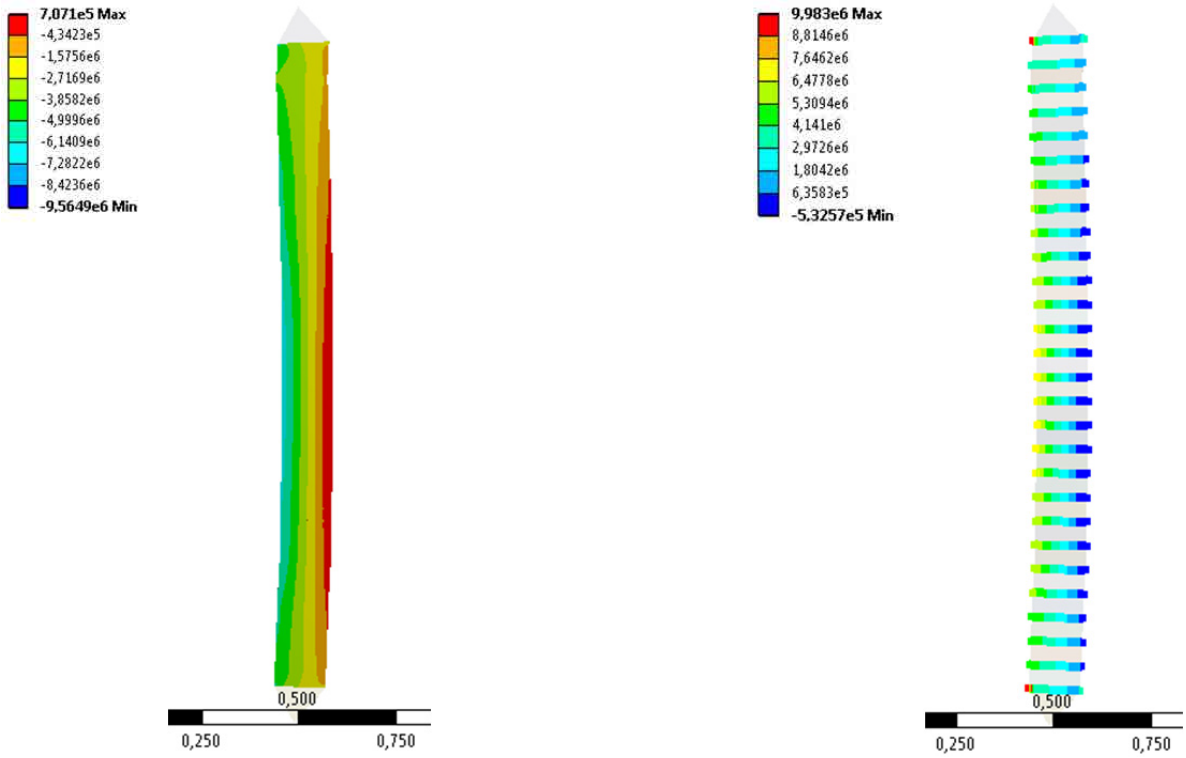


Figure A2. 20 Vertical stress distribution (left) and contact pressure (right) corresponding to the maximum calculated load for wall W#10. Values in Pa

## A2.2.11. Wall W#11

### *A2.2.11.1 Input parameters*

This is the second wall of the construction batch whose material characteristics are summarised in Table A2. 4. Poisson's coefficient and the mesh size are the same than in the previous simulations (0.35 and 5mm respectively).

### *A2.2.11.2 Results*

The maximum load-bearing capacity of the wall W#11 ranged from 78.0kN to 238.3kN for the extreme possible values of the input variables. For the most representative set of values and the real geometry, the load-bearing capacity was 161.4kN.

In Figure A2. 21 an almost linear response might be observed for both curves. The maximum applied load is a half of the previous case, so the second order effects, whose significance increases with the applied load, are almost negligible for wall W#11. The applied force vs. the lateral displacement at mid-height curve (black continuous line) is not as linear as the curve which represent the relationship between the vertical and lateral displacements (blue dotted one). This last one only changes its slope after reaching the maximum load.

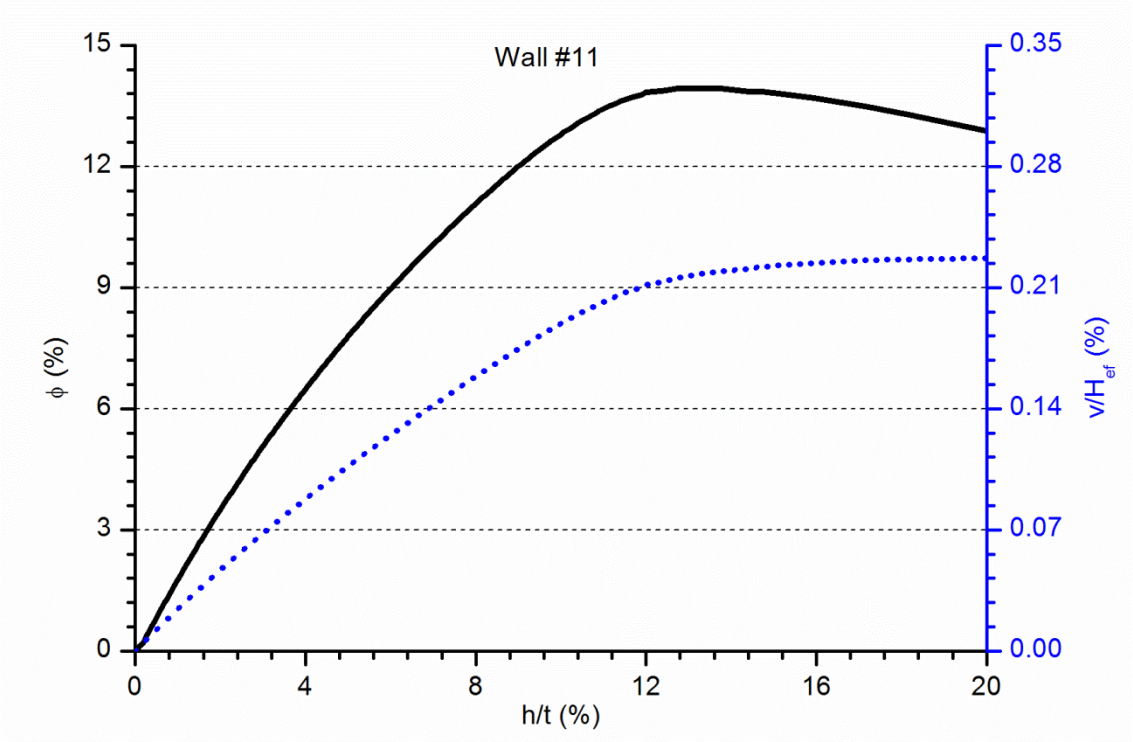


Figure A2. 21 Vertical and lateral calculated response of the wall W#11

Regarding the collapse mode, it is associated, one more time, with the opening of a mortar joint of masonry as results from analysing the contour results presented in Figure A2. 22. The maximum compressive stress is littler than the compressive strength whereas the maximum flexural strength of the masonry is overpassed in a point near the mid-height of the wall.

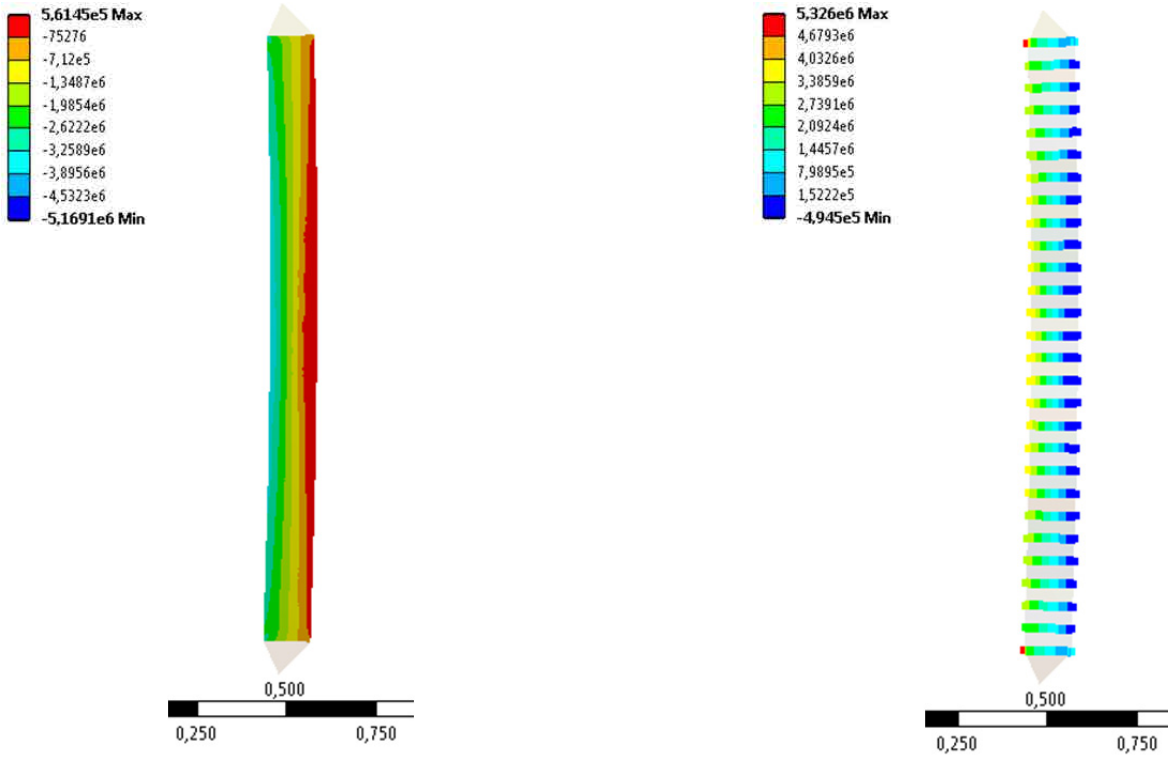


Figure A2. 22 Vertical stress distribution (left) and contact pressure (right) corresponding to the maximum calculated load for wall W#11. Values in Pa

## A2.2.12. Wall W#12

### *A2.2.12.1 Input parameters*

This is the third wall of the construction batch including walls W#10 to W#17. The material characteristics are summarised in Table A2. 4. Poisson's coefficient and the mesh size are the same than in the previous simulations (0.35 and 5mm respectively).

### *A2.2.12.2 Results*

The maximum load-bearing capacity of the wall W#12 ranged from 178.1kN to 501.3kN for the extreme possible values of the input variables. For the most representative set of values and the real geometry, the load-bearing capacity was 352.8kN.

The non-linear response of wall W#12 is noticed when observing Figure A2. 23. Both curves show a decreasing slope corresponding with the quicker raise of the lateral displacement at mid-height (x axis)

during the increase of the applied force (black continuous line) or the descending movement of the top of the wall (blue dotted line).

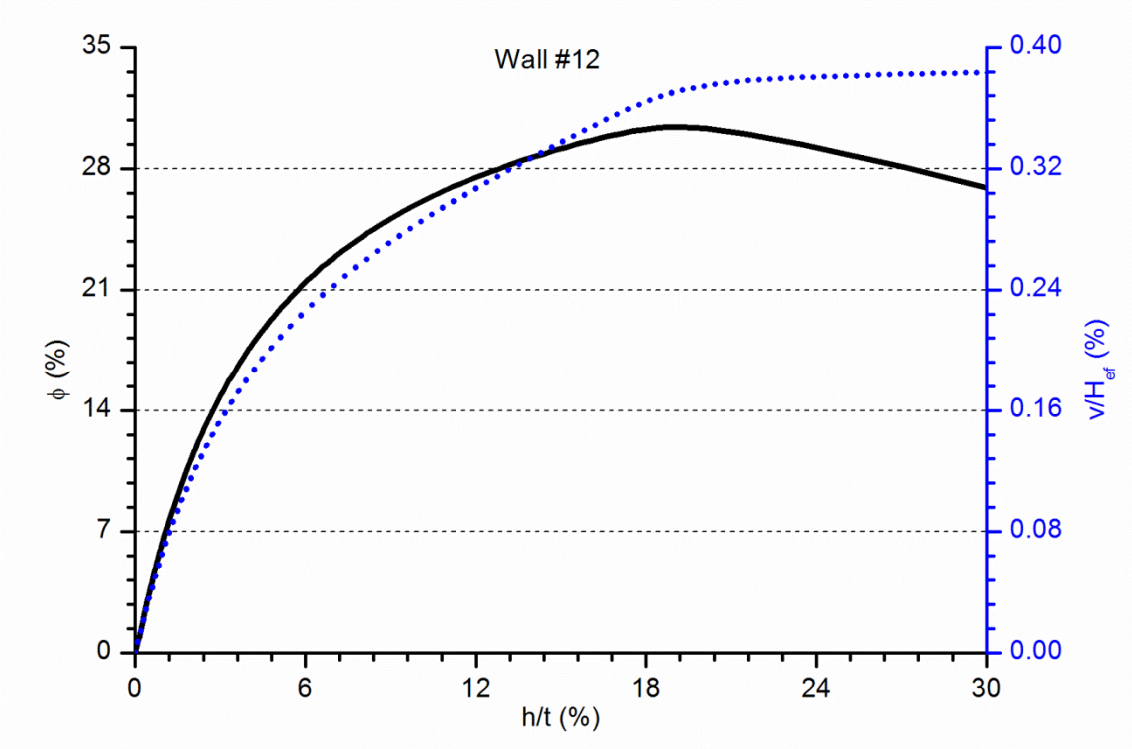


Figure A2. 23 Vertical and lateral calculated response of the wall W#12

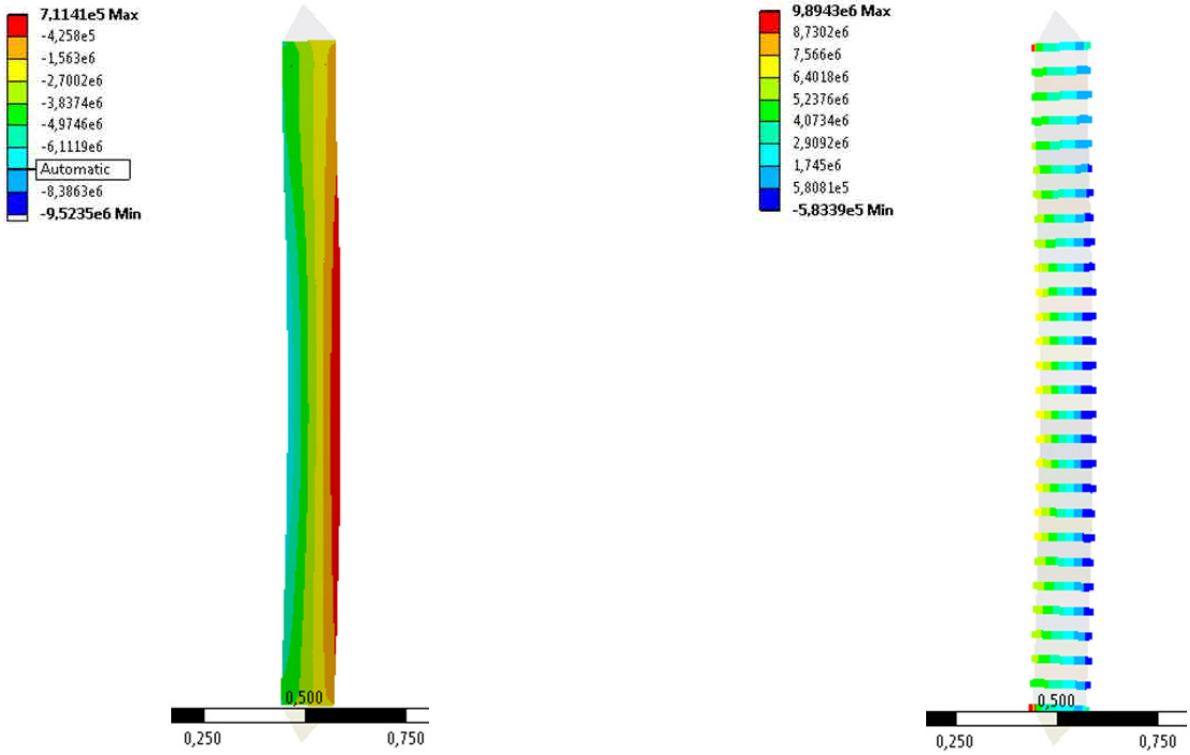


Figure A2. 24 Vertical stress distribution (left) and contact pressure (right) corresponding to the maximum calculated load for wall W#12. Values in Pa

Once again the wall is close to a compressive failure (the maximum compressive stress is 9.5MPa) but the collapse happens, according with the simulation, when one masonry joint reaches the flexural strength. This local failure is placed below the mid-height (see Figure A2. 24).

## A2.2.13. Wall W#13

### *A2.2.13.1 Input parameters*

This is one more case corresponding to the construction batch which included walls W#10 to W#17. The material characteristics are summarised in Table A2. 4. Poisson's coefficient is 0.35 and the mesh size is 5mm.

### *A2.2.13.2 Results*

The maximum load-bearing capacity of the wall W#13 ranged from 40.8kN to 140.6kN for the extreme possible values of the input variables. For the most representative set of values and the real geometry, the load-bearing capacity was 88.0kN.

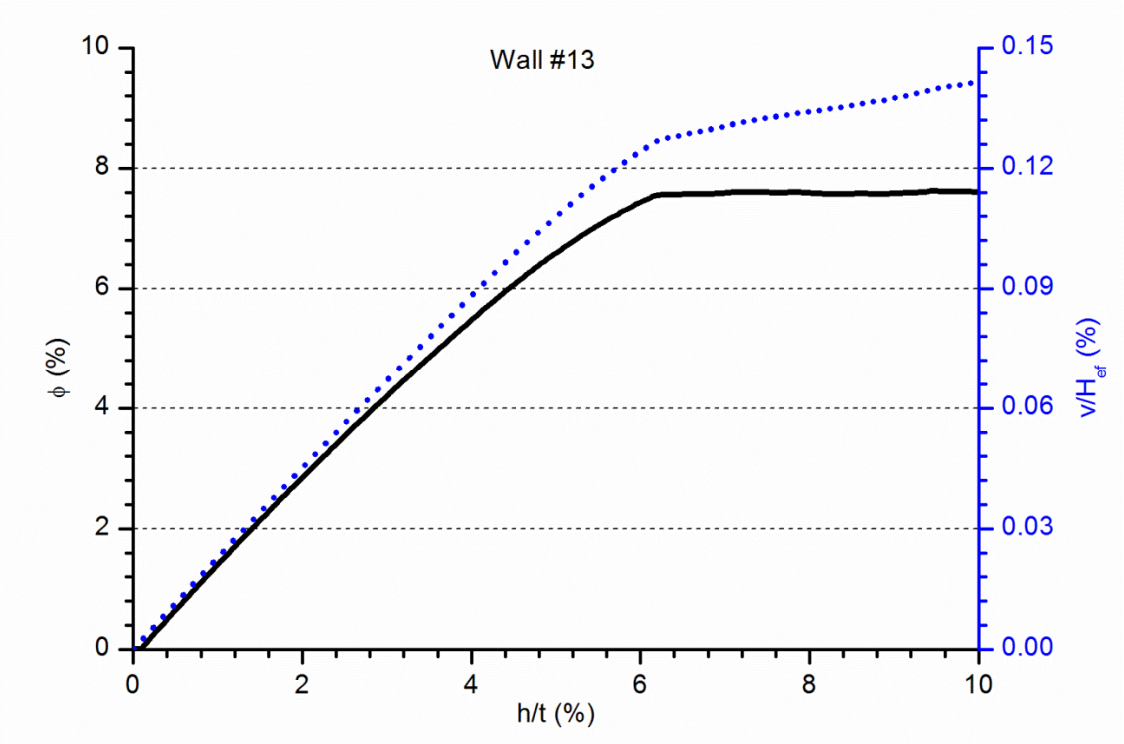


Figure A2. 25 Vertical and lateral calculated response of the wall W#13

Like in the previous wall of the M series which collapsed for a relatively low load (wall W#11), the force vs. lateral displacement at mid-height is almost linear (black continuous line in Figure A2. 25). The same response is observed in the relationship between the vertical and lateral movements (blue dotted

line). The slope of both curves only changes after reaching the maximum load. In this case it is more evident than for wall W#11.

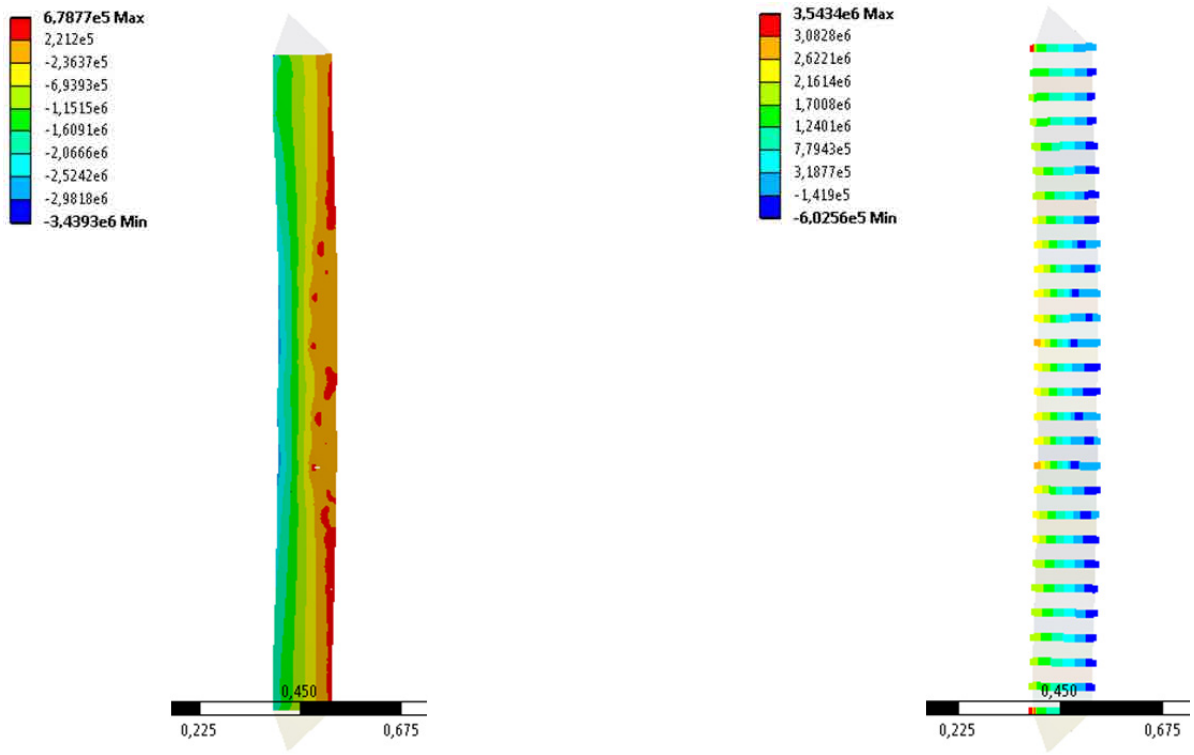


Figure A2. 26 Vertical stress distribution (left) and contact pressure (right) corresponding to the maximum calculated load for wall W#13. Values in Pa

Regarding the collapse mode and according with the simulation results (see Figure A2. 26), several masonry joints failed simultaneously around mid-height. The compressive stresses little in comparison with the compressive strength of the masonry.

## A2.2.14. Wall W#14

### *A2.2.14.1 Input parameters*

This is one more case corresponding to the construction batch which included walls W#10 to W#17. The material characteristics are summarised in Table A2. 4. Poisson's coefficient is 0.35 and the mesh size is 5mm.

### *A2.2.14.2 Results*

The maximum load-bearing capacity of the wall W#14 ranged from 67.0kN to 207.5kN for the extreme possible values of the input variables. For the most representative set of values and the real geometry, the load-bearing capacity was 140.8kN.

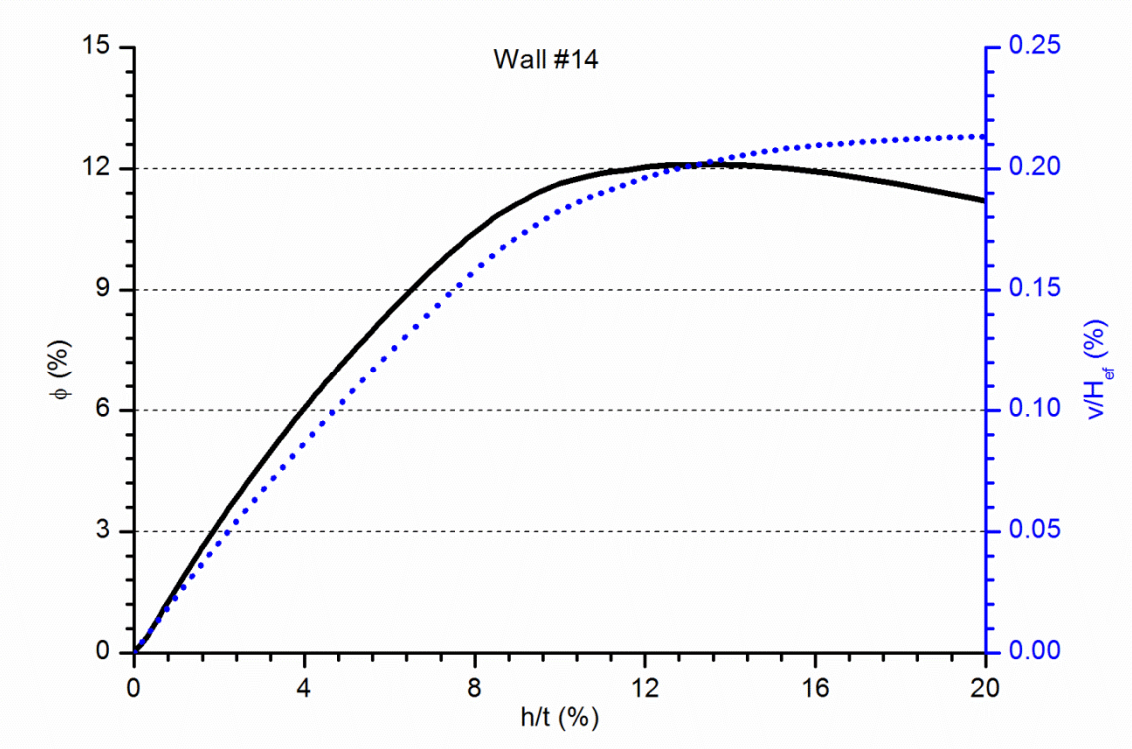


Figure A2. 27 Vertical and lateral calculated response of the wall W#14

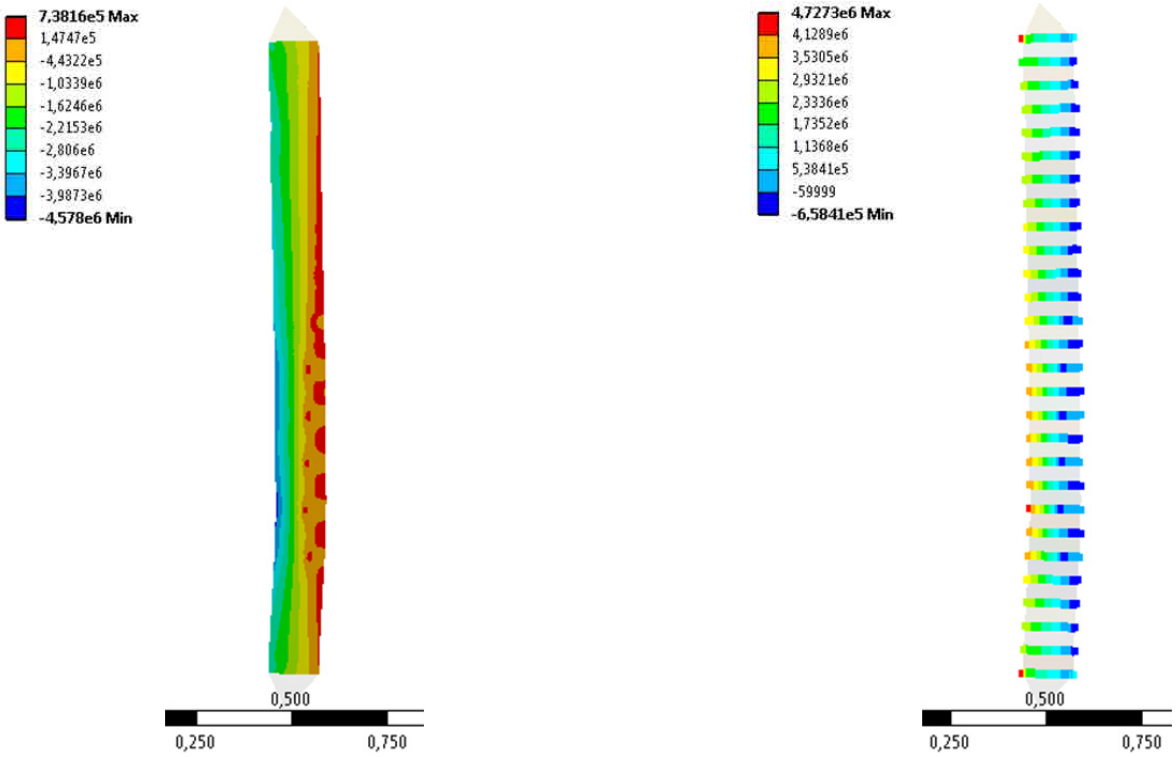


Figure A2. 28 Vertical stress distribution (left) and contact pressure (right) corresponding to the maximum calculated load for wall W#14. Values in Pa

According with the simulation results, the second order effects are no so evident than in other previous cases, and the loss of strength after the failure is significantly slower than in other walls as can be seen in Figure A2. 27. The black continuous line plots the applied force versus the lateral displacement at mid-height. In the same graph, the relationship between the vertical and lateral displacements (blue dotted line) is approximately linear up to 8% of the lateral displacement over the wall's thickness.

Regarding the collapse mode, in Figure A2. 28 it is observed that several masonry joints reached the maximum flexural strength whilst the maximum compressive stress is under 5MPa. Thus, the results suggest the collapse is due to opening of the horizontal contacts. Observing the contour plot, the opening is located in the lower half of the wall.

## A2.2.15. Wall W#15

### *A2.2.15.1 Input parameters*

Table A2. 4 summarises the materials characteristics of wall W#15 as part of the construction batch which included walls W#10 to W#17. Poisson's coefficient is 0.35 and the mesh size is 5mm.

### *A2.2.15.2 Results*

The maximum load-bearing capacity of the wall W#15 ranged from 39.0kN to 139.0kN for the extreme possible values of the input variables. For the most representative set of values and the real geometry, the load-bearing capacity was 87.8kN.

Like for the other wall of the M series which collapse for a load under the 10% of the maximum capacity of the material (W#13), the lateral displacement at mid-height is proportional to the applied load. It is noticed observing the straight line (black continuous) in Figure A2. 29. In the same way, the relationship between the vertical descending movement of the top of the wall and the lateral displacement at mid-height is linear (blue dotted line) up to the collapse load.

According with the model results, the collapse of the wall is due to the opening of several masonry joints (slightly centred below mid-height, see Figure A2. 30) which reached, and punctually overpassed, the maximum masonry flexural strength whereas the compression stress do not raise more than a quarter of the strength of the masonry. In Figure A2. 30 it is noticed that the maximum load is reached when several joint are already opened.

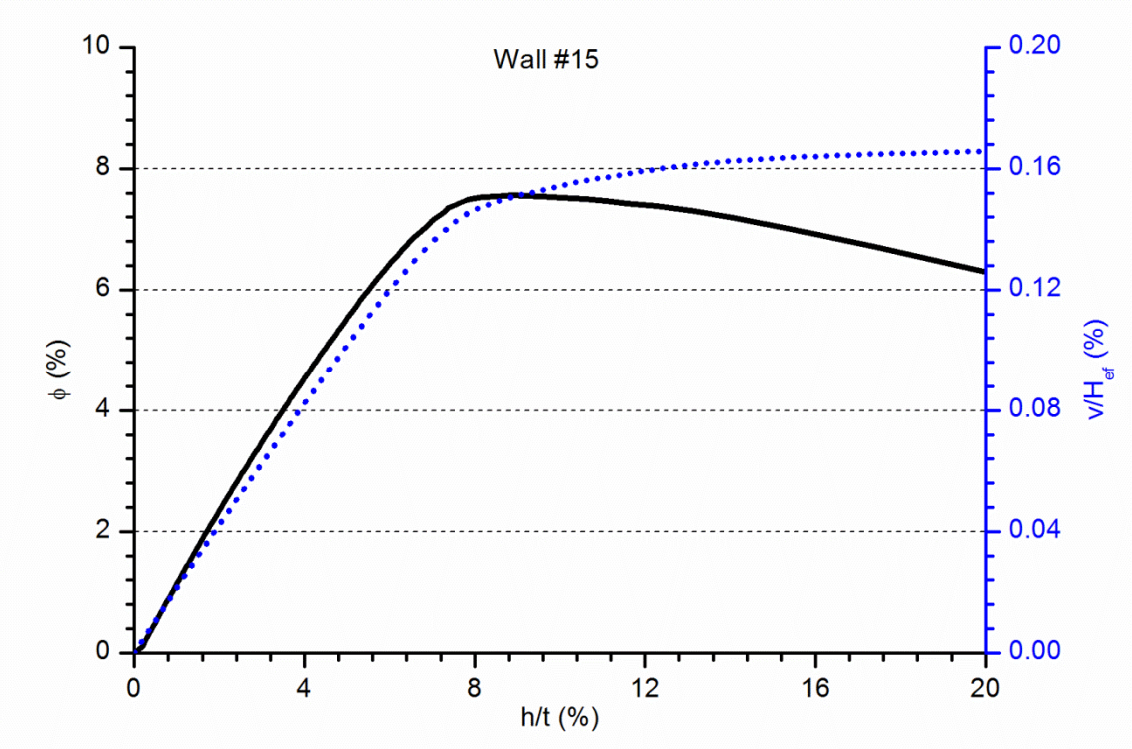


Figure A2. 29 Vertical and lateral calculated response of the wall W#15

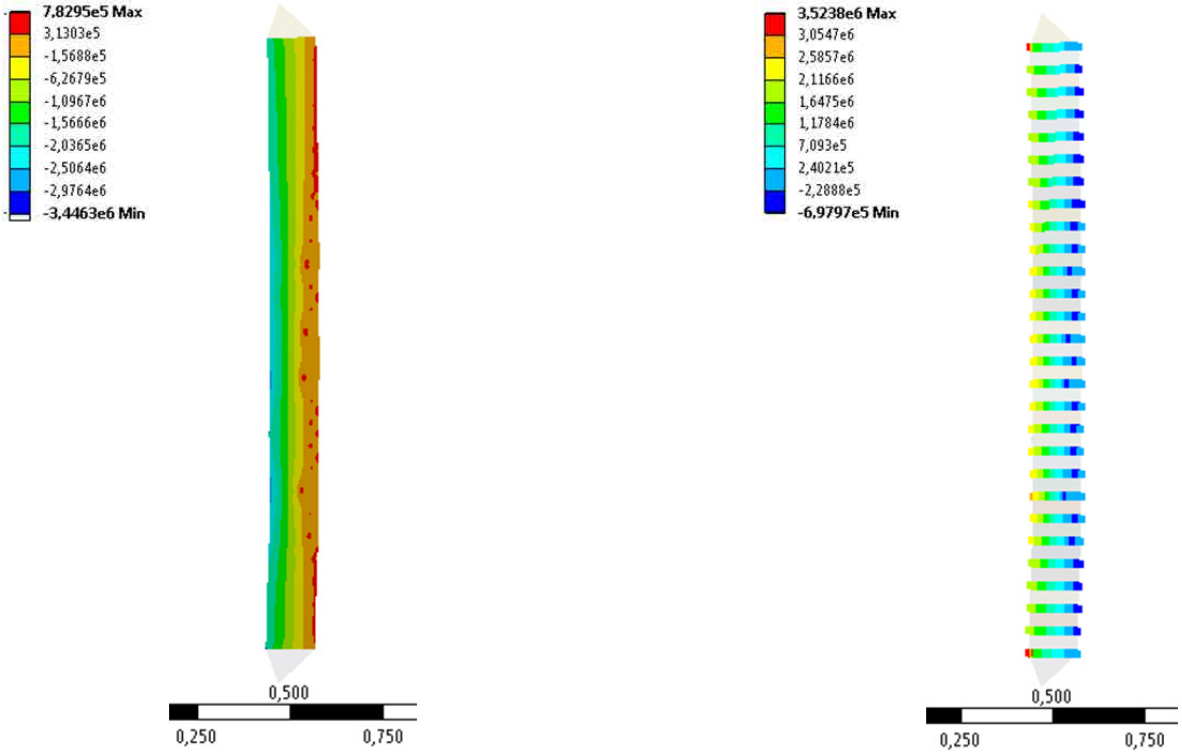


Figure A2. 30 Vertical stress distribution (left) and contact pressure (right) corresponding to the maximum calculated load for wall W#15. Values in Pa

## A2.2.16. Wall W#16

### *A2.2.16.1 Input parameters*

W#16 is the last wall of the M series. Table A2. 4 summarises the materials characteristics used for the simulations. They are the same than for the other walls of the construction batch which included walls W#10 to W#17. Poisson's coefficient is 0.35 and the mesh size is 5mm.

### *A2.2.16.2 Results*

The maximum load-bearing capacity of the wall W#16 ranged from 81.7kN to 248.2kN for the extreme possible values of the input variables. For the most representative set of values and the real geometry, the load-bearing capacity was 168.7kN.

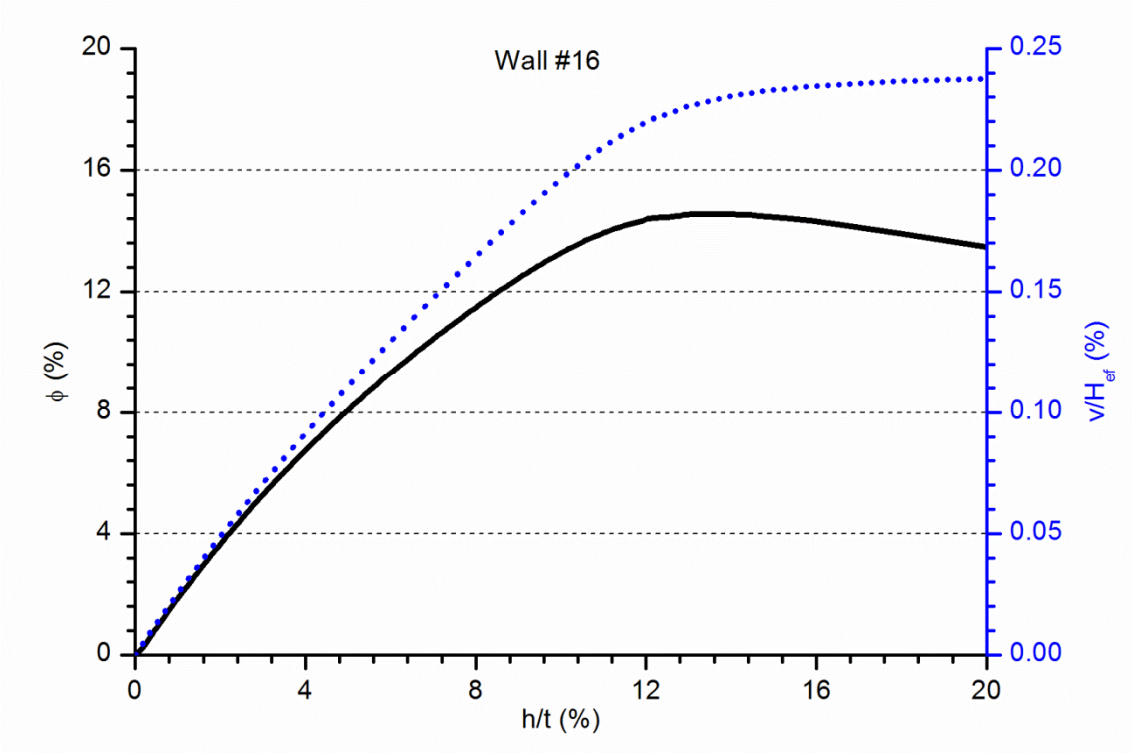


Figure A2. 31 Vertical and lateral calculated response of the wall W#16

Although the relationship between the vertical displacement of the top of the wall and the lateral displacement at mid-height (blue dotted line in Figure A2. 31) is almost linear up to the failure load, the force-lateral displacement correlation (black continuous line) is noticeably affected by the second order bending effects which caused the increase of the speed the lateral displacement grow at. Reaching the maximum load does not produce a sudden slope change in the graph which softly continues its slope variation.

Regarding the collapse causes according with the simulation, it is remarkable that the maximum compressive stress is kept far from the masonry strength values whereas the tensile stress in the contacts

which represent masonry joint reached and punctually overpassed the flexural strength of the material. According with the results in Figure A2. 32, the response of the wall would be almost symmetric.

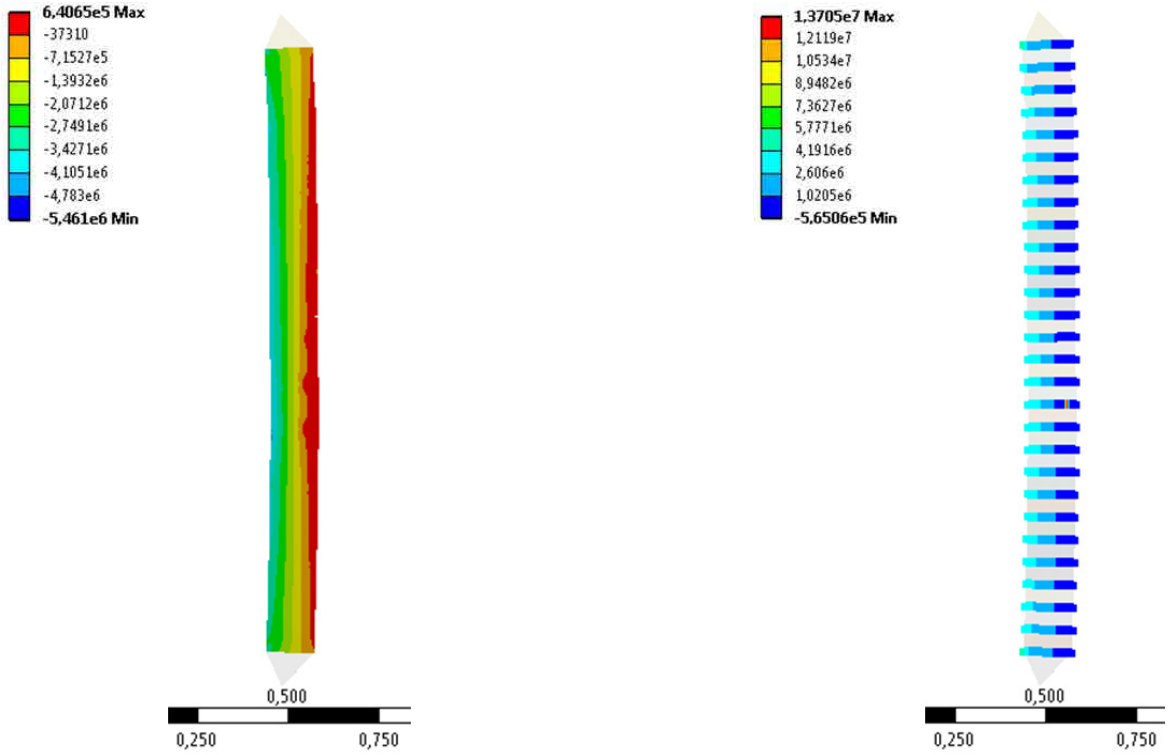


Figure A2. 32 Vertical stress distribution (left) and contact pressure (right) corresponding to the maximum calculated load for wall W#16. Values in Pa

## A2.2.17. Wall W#17

### *A2.2.17.1 Input parameters*

This is the only wall of the T series whose thickness is double. The materials properties are the same than for the seven previous walls as the construction batch is the same. These are summarised in Table A2. 4. Poisson's coefficient is 0.35 and the mesh size is 5mm.

### *A2.2.17.2 Results*

The maximum load-bearing capacity of the wall W#17 ranged from 106.8kN to 391.8kN for the extreme possible values of the input variables. For the most representative set of values and the real geometry, the load-bearing capacity was 325.0kN.

The wall response is divided in three main ranges. For the lower loads the response (force vs. lateral displacement at mid-height) is linear (see black continuous line in Figure A2. 33). After this, the slope of the curve decrease but it stays linear. Finally a non-linear relationship is observed. The lateral displacement grows quicker than the applied load in this last range up to the failure. The relation between

the vertical descending movement of the top of the wall and the lateral movement at mid-height (blue dotted line) follows the same shape.

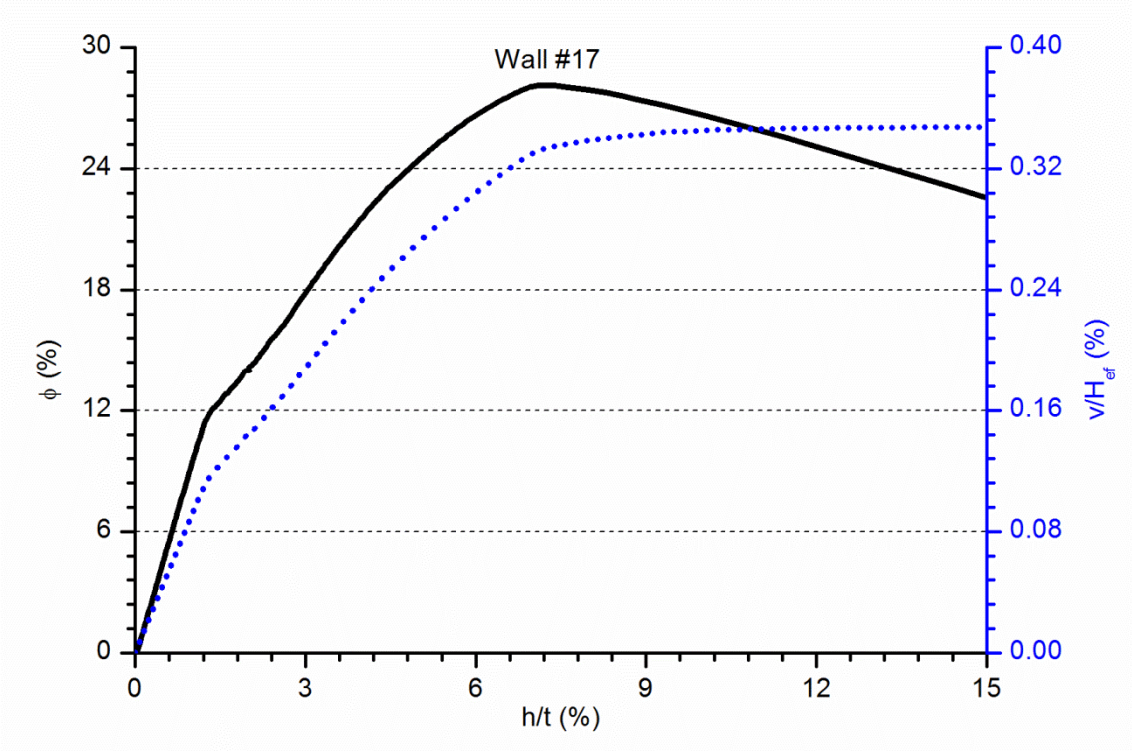


Figure A2. 33 Vertical and lateral calculated response of the wall W#17

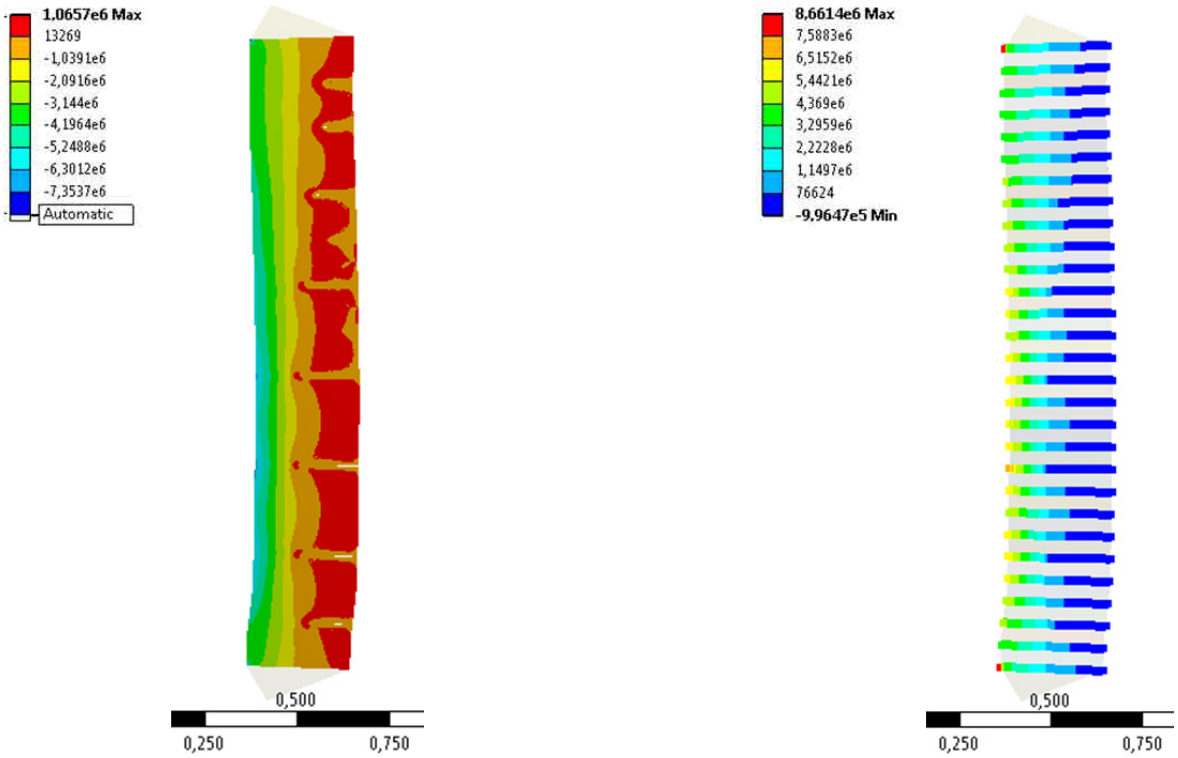


Figure A2. 34 Vertical stress distribution (left) and contact pressure (right) corresponding to the maximum calculated load for wall W#17. Values in Pa

In the contour plot presented in Figure A2. 34, it is observed that the maximum tensile stress in the contacts is higher than the flexural strength of the masonry so the failure of the wall is due to a joint opening. Looking at the left side of Figure A2. 34 it is noticed that the major part of the wall is compressed. The maximum compressive stress (8.4MPa) does not reach the maximum masonry strength (10.8MPa) although it is close to it.

## A2.2.18. Wall W#18

### *A2.2.18.1 Input parameters*

This is the first of the three walls of the S series. The values of the main properties for the simulations are the same than for previous walls (as explained in Chapter 4), so they are summarised in Table A2. 4. Like in previous cases, the Poisson's coefficient was set to 0.35 and the used mesh size was 5mm.

### *A2.2.18.2 Results*

The maximum load-bearing capacity of the wall W#18 ranged from 183.7kN to 515.8kN for the extreme possible values of the input variables. For the most representative set of values and the real geometry, the load-bearing capacity was 362.4kN.

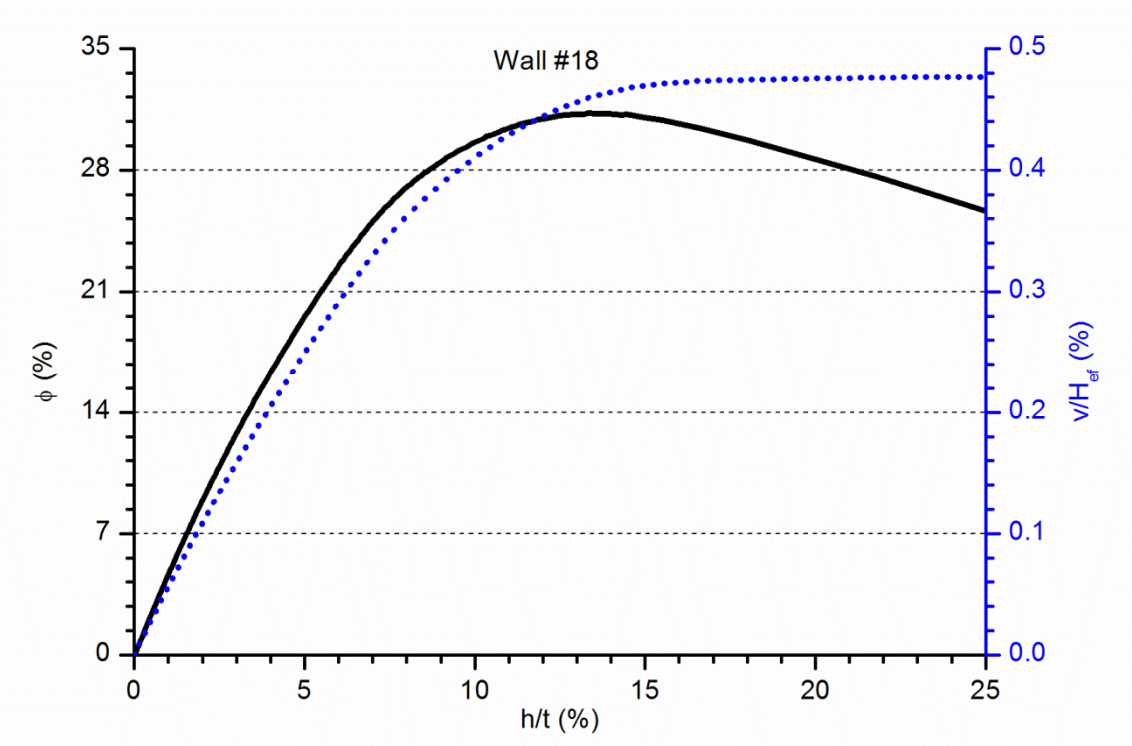


Figure A2. 35 Vertical and lateral calculated response of the wall W#18

Observing the plots in Figure A2. 35 it is noticed that the response was linear up to half the applied load when the second order effects became evident and the lateral displacement at mid-height increased faster than the applied load (black continuous line) or the vertical descending movement of the top of the wall (blue dotted line). For the maximum load the curves show a soft and progressive change in the slope.

Regarding the cause of the failure it has to be highlighted that according with the numerical results (see Figure A2. 36), the maximum compressive stress has reached the strength of the masonry but at the same time, the maximum tensile stress in the contacts has reached the flexural capacity of masonry. Thus, a combined failure cause (buckling and crushing) is expected for wall W#18 according with the finite element analysis results.

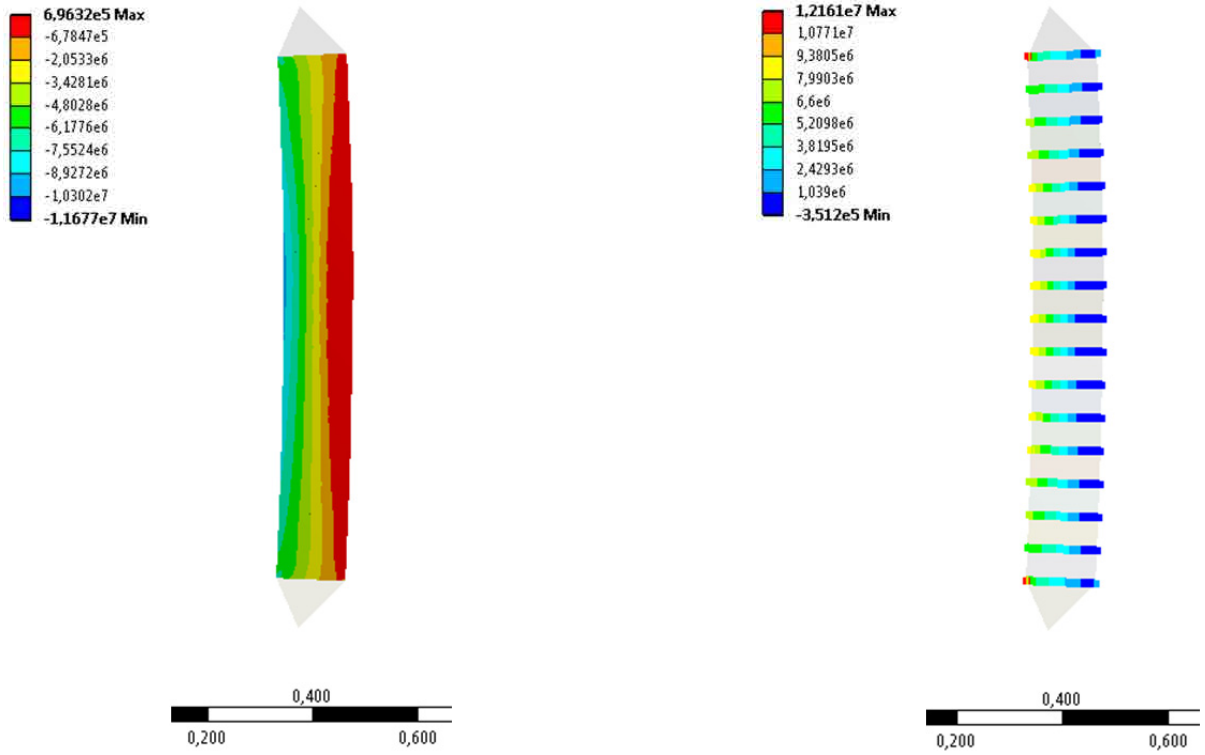


Figure A2. 36 Vertical stress distribution (left) and contact pressure (right) corresponding to the maximum calculated load for wall W#18. Values in Pa

## A2.2.19. Wall W#19

### *A2.2.19.1 Input parameters*

This is the second wall of the S series. The values of the main properties for the simulations are summarised in Table A2. 4 and the Poisson's coefficient is set to 0.35 and the used mesh size was 5mm.

### *A2.2.19.2 Results*

The maximum load-bearing capacity of the wall W#19 ranged from 83.4kN to 256.0kN for the extreme possible values of the input variables. For the most representative set of values and the real geometry, the load-bearing capacity was 169.0kN.

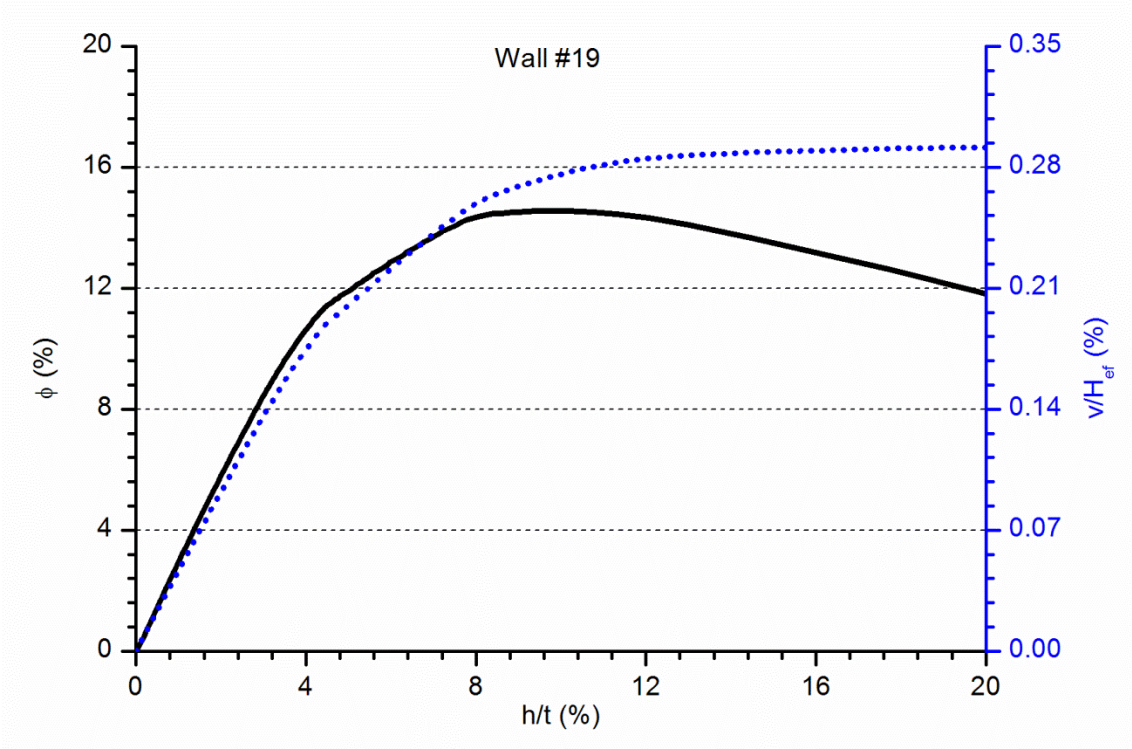


Figure A2. 37 Vertical and lateral calculated response of the wall W#19

Observing the graph in Figure A2. 37 three parts are distinguished. In the first two, the lateral displacement of the wall at mid-height is proportional to the applied load (black continuous line) or the descending displacement (blue dotted line). It is only close to the maximum load that the second order effects are noticeable. Between the first and the second parts the lateral deformation increases its growing speed and the slope of the curves decreases.

Regarding the stress distribution it is observed (Figure A2. 38) that the wall W#19 behaves symmetrically according with the numerical results. It is also worth noticing that the maximum compressive stress is lower than the corresponding strength and the maxim tensile stress overpasses the flexural strength of masonry. Thus, the failure of the wall is due to the opening of some masonry joints.

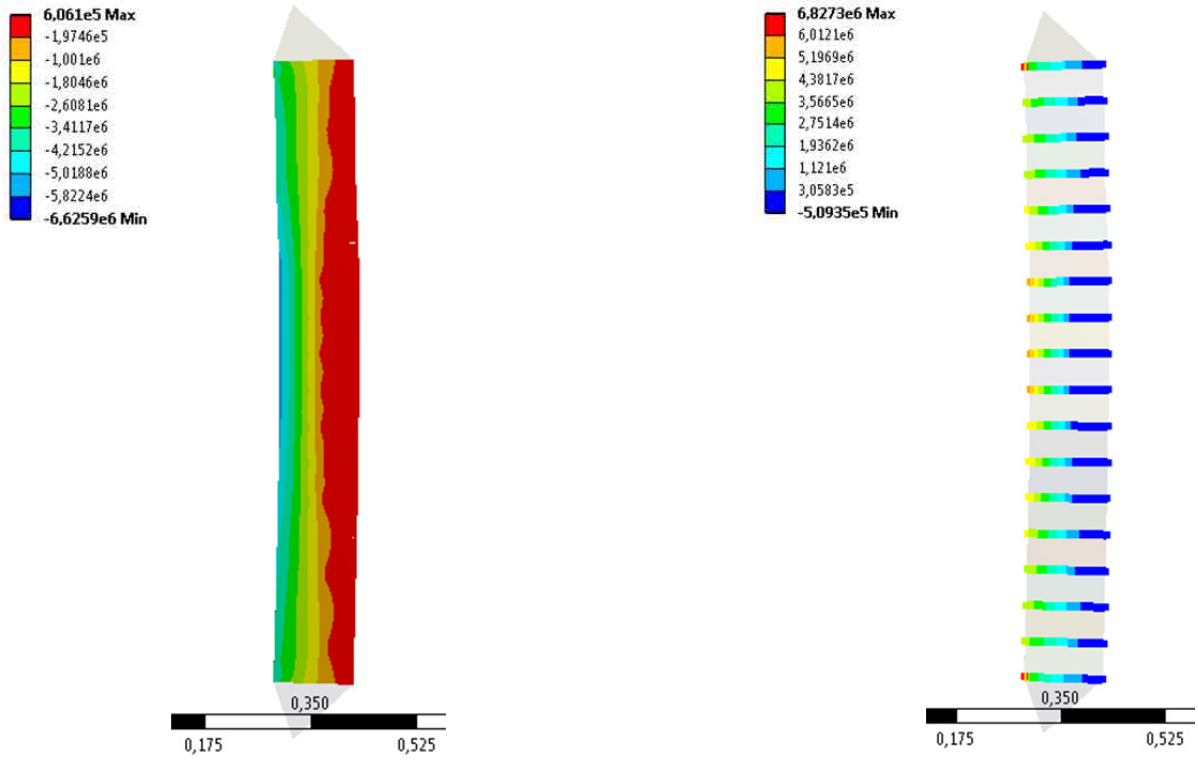


Figure A2. 38 Vertical stress distribution (left) and contact pressure (right) corresponding to the maximum calculated load for wall W#19. Values in Pa

## A2.2.20. Wall W#20

### *A2.2.20.1 Input parameters*

This is the last unreinforced tested wall and also the last of the S series. The values of the main properties for the simulations are summarised in Table A2. 4 and the Poisson's coefficient is set to 0.35 and the used mesh size was 5mm.

### *A2.2.20.2 Results*

The maximum load-bearing capacity of the wall W#20 ranged from 34.5kN to 114.4kN for the extreme possible values of the input variables. For the most representative set of values and the real geometry, the load-bearing capacity was 72.0kN.

Like in the previous cases in which the wall collapses for relatively low loads (compared with other simulated walls), the lateral displacement at mid-height is proportional to the applied load (black continuous line) and to the descending movement of the top of the wall (blue dotted line) as can be observed in Figure A2. 39. This behaviour is maintained almost to the maximum load when the lateral displacement grows with an extreme velocity.

According with the contour plots in Figure A2. 40 the wall collapsed because of the opening of a masonry joint in which the tensile stress was slightly bigger than the flexural strength of the masonry.

However, the maximum load was reached with several joint opened. Finally it has to be noticed that the compressive stresses are lower than the strength values for the masonry so the crushing failure was not probable according with the simulation.

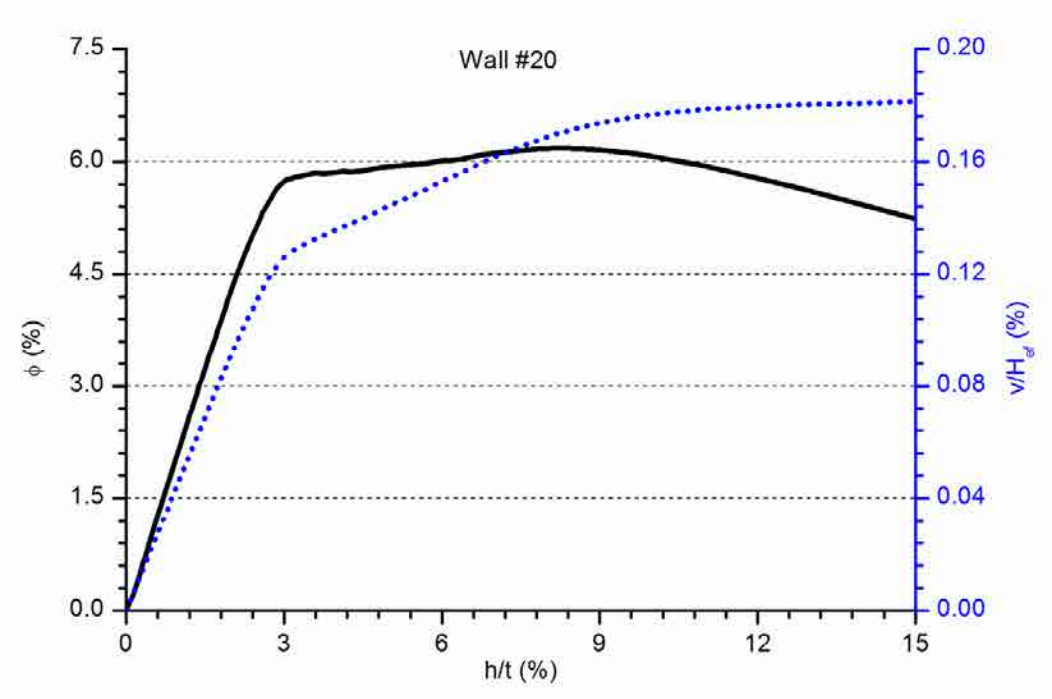


Figure A2. 39 Vertical and lateral calculated response of the wall W#20

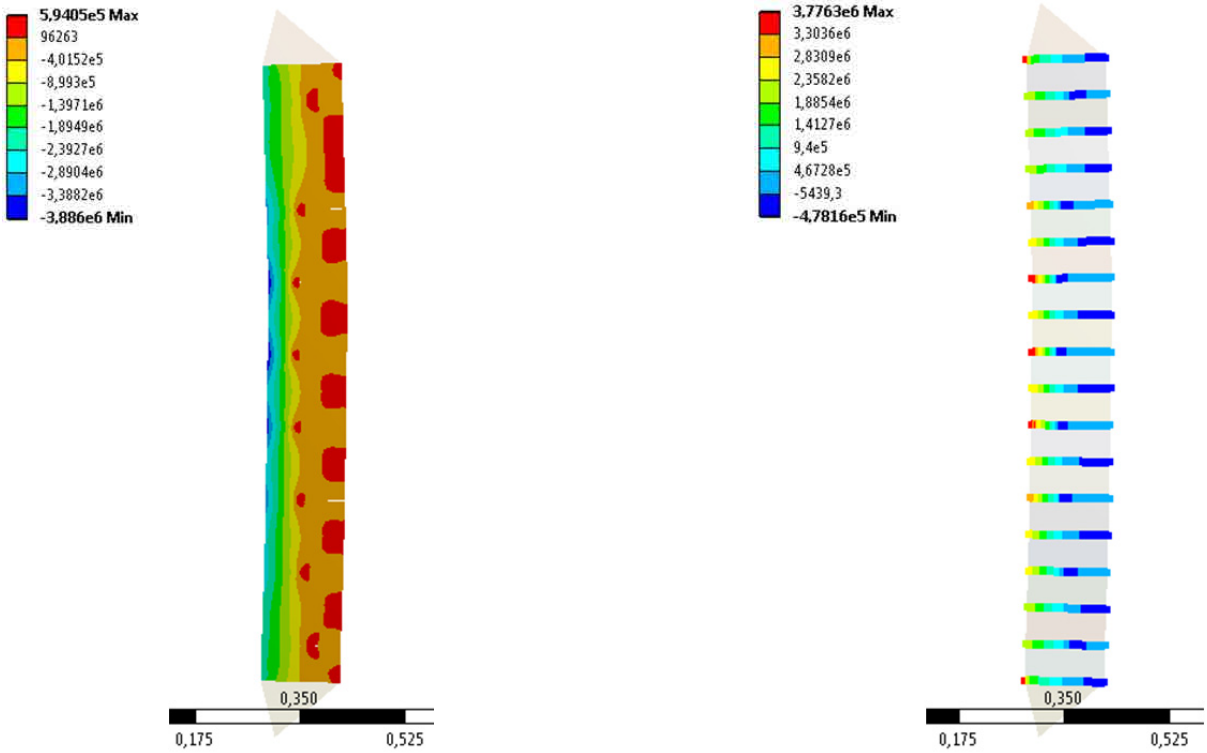


Figure A2. 40 Vertical stress distribution (left) and contact pressure (right) corresponding to the maximum calculated load for wall W#20. Values in Pa

## A2.3 FEA of TRM Strengthened Masonry Walls

In the same way than for the unreinforced walls, three models were run for each experimentally tested TRM strengthened wall. The most significant model, which results are analysed with detail, considered a deterministic set of values for the main variables of the problem. The average values of compressive and flexural strength and Young's modulus of masonry were taken into account to carry out the calculus. The experimental compressive strength of the strengthening mortar and the theoretical values of the tensile strength of the strengthening fibre grid as well as the modulus of elasticity of this grid were used to model the TRM. To complete the analysis, and have a measure of the sensitivity of the model, two extra simulations, one corresponding with the "lowest" values of the masonry properties (the combination of which leaded to the minimum load-bearing capacity) according with the experimental research, and other corresponding with the "highest" values were considered. This is a simplified way to analyse how the scattering in the masonry input data affects the calculated load-bearing capacity in the current finite element analysis. The only result of these two extra simulations analysed herein is the maximum load.

### A2.3.1. Wall W#21

#### *A2.3.1.1 Input parameters*

This is the first wall of the construction batch corresponding with all strengthened walls (W#21 to W#29). The masonry properties are considered to be identical to previous walls as average values were considered for the same construction material (see Chapter 4). The masonry characterisation values are summarised in Table A2. 4. Like in previous cases, the Poisson's coefficient was set to 0.35 for all materials and the used average mesh size was 5mm for masonry and 3mm for the TRM elements.

| ***Variable*** | ***Comment*** | ***Average values*** | ***Lowest values*** | ***Highest values*** |
|---|---|---|---|---|
| $f_{cm}$ *(MPa)* | Masonry compressive strength | 10.80 | 7.00 | 15.00 |
| $f_{xt}$ *(MPa)* | Bed joint tensile strength | 0.36 | 0.10 | 0.70 |
| $G_f^I$ *(N/m)* | Bed joint tensile fracture energy | 13 | 4 | 26 |
| $f_{st}$ *(MPa)* | Inclined plane tensile strength | 2.8 | --- | --- |
| $G_{fs}^I$ *(MPa)* | Inclined plane tensile fracture energy | 100 | --- | --- |
| $f_{ss}$ *(MPa)* | Inclined plane shear strength | 0.56 | --- | --- |
| $G_{fs}^{II}$ *(MPa)* | Inclined plane shear fracture energy | 20 | --- | --- |
| *E (MPa)* | Masonry Young's modulus | 780 | 400 | 1100 |

Table A2. 5 Input data for the masonry considered in the FEA for walls W#21 to W#29

| ***Strengthening System*** | ***Density (kg/m$^3$)*** | ***$f_{cm}$ (MPa)*** | ***E (MPa)*** | ***$f_{xt}$ (MPa)*** | ***$G_f^I$ (N/m)*** |
|---|---|---|---|---|---|
| Planitop HDM Maxi | 1850 | 42.20 | 11000 | 8.1 | 295 |

Table A2. 6 Input data for the TRM strengthening system for walls W#21 and W#22

An inclined contact was defined in the masonry area near the extremes of the wall to allow a compressive-shear mixed masonry failure which had been previously observed when testing strengthened walls (see Table A2. 5 for the values of the definition variables of this contact). The effect of considering

this possible failure is studied in Chapter 4 by comparing the results of the simulations presented later on in subsection A2.4.1 with A2.4.2, A2.4.3 with A2.4.4, A2.4.8 with A2.4.9 and A2.4.10 with A2.4.11.

Contacts between TRM and masonry substrate have been defined to be always perfectly bonded (as experimentally observed for the studied cases). In addition, fictitious joints of TRM (coincident with masonry bed joints, see Chapter 4) have been defined to allow the TRM tensile failure mode. The values of the variables used to define the TRM strengthening system are summarised in Table A2. 6. Further explanations and justification about the selected values are included in Chapter 4. This wall was strengthened with one glass fibre grid (MapeGrid G220) embedded into a 13mm layer of Portland based mortar (Planitop HDM Maxi) which is characterised by the values in Table A2. 6.

#### *A2.3.1.2 Results*

The maximum load-bearing capacity of the wall W#21 ranged from 178.0kN to 320.1kN for the extreme possible values of the masonry input variables. For the most representative set of values and the real geometry, the load-bearing capacity was 264.6kN.

Observing Figure A2. 41 it is noticed that the force-lateral displacement response (black continuous line) is more linear than for the previous unreinforced masonry walls and the observed curvature might be the result of the second order effects. The relationship between the two movements represented in Figure A2. 41 (vertical displacement of the top of the wall and lateral displacement at mid-height) is proportional so it is represented by a straight (blue dotted) line.

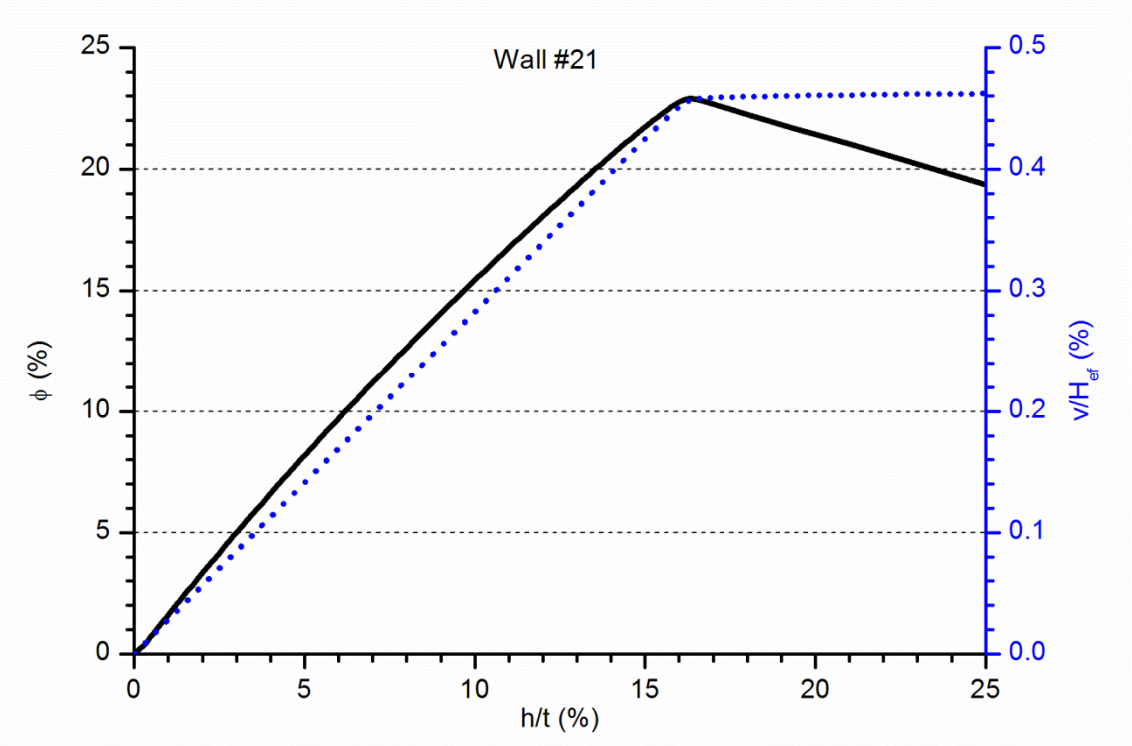


Figure A2. 41 Vertical and lateral calculated response of the wall W#21

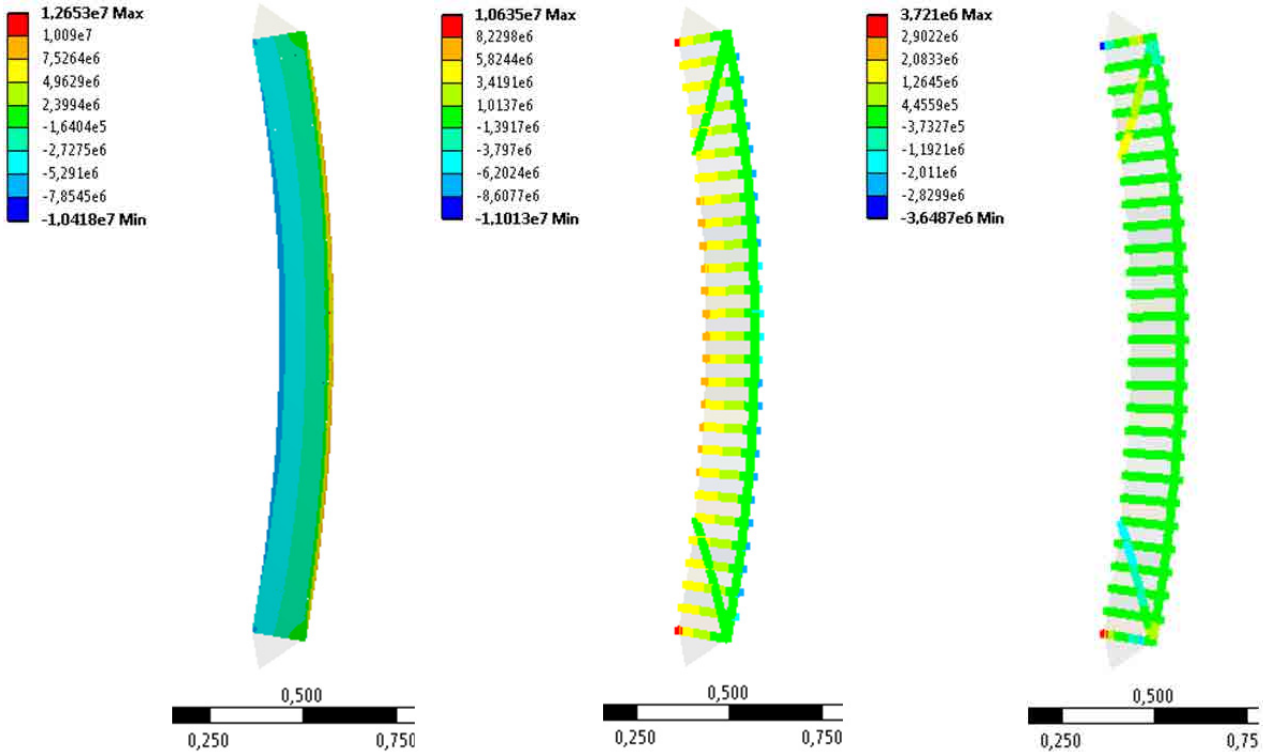


Figure A2. 42 Vertical stress distribution (left), contacts pressure (middle) and contacts shear (right) corresponding to the maximum calculated load for wall W#21. Values in Pa

Form the values plotted in the contour representations in Figure A2. 42 it is observed that the masonry compressive strength is enough to resist the vertical compressive stresses caused by the maximum load (left). In contrast, the tensile strength of the TRM (8.1MPa) is lower than the maximum punctual normal stress (11MPa, middle image) so the horizontal contacts of the TRM are opening pointing out the possibility of a tensile failure of TRM. Furthermore, the shear stresses on the inclined contacts in the masonry are higher than 1MPa in more than half of the line length whilst the maximum strength was 0.56MPa. It indicates that these contacts were sliding and the compressive-shear failure of the masonry near the ends of the wall is also possible.

## A2.3.2. Wall W#22

### *A2.3.2.1 Input parameters*

This is the second TRM strengthened wall. Materials and strengthening system properties are exactly the same than for the wall W#21, so Table A2. 5 and Table A2. 6 summarise the values of the definition variables. This wall was strengthened with one glass fibre grid (MapeGrid G220) embedded into an 8mm layer of Portland based mortar (Planitop HDM Maxi).

#### *A2.3.2.2 Results*

The maximum load-bearing capacity of the wall W#22 ranged from 144.4kN to 252.0kN for the extreme possible values of the masonry input variables. For the most representative set of values and the real geometry, the load-bearing capacity was 208.2kN.

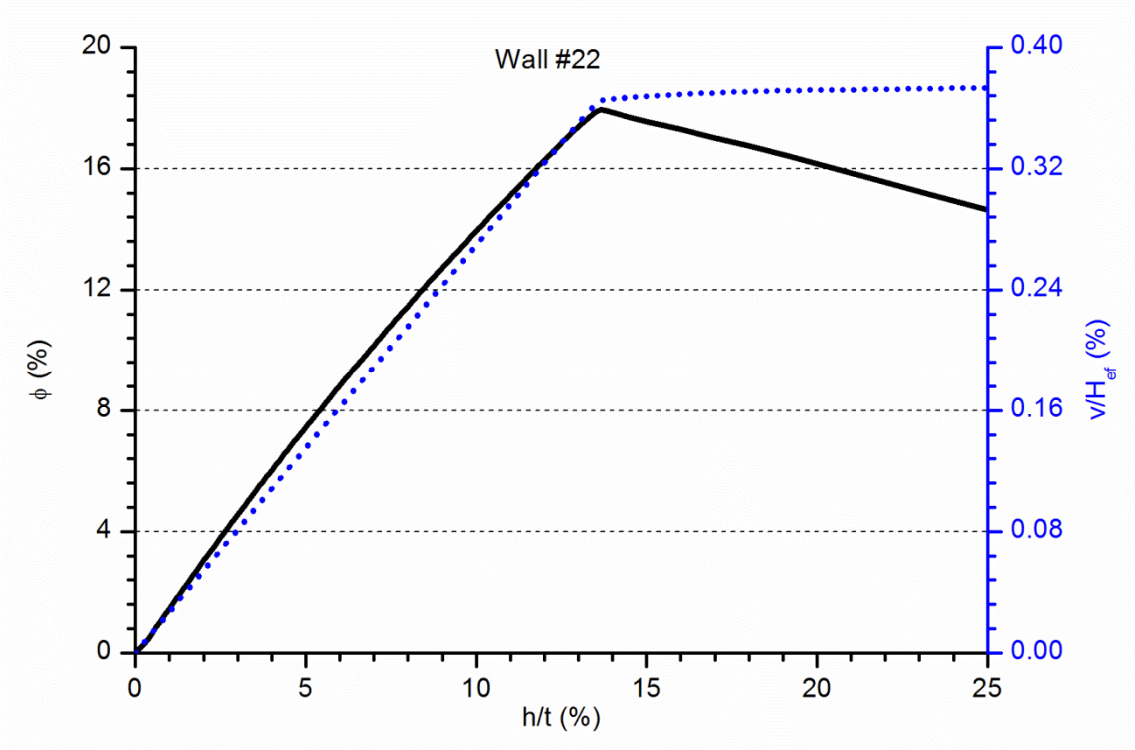


Figure A2. 43 Vertical and lateral calculated response of the wall W#22

The force-lateral displacement response (black continuous line in Figure A2. 43) is even more linear than for the previous wall. This fact agrees with the condition that the maximum resisted load is lower. As the load-bearing capacity becomes lower, the force-lateral displacement results more linear. Thus relation was the same for unreinforced walls. Regarding the relationship between the two movements represented in Figure A2. 43 (vertical displacement of the top of the wall and lateral displacement at mid-height), its proportionality is shown and represented by a straight (blue dotted) line.

Looking at the contour plots in Figure A2. 44, the first noteworthy fact to be observed is that the maximum compressive stress in the compression side of the wall (8MPa) is far lower than the masonry strength (10.8MPa) so the masonry crushing failure is discarded according with the model. In contrast, both, tensile failure of TRM and shear sliding of the masonry near the ends were possible. The maximum tensile stress on TRM is 9.7MPa (over the threshold value of 8.1MPa for this strengthening case) and the shear stress on the inclined fictitious discontinuity of the masonry is over the strength limit (0.56MPa) along more than the half of the length. In conclusion, both failure modes were possible but the tensile stress on TRM is lower than for the previous case.

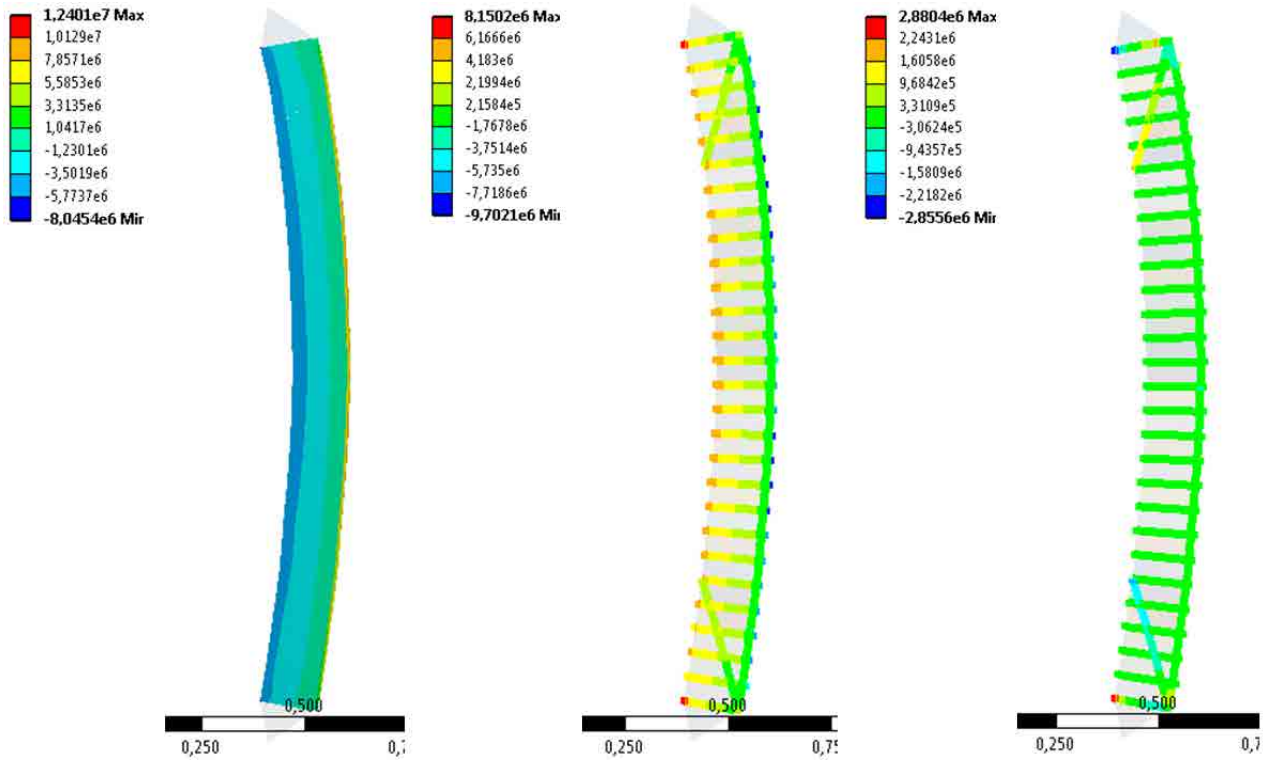


Figure A2. 44 Vertical stress distribution (left), contacts pressure (middle) and contacts shear (right) corresponding to the maximum calculated load for wall W#22. Values in Pa

## A2.3.3. Wall W#23

### *A2.3.3.1 Input parameters*

The masonry parameters are the same for all strengthened walls (W#21 to W#29) as they belong to the same construction batch. For this reason, the values of the definition variables to be used in the masonry elements and contacts are summarised in Table A2. 5. However, the strengthening system is different for this case (and the next one, W#24) than for the previous two. The TRM is composed of one glass fibre grid (MapeGrid G220) embedded into a 9.5mm layer of lime based mortar (Planitop HDM Restauro). The values of the characterisation variables required by the model are summarised in Table A2. 7.

| ***Strengthening System*** | ***Density (kg/m$^3$)*** | ***$f_{cm}$ (MPa)*** | ***E (MPa)*** | ***$f_{xt}$ (MPa)*** | ***$G_f^I$ (N/m)*** |
|---|---|---|---|---|---|
| Planitop HDM Restauro | 1900 | 14.53 | 8000 | 6.6 | 240 |

Table A2. 7 Input data for the TRM strengthening system for walls W#23 and W#24

### *A2.3.3.2 Results*

The maximum load-bearing capacity of the wall W#23 ranged from 146.8kN to 263.6kN for the extreme possible values of the masonry input variables. For the most representative set of values and the real geometry, the load-bearing capacity was 215.4kN.

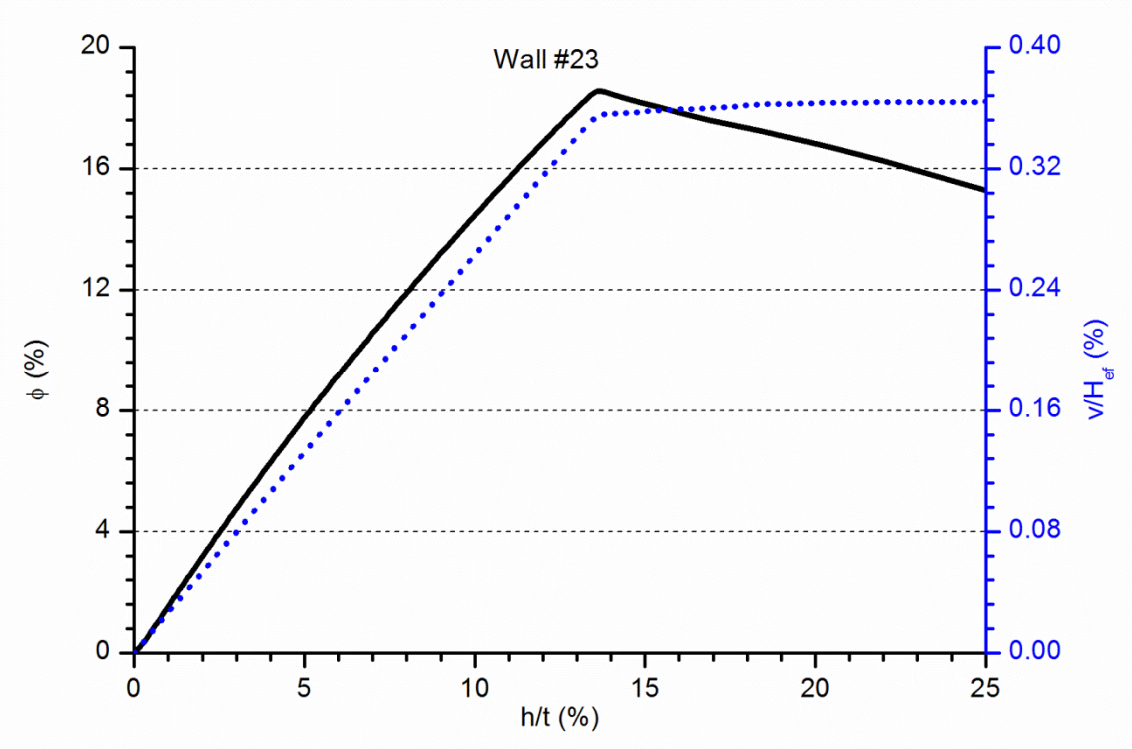


Figure A2. 45 Vertical and lateral calculated response of the wall W#23

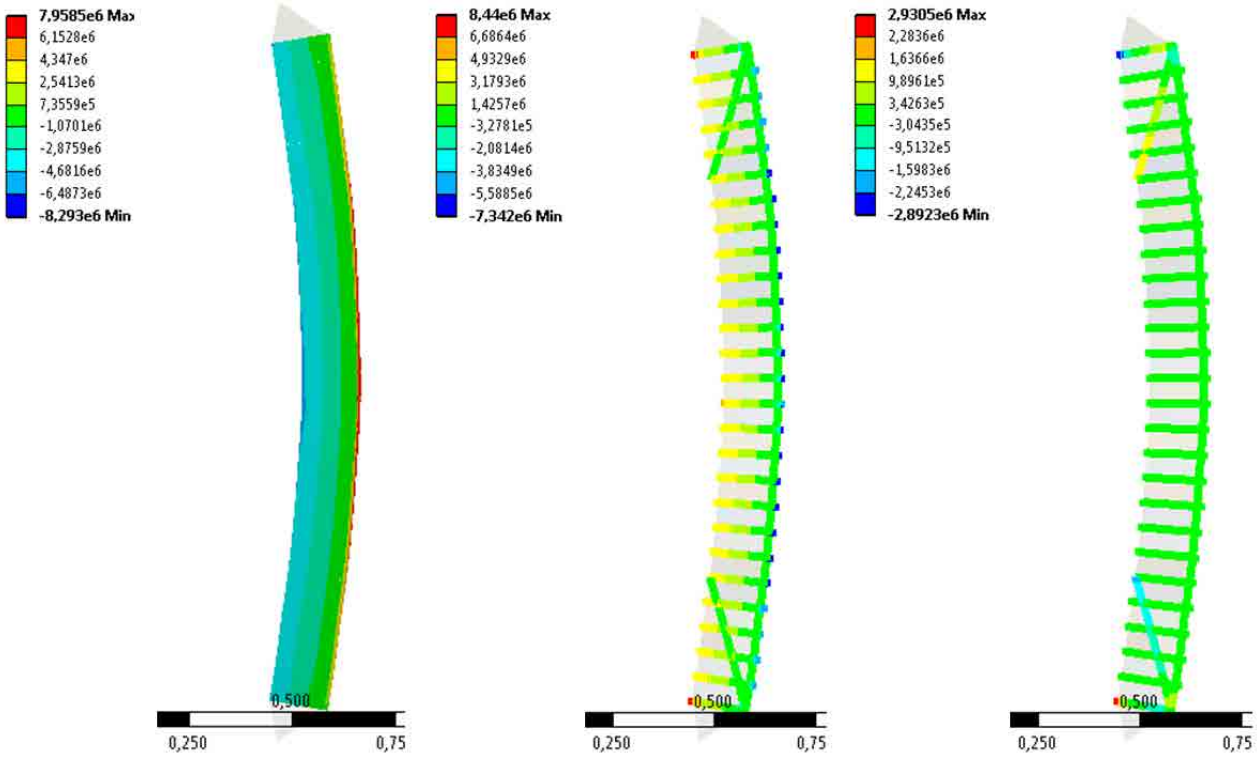


Figure A2. 46 Vertical stress distribution (left), contacts pressure (middle) and contacts shear (right) corresponding to the maximum calculated load for wall W#23. Values in Pa

The force-lateral displacement response (black continuous line in Figure A2. 45) and the vertical displacement of the top of the wall versus the lateral displacement at mid-height (blue dotted line in Figure A2. 45) are almost equal to the previous simulation (wall W#22) although the strengthening system is different. A linear relationship is observed between the two displacements and only a slight non-linearity is noticeable in the force-lateral displacement curve due to the second order bending.

Regarding the possible failure mode according with the simulation results, it has to be noticed (see Figure A2. 46) that the masonry crushing at the compression side of the wall is not possible because the maximum stress (8.3MPa) is lower than the corresponding strength (10.8MPa). In contrast, the tensile strength of the TRM (6.6MPa) is overpassed in most of the horizontal TRM joints so this failure mode is likely to be observed. However, this is not the only possible failure mode for this structure and loading case. The shear stress calculated in the fictitious inclined joints in the masonry near the ends of the wall is over the maximum strength (0.56MPa) along more than half the length of these contacts (see the image of the right in Figure A2. 46).

### A2.3.4. Wall W#24

#### *A2.3.4.1 Input parameters*

The input parameters are exactly the same than for wall W#23 because the masonry and strengthening are the same. The only difference is the TRM thickness: 9mm in this case.

#### *A2.3.4.2 Results*

The maximum load-bearing capacity of the wall W#24 ranged from 162.7kN to 298.7kN for the extreme possible values of the masonry input variables. For the most representative set of values and the real geometry, the load-bearing capacity was 247.1kN.

Qualitatively, the calculated response is analogue to the previous ones, with an almost perfectly linear relationship between the descending displacement of the top of the wall and the lateral displacement at mid-height (blue dotted line in Figure A2. 47). The force-lateral displacement curve (black continuous line in Figure A2. 47) is slightly affected by the second order effects due to the eccentricity of the load application point.

Observing the contour plots presented in Figure A2. 48 it is noticed that the crushing failure of the compressed side of the wall is not likely although the calculated maximum stress (10MPa) is closer to the strength (10.8MPa) than for previous cases. On the contrary, the shear stresses in the contact representing the inclined failure plane at both ends of the wall is higher than the strength (0.56MPa) in more than 2/3 of the length making this failure mode likely. However, the possibility of TRM tensile failure has to be

considered too because the tensile strength (6.6MPa) is lower than the maximum calculated stress (7.9MPa) in several joints near the mid-height (see the image of the right in Figure A2. 48).

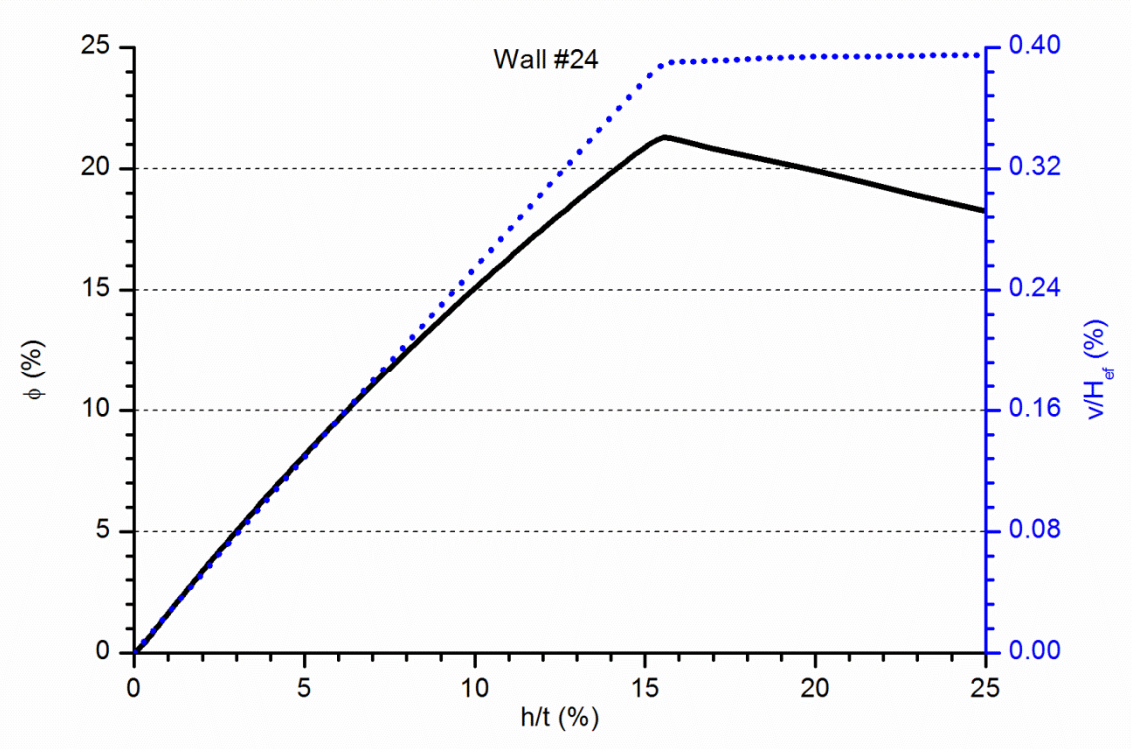


Figure A2. 47 Vertical and lateral calculated response of the wall W#24

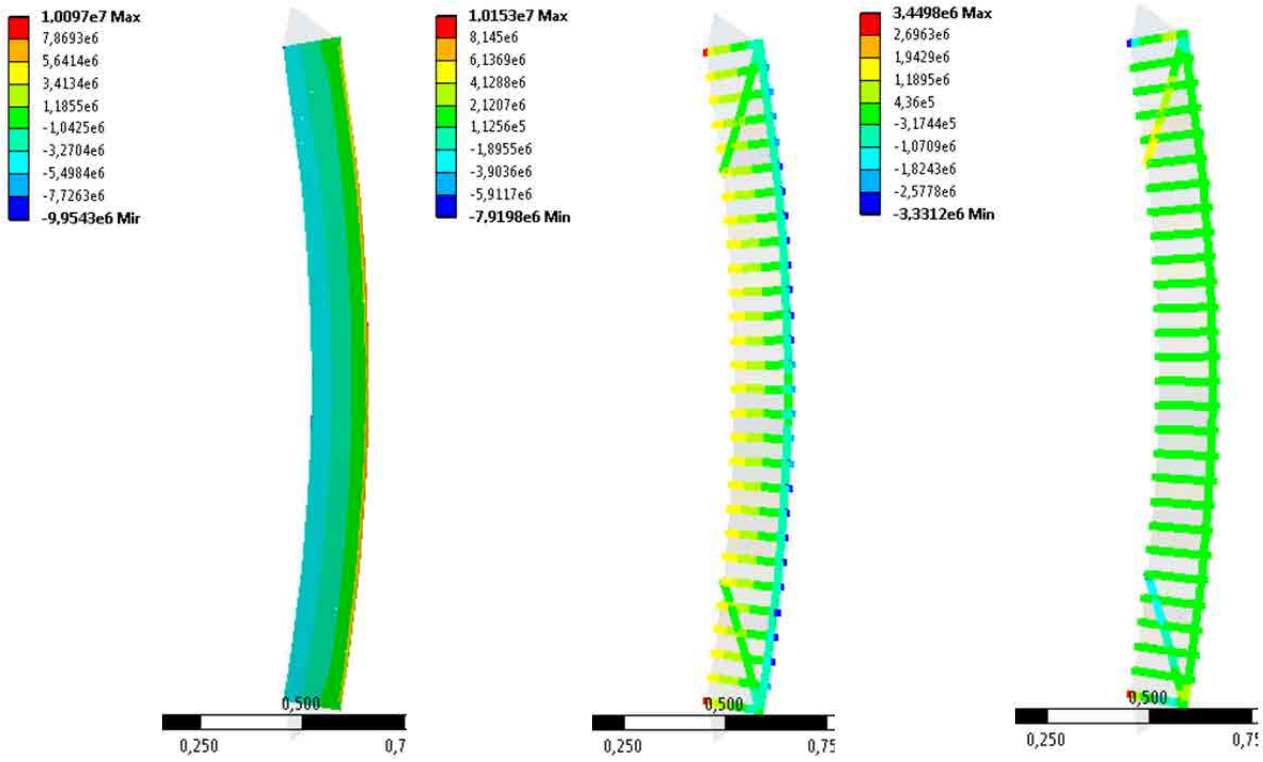


Figure A2. 48 Vertical stress distribution (left), contacts pressure (middle) and contacts shear (right) corresponding to the maximum calculated load for wall W#24. Values in Pa

## A2.3.5. Wall W#25

### *A2.3.5.1 Input parameters*

The values of the definition parameters of the masonry are the same than for the previous strengthened walls. These are summarised in Table A2. 5. The strengthening system is composed of two glass fibre grids (MapeGrid G220) embedded into a 7.5mm layer of lime based mortar (Planitop HDM Restauro). This TRM combination was used only for wall W#25 and the characterisation values are summarised in Table A2. 8.

| ***Strengthening System*** | ***Density (kg/m$^3$)*** | ***$f_{cm}$ (MPa)*** | ***E (MPa)*** | ***$f_{xt}$ (MPa)*** | ***$G_f^I$ (N/m)*** |
|---|---|---|---|---|---|
| Planitop HDM Restauro | 1900 | 14.53 | 8000 | 12.0 | 440 |

Table A2. 8 Input data for the TRM strengthening system for wall W#25

### *A2.3.5.2 Results*

The maximum load-bearing capacity of the wall W#25 ranged from 178.1kN to 319.0kN for the extreme possible values of the masonry input variables. For the most representative set of values and the real geometry, the load-bearing capacity was 263.0kN.

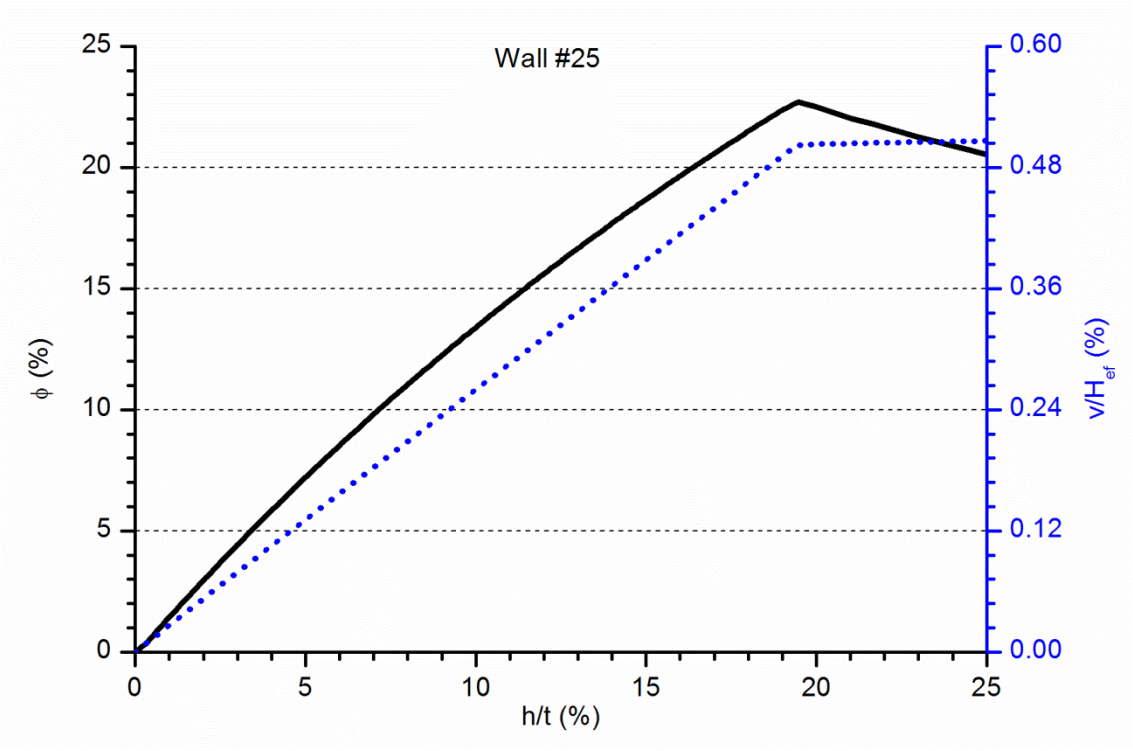


Figure A2. 49 Vertical and lateral calculated response of the wall W#25

The qualitatively response of wall W#25 is similar to the response of previously presented walls as can be observed in Figure A2. 49. The force versus lateral displacement at mid-height curve (black

continuous line) shows a little nonlinearity because of the second order effects. The relationship between the vertical displacement at the top of the wall and the lateral displacement at mid-height is linear up to failure like in all previous cases. Nevertheless, it has to be remarked that the lateral displacement for the maximum applied load is greater in this case.

Observing the Figure A2. 50 corresponding with three resulting contour plots (vertical stress, contact pressure and contact shear stress), it has to be highlighted that the crushing failure of the masonry at the compression side is almost possible because the maximum compressive stress is 10.4MPa is near to the strength (10.8MPa). However, the tensile failure of TRM and the compression-shear failure of the masonry near the wall's extremes are more likely. The maximum punctual tensile stress on TRM is 15.4kN (for strength of 12MPa) and the shear stress is over the corresponding strength (0.56kN) in more than half the length of the inclined contacts.

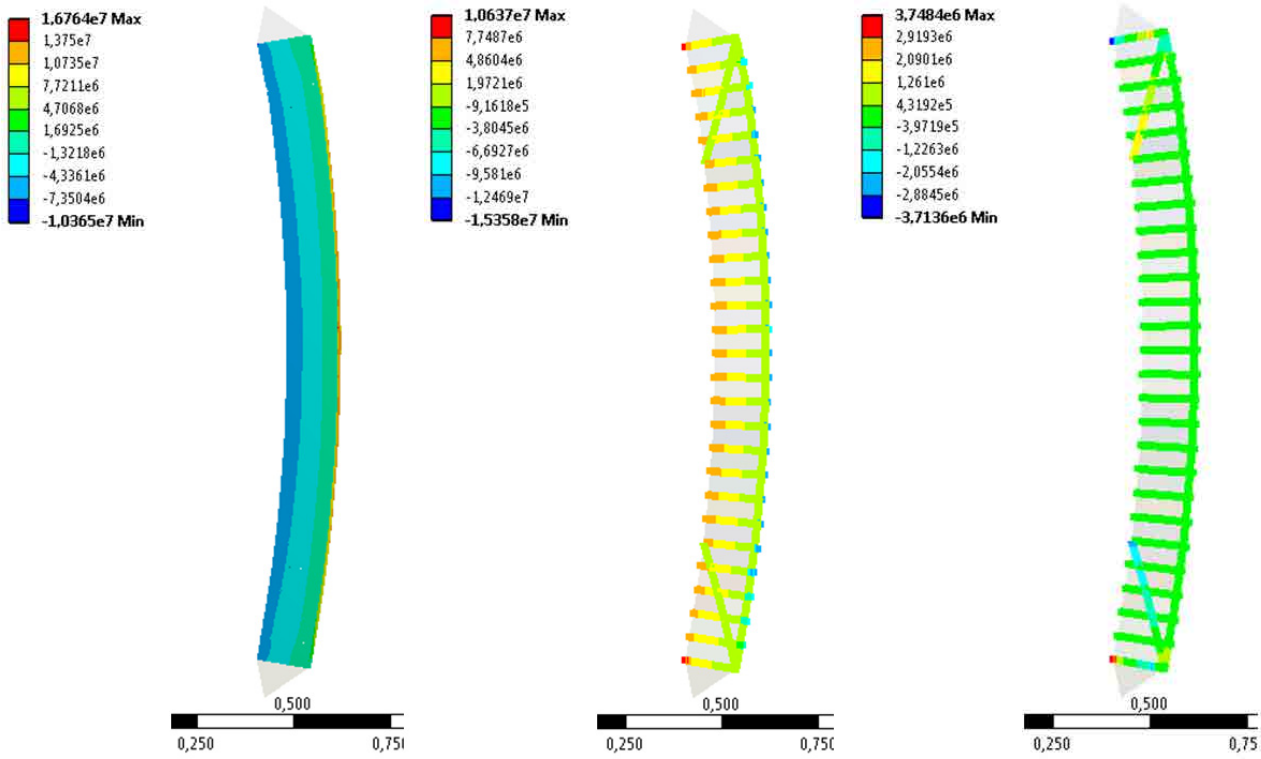


Figure A2. 50 Vertical stress distribution (left), contacts pressure (middle) and contacts shear (right) corresponding to the maximum calculated load for wall W#25. Values in Pa

## A2.3.6. Wall W#26

### *A2.3.6.1 Input parameters*

The values of the definition parameters of the masonry are the same than for the previous strengthened walls. These are summarised in Table A2. 5. Like in the previous case, the only change in the variables

definition is the TRM strengthening system which is composed of two glass fibre grids (MapeGrid G220) embedded into an 8mm layer of Portland cement based mortar (Planitop HDM Maxi). This TRM combination was used only for wall W#26 and the characterisation values are summarised in Table A2. 9.

| ***Strengthening System*** | ***Density (kg/m$^3$)*** | ***$f_{cm}$ (MPa)*** | ***E (MPa)*** | ***$f_{xt}$ (MPa)*** | ***$G_f^I$ (N/m)*** |
|---|---|---|---|---|---|
| Planitop HDM Maxi | 1850 | 42.20 | 11000 | 11.3 | 412 |

Table A2. 9 Input data for the TRM strengthening system for wall W#26

### *A2.3.6.2 Results*

The maximum load-bearing capacity of the wall W#26 ranged from 189.9kN to 342.5kN for the extreme possible values of the masonry input variables. For the most representative set of values and the real geometry, the load-bearing capacity was 282.4kN.

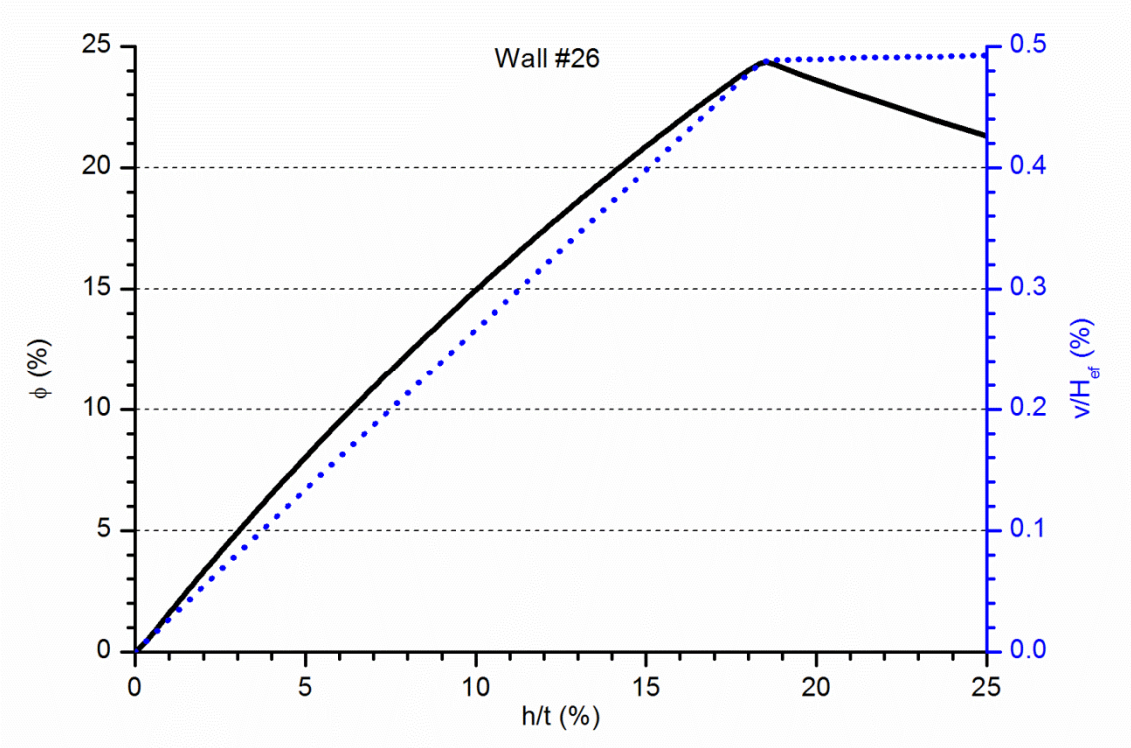


Figure A2. 51 Vertical and lateral calculated response of the wall W#26

Observing the graphs in Figure A2. 51, the lateral displacement increase associated with using two glass fibre grids is observable but less evident than for the previous wall. However, the general response is consistent and it is analogue to all strengthened cases with a linear relationship between the vertical descending displacement of the top of the wall and the lateral displacement at mid-height. This linearity is kept up to the failure of the wall (see the blue dotted line in Figure A2. 51). The force versus lateral displacement at mid-height curve (black continuous line) is nonlinear but always increasing. The second order effects are evident.

In Figure A2. 52 it can be observed that the compressive crushing of the masonry is, for the first time, a possible failure mode as the maximum punctual vertical stress (11.2MPa) is slightly higher than the corresponding strength (10.8MPa). However, the stress values which are far higher than the strength properties are the ones corresponding with the tensile stress in the TRM (reaching a value of 16.3kN in comparison with the 11.3kN strength value) and the shear stress on the fictitious inclined plane defined to make it possible a compression-shear combined failure near the boundary restraints (stresses overpass the strength of 0.56kN along more than a half of the contact length).

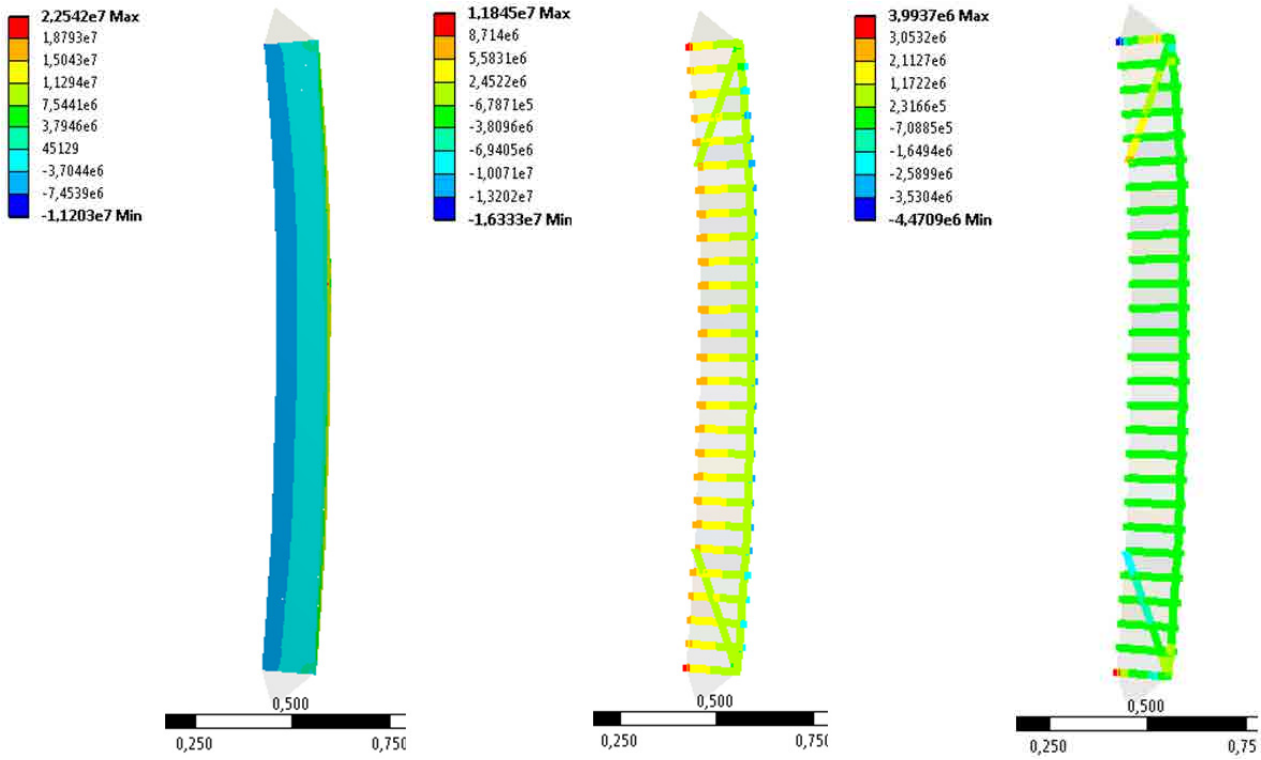


Figure A2. 52 Vertical stress distribution (left), contacts pressure (middle) and contacts shear (right) corresponding to the maximum calculated load for wall W#26. Values in Pa

## A2.3.7. Wall W#27

### *A2.3.7.1 Input parameters*

This is the first wall strengthened with a carbon fibre grid. The values to define the masonry are the same than for the previous strengthened walls (summarised in Table A2. 5). The TRM strengthening system is composed of one carbon fibre grid (Ruredil XMesh C10) embedded into an 8mm layer of pozzolana based mortar (Ruredil XMesh M25). This TRM combination was used only for wall W#27. The characterisation values are summarised in Table A2. 10.

| ***Strengthening System*** | ***Density (kg/m$^3$)*** | ***$f_{cm}$ (MPa)*** | ***E (MPa)*** | ***$f_{xt}$ (MPa)*** | ***$G_f^I$ (N/m)*** |
|---|---|---|---|---|---|
| XMesh M25 | 1900 | 34.47 | 15000 | 20.0 | 733 |

Table A2. 10 Input data for the TRM strengthening system for wall W#27

#### *A2.3.7.2 Results*

The maximum load-bearing capacity of this wall ranged from 245.4kN to 414.7kN for the extreme possible values of the masonry input variables. For the most representative set of values and the real geometry, the load-bearing capacity was 333.1kN.

The calculated response of the wall is characterised by a linear relationship between the vertical displacement of the top of the wall and the lateral displacement at mid-height (see the blue dotted line in Figure A2. 53) and a nonlinear force versus lateral displacement relationship (black continuous line in Figure A2. 53). In this case the second order bending effects are more evident than in previous cases with agrees with the major lateral displacement.

Observing the contour plots in Figure A2. 54 it is noticed that, for the first time, the TRM tensile failure is not likely as the maximum calculated stress is 18.6MPa which is lower than the corresponding strength (20MPa). For wall W#27, the crushing of the masonry at the compression side (were the vertical maximum stress is 13.2MPa, which is higher than the corresponding strength, 10.8MPa) and the sliding along inclined cracks placed at the extremes of the wall (where the shear stress is higher than the corresponding strength 0.56MPa for all the length of the contact) are the two most probable failure modes. The tangential stress distribution for the maximum load (image at the right of Figure A2. 54) is different from the other studied cases, with a punctual stress concentrator near the tensile side of the wall.

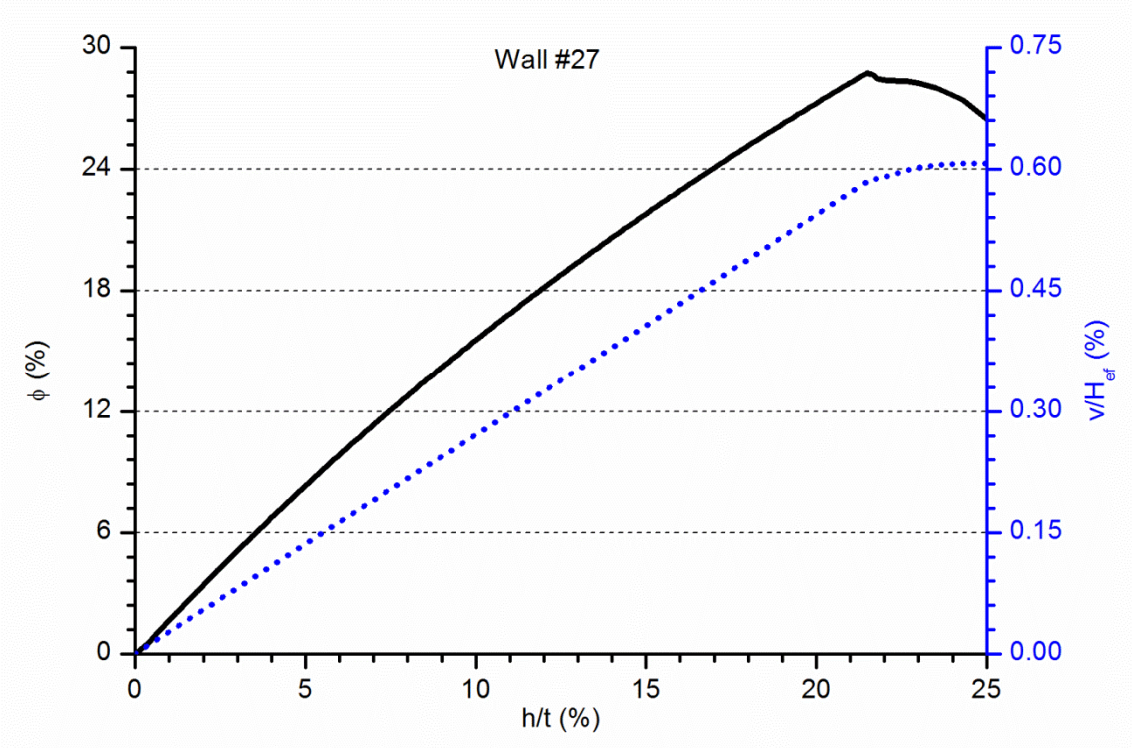


Figure A2. 53 Vertical and lateral calculated response of the wall W#27

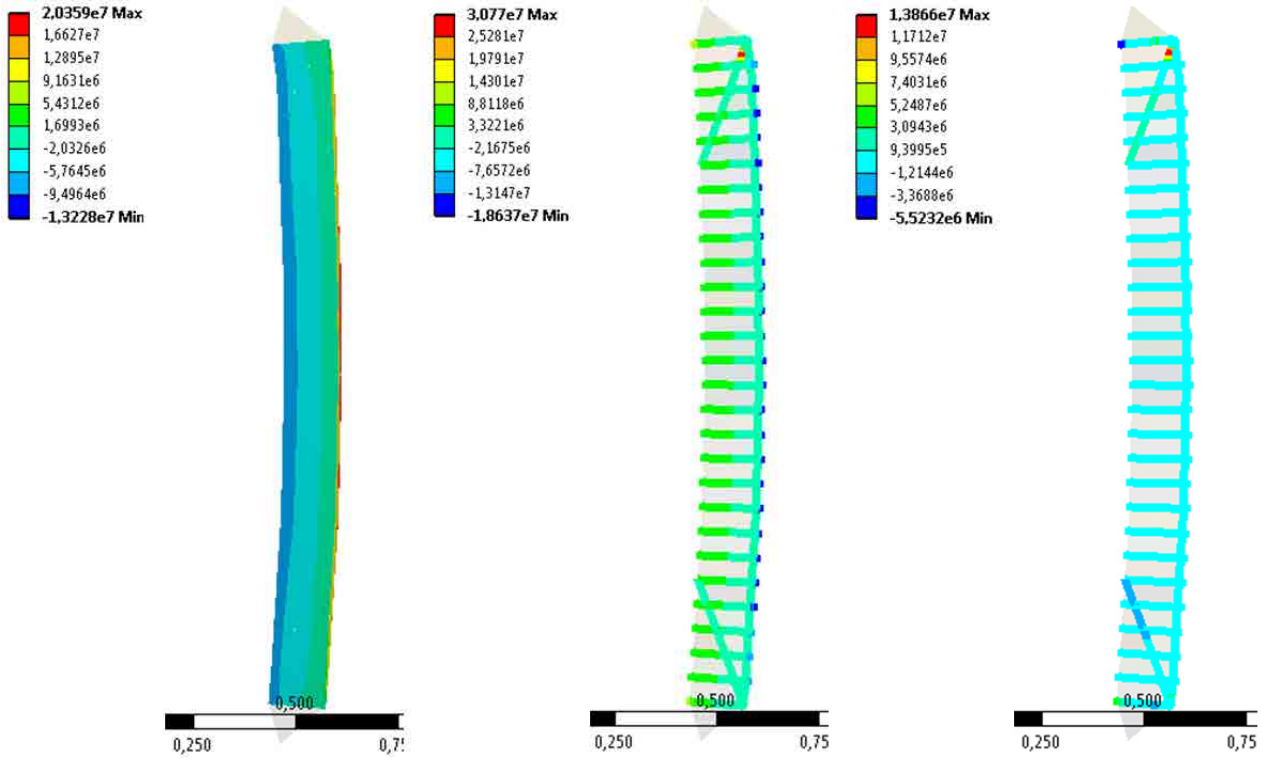


Figure A2. 54 Vertical stress distribution (left), contacts pressure (middle) and contacts shear (right) corresponding to the maximum calculated load for wall W#27. Values in Pa

## A2.3.8. Wall W#28

### *A2.3.8.1 Input parameters*

This is the second wall strengthened with a carbon fibre grid. The only difference with wall W#27 is the TRM thickness (9mm). The values to define the masonry are summarised in Table A2. 5. Table A2. 11 presents the definition values of the specific TRM used in wall W#28.

| ***Strengthening System*** | ***Density (kg/m$^3$)*** | ***$f_{cm}$ (MPa)*** | ***E (MPa)*** | ***$f_{xt}$ (MPa)*** | ***$G_f^I$ (N/m)*** |
|---|---|---|---|---|---|
| XMesh M25 | 1900 | 34.47 | 15000 | 17.8 | 652 |

Table A2. 11 Input data for the TRM strengthening system for wall W#28

### *A2.3.8.2 Results*

The maximum load-bearing capacity of wall W#28 ranged from 252.4kN to 473.3kN for the extreme possible values of the masonry input variables. For the most representative set of values and the real geometry, the load-bearing capacity was 381.1kN.

A discontinuity in the resulting curve representing the force versus the lateral displacement at mid-height (black continuous line in Figure A2. 55) is observed. It might correspond to a partial failure of the structure. After this discontinuity the load is increased again up to its maximum. The nonlinearity of this plot is significant which agrees with the greater load-bearing capacity in comparison with previous

simulations. Apart from the discontinuity, the relationship between the vertical displacement of the top of the wall and the lateral movement at mid-height is linear up to failure (blue dotted line in Figure A2. 55).

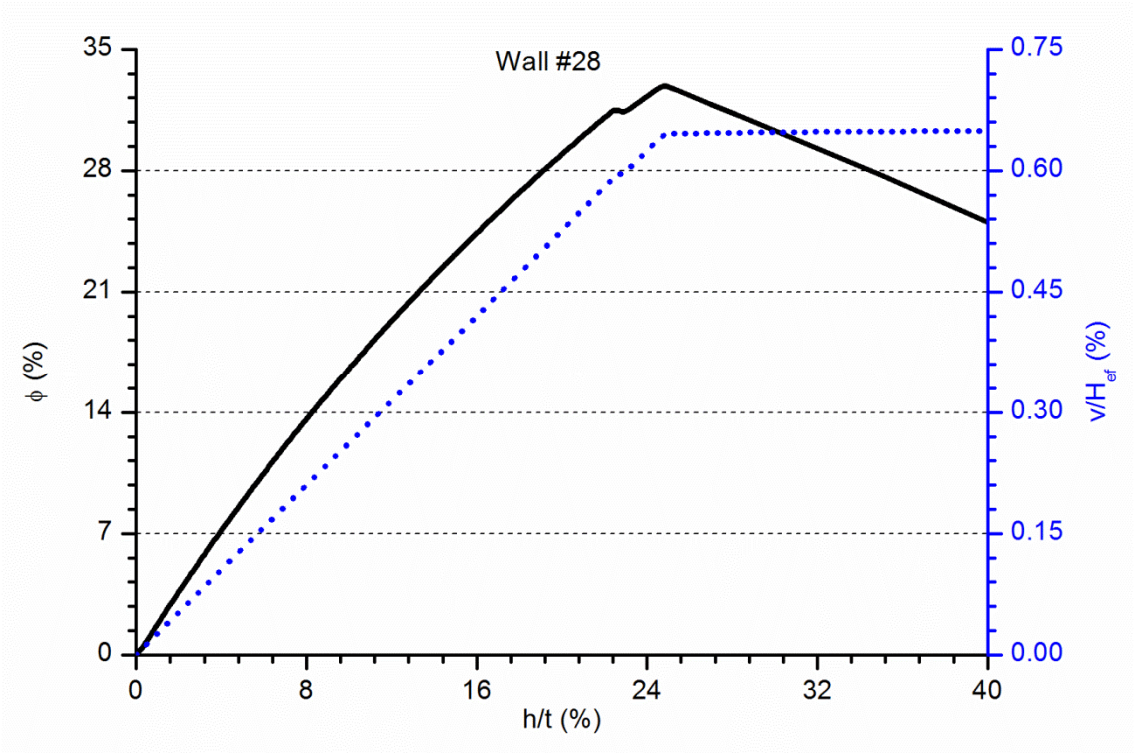


Figure A2. 55 Vertical and lateral calculated response of the wall W#28

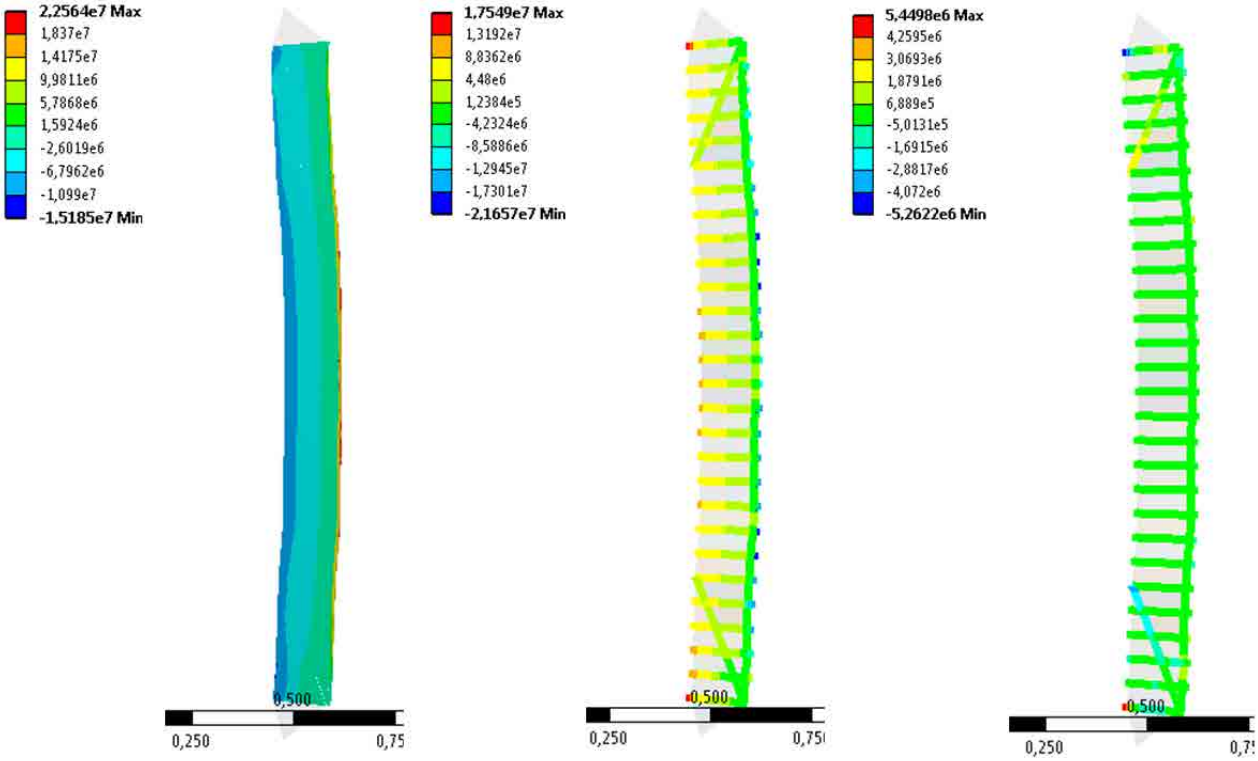


Figure A2. 56 Vertical stress distribution (left), contacts pressure (middle) and contacts shear (right) corresponding to the maximum calculated load for wall W#28. Values in Pa

For the first time, the three considered failure modes are simultaneously possible (see the contour plots in Figure A2. 56). For the maximum applied load, the masonry of the compression side of the wall at mid-height shows vertical stresses (maximum 15.2MPa) which are punctually higher than the corresponding strength (10.8MPa). At the same time most of the TRM joints near mid-height have opened because the maximum stresses (up to 21.7MPa when the strength is only 17.8MPa) are placed above and under the mid-height area. Finally, the shear stresses in the inclined possible cracks near the wall endings higher than the corresponding strength (0.56MPa) along all contacts length.

## A2.3.9. Wall W#29

### *A2.3.9.1 Input parameters*

This is last strengthened wall. The TRM, including one carbon fibre grid, is 11mm thick. The values to define the masonry are summarised in Table A2. 5 like in several previous analysis. Table A2. 12 presents the definition values of the specific TRM used in wall W#29.

| ***Strengthening System*** | ***Density (kg/m$^3$)*** | ***$f_{cm}$ (MPa)*** | ***E (MPa)*** | ***$f_{xt}$ (MPa)*** | ***$G_f^I$ (N/m)*** |
|---|---|---|---|---|---|
| XMesh M25 | 1900 | 34.47 | 15000 | 14.5 | 533 |

Table A2. 12 Input data for the TRM strengthening system for wall W#29

### *A2.3.9.2 Results*

The maximum load-bearing capacity of wall W#29 ranged from 227.9kN to 349.2kN for the extreme possible values of the masonry input variables. For the most representative set of values and the real geometry, the load-bearing capacity was 344.1kN.

In Figure A2. 57 a similar response to wall W#27 is observed, with a nonlinear force versus lateral displacement at mid-height relationship (black continuous line) due to the second order bending effects. The curve relating the lateral and vertical displacement (blue dotted line) is a straight line showing a linear relationship which lasts up to the maximum load.

Regarding the resulting possible failure modes, it has to be highlighted that the compressive strength is only overpassed in punctual points at the compression side of the wall so the crushing failure is possible but not the most likely according with the results (see the image on the left of Figure A2. 58). The TRM tensile failure is more likely because several contacts in the mid-height area have already partially opened for the maximum load (the maximum stress is 22.6MPa and the corresponding calculated strength is limited to 14.5MPa, see Figure A2. 58). Finally, the tangential stress along the inclined contact placed on the masonry area near the extremes of the wall, is higher than the corresponding strength (0.56kN) in almost all the contact length (see the image at the right side of Figure A2. 58).

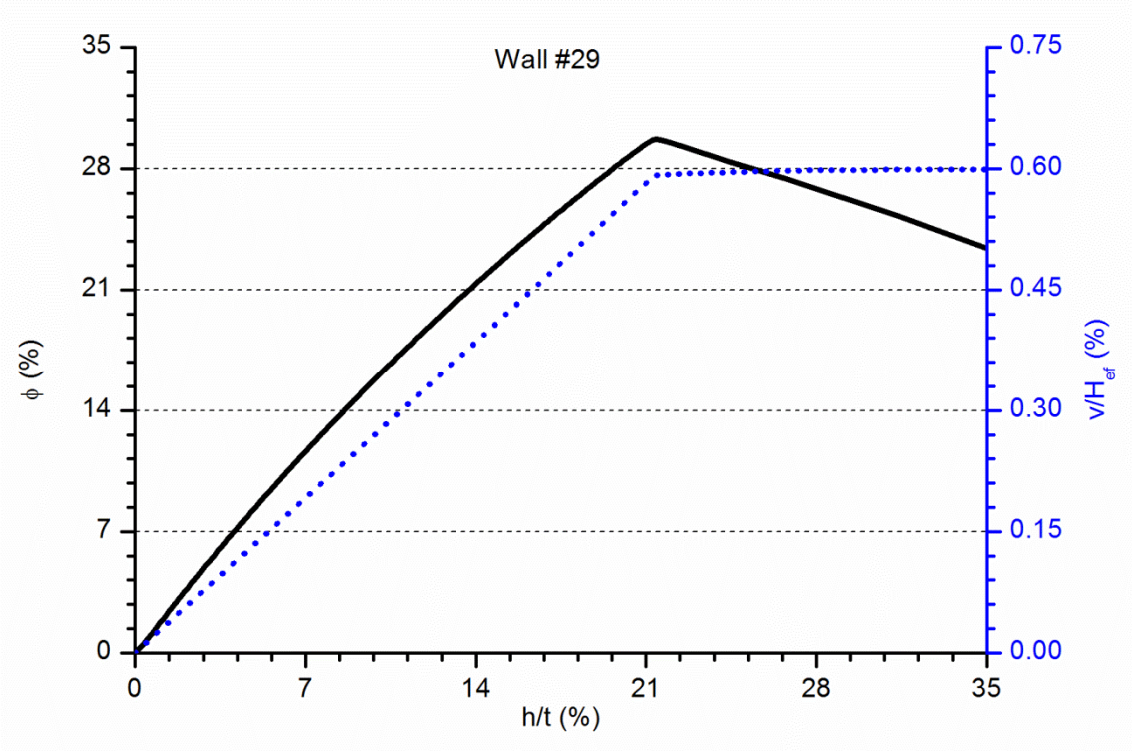


Figure A2. 57 Vertical and lateral calculated response of the wall W#29

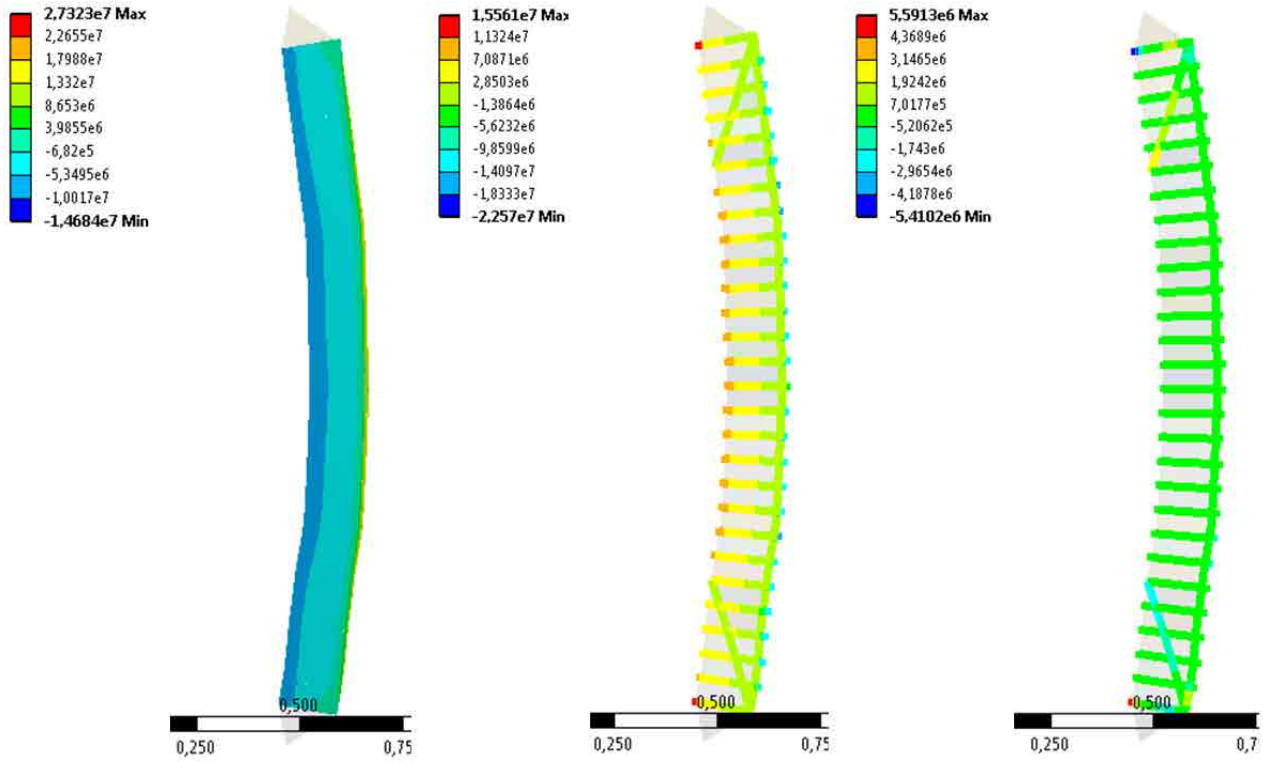


Figure A2. 58 Vertical stress distribution (left), contacts pressure (middle) and contacts shear (right) corresponding to the maximum calculated load for wall W#29. Values in Pa

For comparison purposes the same simulation of W#29 has been carried out with a littler mesh with the following result:

Using a mesh size of 5mm for the masonry and 3mm for the TRM, the maximum load was 344.1kN, whereas using a mesh size of 3.5mm for the masonry and 2mm for the TRM the load bearing capacity was 344.0kN.

## A2.4 FEA on Theoretical Walls

There are two main aims for the analyses herein summarised. First of all, it is intended to analyse the effect of considering a possible inclined plain of failure in the masonry near the extremes of the wall. Two equivalent simulations were carried out with theoretical walls with and without strengthening and for two heights (see walls H0, H0S, HS11, HS11S for the highest slenderness and walls M0, M0S, MS11 and MS11S for the shortest walls). The second aim was to analyse the theoretical effect of the strengthening by comparing different strengthening configurations (using 1, 2 or 4 fibre grids and applying TRM in one or two sides). The geometric configuration of the walls maintained the same eccentricity at both extremes for all cases and there were perfectly vertical aligned. Thus, $e_b = e_t = e_m = 20mm$ and $d = 0mm$.

### A2.4.1. Wall H0

#### *A2.4.1.1 Input parameters*

This is the first theoretical wall analysed. For the wall H0 and all the following cases the same masonry properties have been considered (see Table A2. 13). The average mesh size used to define the elements representing the masonry was 20mm.

| ***Variable*** | ***Comment*** | ***Value*** |
|---|---|---|
| $f_{cm}$ *(MPa)* | Masonry compressive strength | 10.80 |
| $f_{xt}$ *(MPa)* | Bed joint tensile strength | 0.36 |
| $G_f^I$ *(N/m)* | Bed joint tensile fracture energy | 13 |
| *E (MPa)* | Masonry Young's modulus | 780 |
| $\upsilon$ | Masonry Poisson's coefficient | 0.35 |

Table A2. 13. Mechanical properties used to characterise the masonry of the FEA on Theoretical Walls which do not consider the inclined failure plain.

#### *A2.4.1.2 Results*

The load-bearing capacity of the wall H0 is 85.9kN. Regarding the response of this generic wall, it is observed (see Figure A2. 59) that the relationship between the applied force and the lateral displacement at mid-height (black continuous line) is clearly non-linear because of the second order effects which are

amplified up to failure. In the same way, the curve relating the vertical descending movement at the top of the wall with the lateral movement at mid-height (blue dotted line) is non-linear. It is observed that the second order effects are related with the existence of an initial eccentricity. The geometric imperfections (not considered in these theoretical cases) only modify the non-linear response.

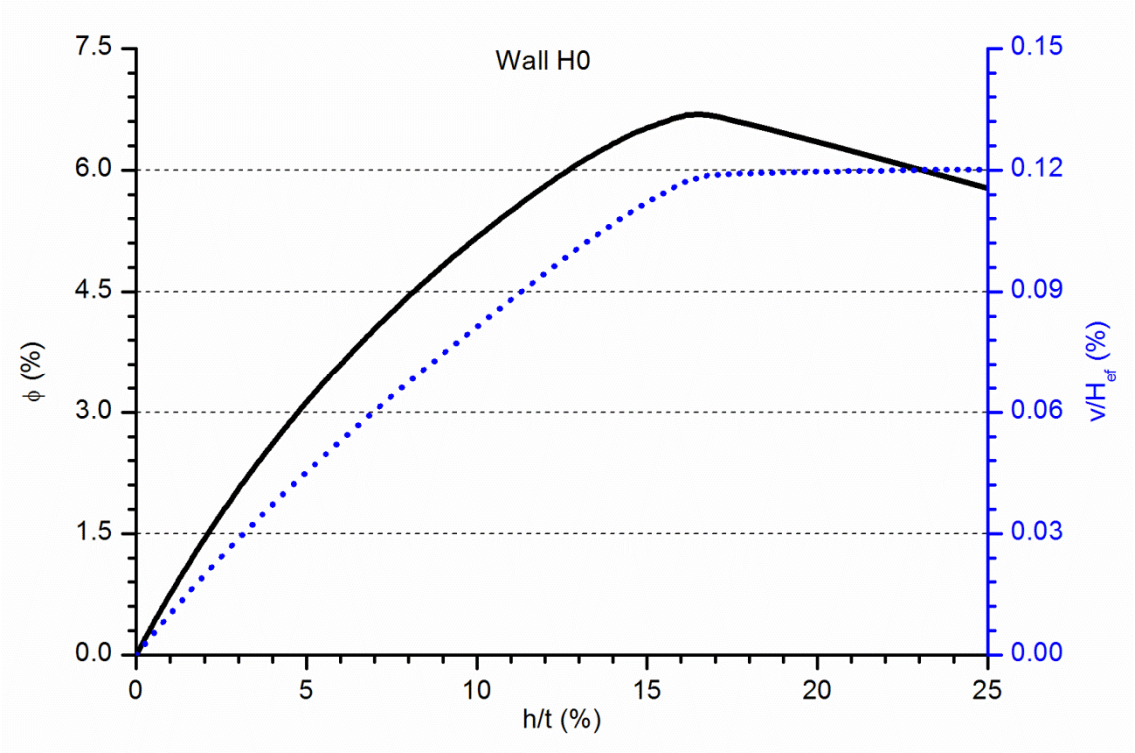


Figure A2. 59 Vertical and lateral calculated response of the wall H0

Observing the contour plot graphs in Figure A2. 60, it has to be remarked that the most probable failure cause is the opening of a horizontal joint. The maximum vertical compressive stress (2.1MPa) is far lower than the corresponding strength (10.8MPa) whilst the maximum tensile stress value (0.36MPa) is reached in some joints near the mid-height position. Looking at the stress distribution, the symmetric response has to be highlighted. It is the main difference between this case and the real comparable cases analysed before.

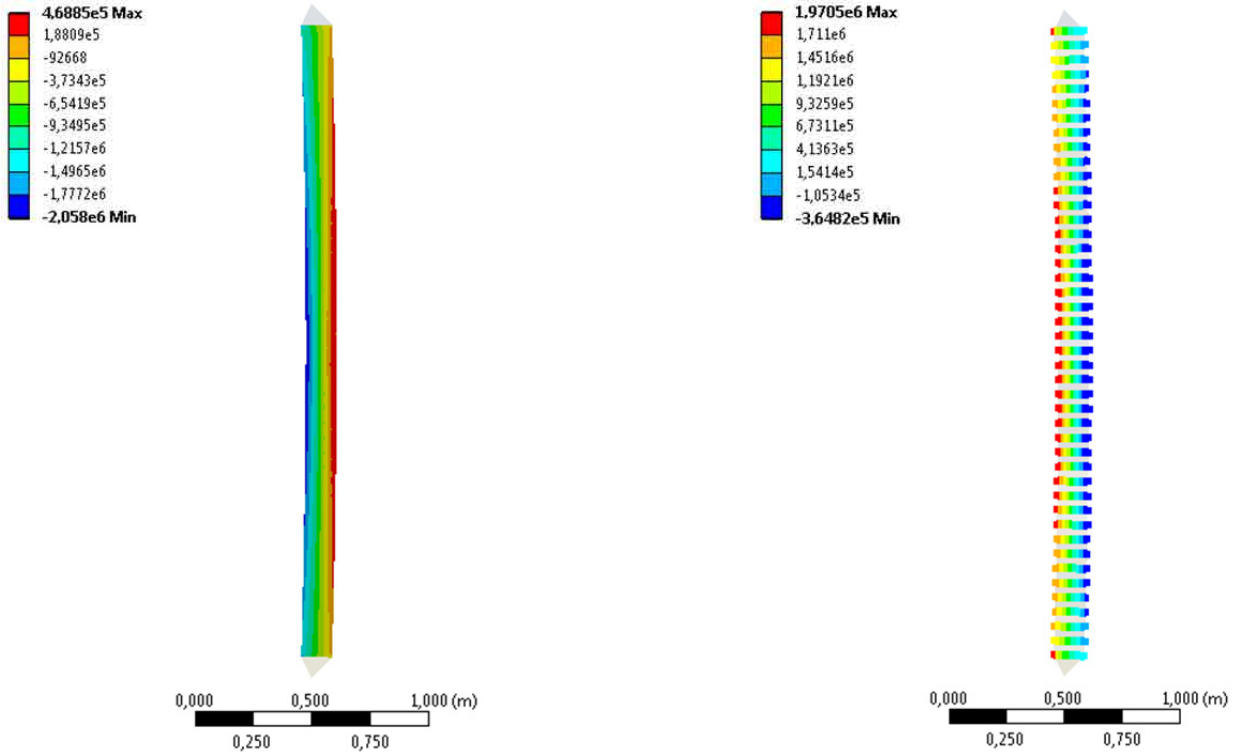


Figure A2. 60 Vertical stress distribution (left) and contact pressure (right) corresponding to the maximum calculated load for wall H0. Values in Pa

## A2.4.2. Wall H0S

### *A2.4.2.1 Input parameters*

Wall H0S is equivalent to the previous one (H0) but considering the possibility of a compression-shear mixed failure with the opening of an inclined crack near one of the extremes of the wall. The definition of this contact uses the variables included in Table A2. 14. Like in the previous model, the average mesh size was 20mm.

| ***Variable*** | ***Comment*** | ***Value*** |
|---|---|---|
| $f_{cm}$ *(MPa)* | Masonry compressive strength | 10.80 |
| $f_{xt}$ *(MPa)* | Bed joint tensile strength | 0.36 |
| $G_f^I$ *(N/m)* | Bed joint tensile fracture energy | 13 |
| $f_{st}$ *(MPa)* | Inclined plane tensile strength | 2.8 |
| $G_{fs}^I$ *(MPa)* | Inclined plane tensile fracture energy | 100 |
| $f_{ss}$ *(MPa)* | Inclined plane shear strength | 0.56 |
| $G_{fs}^{II}$ *(MPa)* | Inclined plane shear fracture energy | 20 |
| *E (MPa)* | Masonry Young's modulus | 780 |
| $\upsilon$ | Masonry Poisson's coefficient | 0.35 |

Table A2. 14. Mechanical properties used to characterise the masonry of the FEA on Theoretical Walls which considered the inclined failure plain.

### *A2.4.2.2 Results*

The load-bearing capacity of the wall H0S is 85.9kN, exactly the same than the case H0.

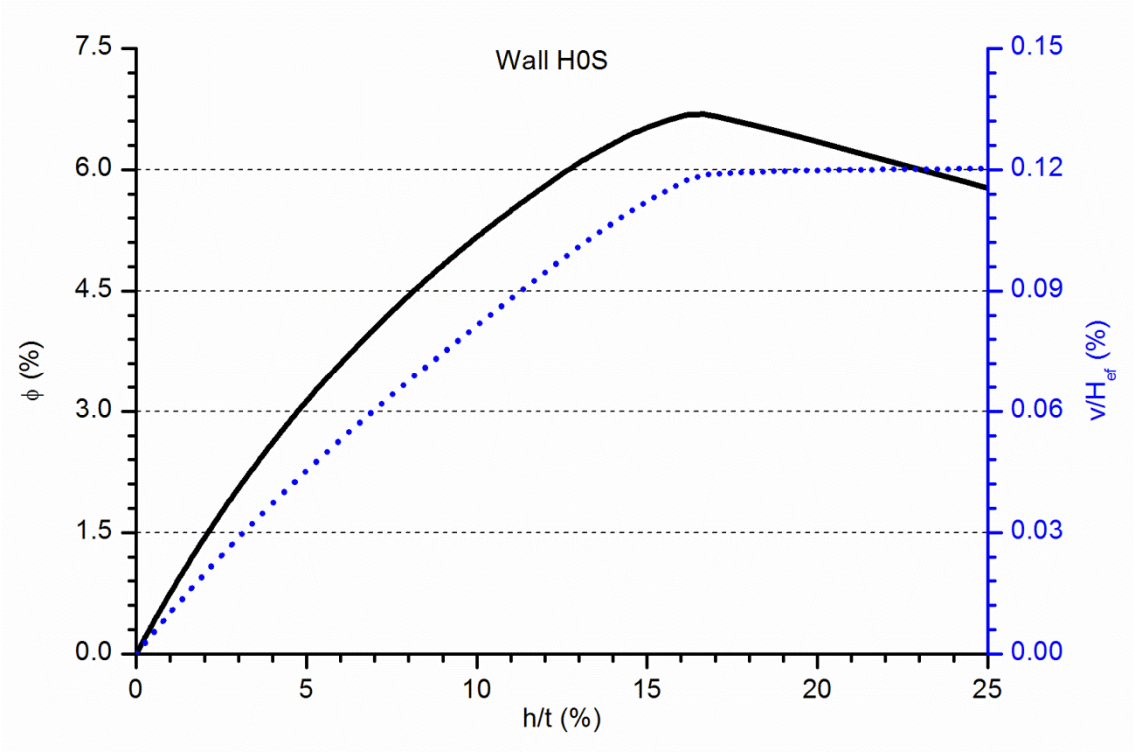


Figure A2. 61 Vertical and lateral calculated response of the wall H0S

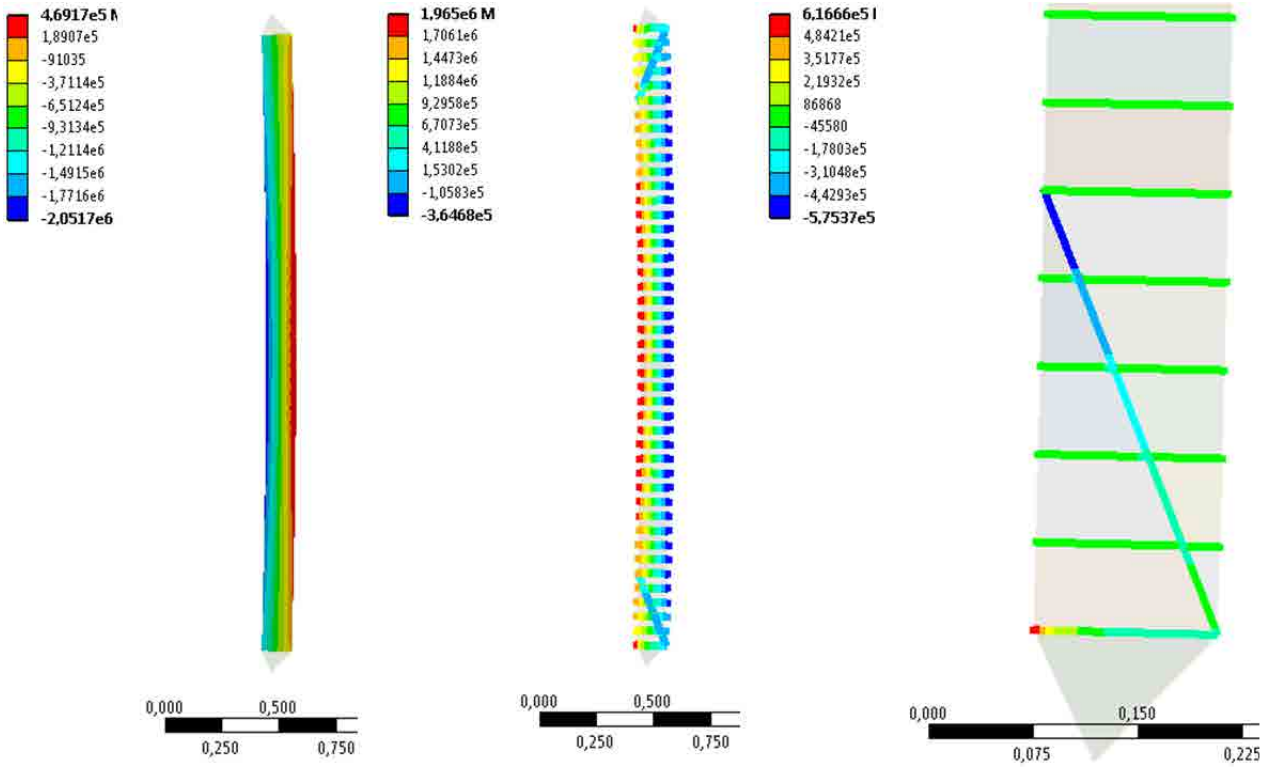


Figure A2. 62 Vertical stress distribution (left), contacts pressure (middle) and contacts shear at the bottom extreme of the wall (right) corresponding to the maximum calculated load for wall H0S. Values in Pa

The curves presented in Figure A2. 61 are equal to the curves in case H0. The non-linear response characterise both presented relationships. The force versus lateral displacement plot (black continuous line) is non-linear with a decreasing slope. The second order effects also rise with the vertical descending movement of the top of the wall (blue dotted line).

Observing the images in Figure A2. 62 it has to be noticed that the most likely failure mode according with the results would be the opening of a horizontal masonry joint. The maximum tensile strength of the joints (0.36MPa) is reached in some joints near de mid-height of the wall (middle image of Figure A2. 62). In addition, the shear stress on the inclined contact is below the corresponding strength (0.56MPa) in almost all the length of these plains (right image of Figure A2. 62). Finally, the maximum compressive vertical stress (2.1MPa) is far lower than the comparison strength (10.8MPa).

### A2.4.3. Wall HS11

#### *A2.4.3.1 Input parameters*

This wall is comparable with wall H0 but considering a TRM strengthening system applied on the tensile side of the wall. The masonry representation does not consider the compressive-shear failure along inclined cracks near wall endings, so the masonry properties to be used are gathered in Table A2. 13. The TRM is composed of one glass fibre grid embedded into a 10mm layer of strengthening Portland-based mortar. The main characteristics of this strengthening are summarised in Table A2. 15. The average mesh size was 20mm in masonry and 3mm in TRM.

| ***TRM thickness (mm)*** | ***Density (kg/m$^3$)*** | ***$f_{cm}$ (MPa)*** | ***E (MPa)*** | ***$f_{xt}$ (MPa)*** | ***$G_f^I$ (N/m)*** |
|---|---|---|---|---|---|
| 10 | 1850 | 42.20 | 11000 | 8.1 | 295 |

Table A2. 15. Input data for the TRM strengthening system for wall HS11

#### *A2.4.3.2 Results*

The load-bearing capacity of the wall HS11 is 199.8kN, which is a remarkable increase in comparison with the non-strengthened comparable cases, and observing the plots in Figure A2. 63 it is noticed that the strengthening has changed the wall's response. For wall HS11 the relationship between the vertical displacement of the top of the wall and the lateral displacement at mid-height (blue dotted line) is linear up to failure in contrast with previous non-strengthened theoretical cases. However, the force versus lateral displacement at mid-height is still non-linear (black continuous line) because of the second order effects like in the previous cases.

In Figure A2. 64 can be observed that the maximum vertical compressive stress (4.6MPa) is far from the masonry strength (10.8MPa) whilst the maximum tensile strength (8.1MPa) of the TRM is punctually

reached in several joints near the mid-height which would support the hypothesis of a tensile failure of the TRM. Finally, the symmetry of the results has to be remarked in contrast with experimental cases.

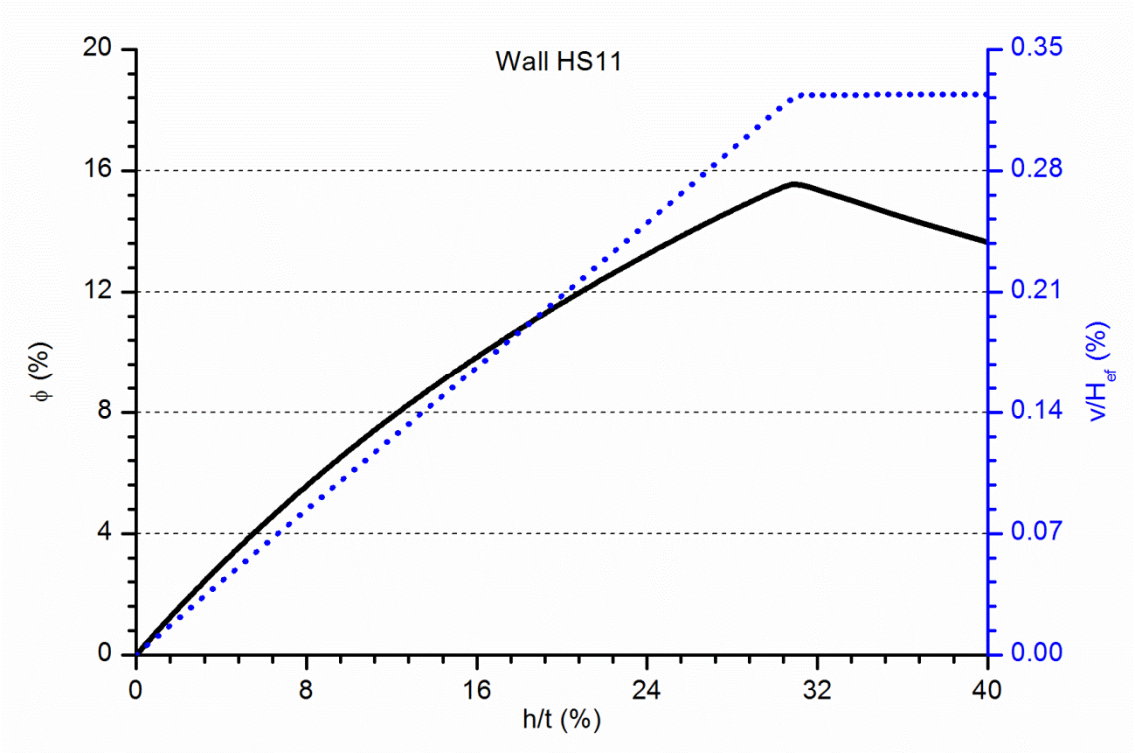


Figure A2. 63 Vertical and lateral calculated response of the wall HS11

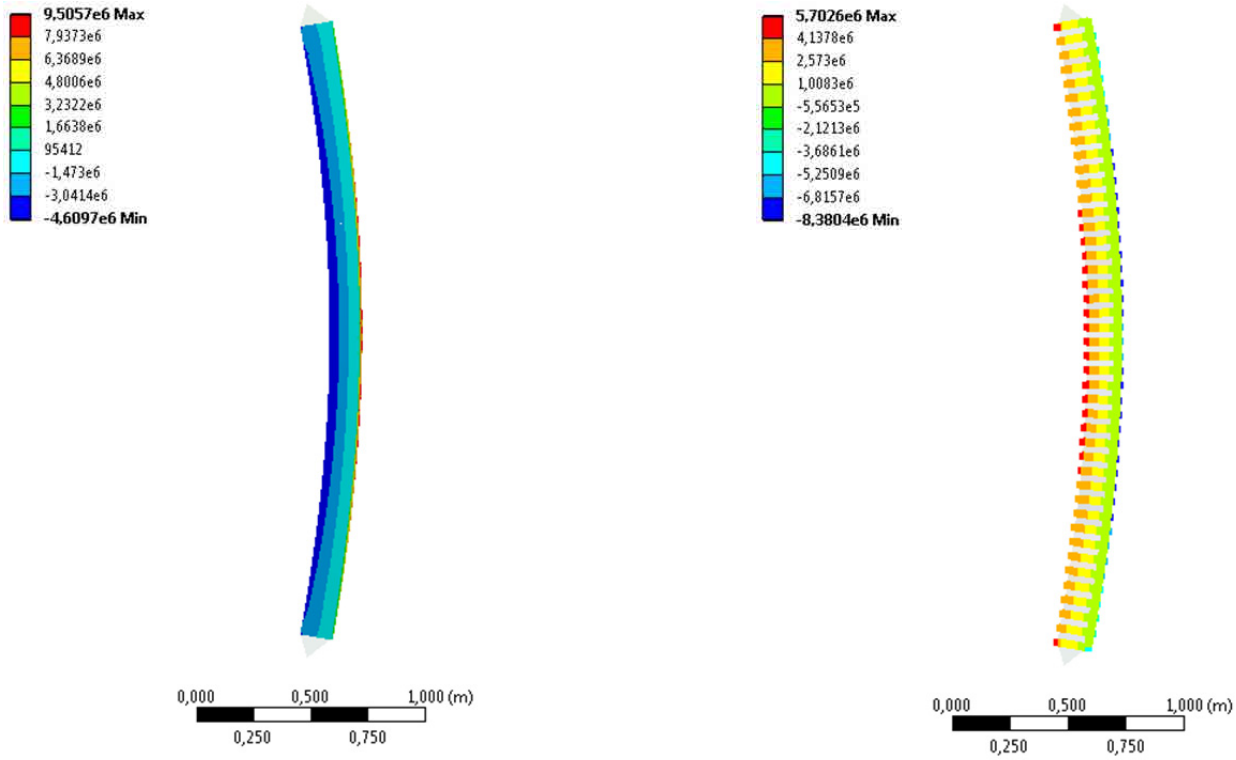


Figure A2. 64 Vertical stress distribution (left) and contact pressure (right) corresponding to the maximum calculated load for wall HS11. Values in Pa

## A2.4.4. Wall HS11S

### *A2.4.4.1 Input parameters*

This wall is comparable with the previous one (HS11) but adding the possibility of a compressive-shear failure in the masonry near the endings of the wall. Thus, the masonry characteristics to be used are the ones presented in Table A2. 14. The values of the defining parameters for the strengthening system are the same than for wall HS11, so they are summarised in Table A2. 15. Finally, the mesh average size is 20mm for masonry and 3mm for TRM.

### *A2.4.4.2 Results*

The maximum load differs so little from the previous considered case (in which the possibility of compression-shear failure along an inclined crack was not taken into account) that it could be said that there had been no change. For wall HS11S the load-bearing capacity was 200.0kN.

The relationship between the applied force and the lateral displacement at mid-height (black continuous line in Figure A2. 65) is non-linear due to the second order bending effects whereas a proportional relationship might be observed between the vertical descending movement of the top of the wall and its lateral displacement at mid-height (blue dotted line). This proportional behaviour lasts up to the failure of the wall.

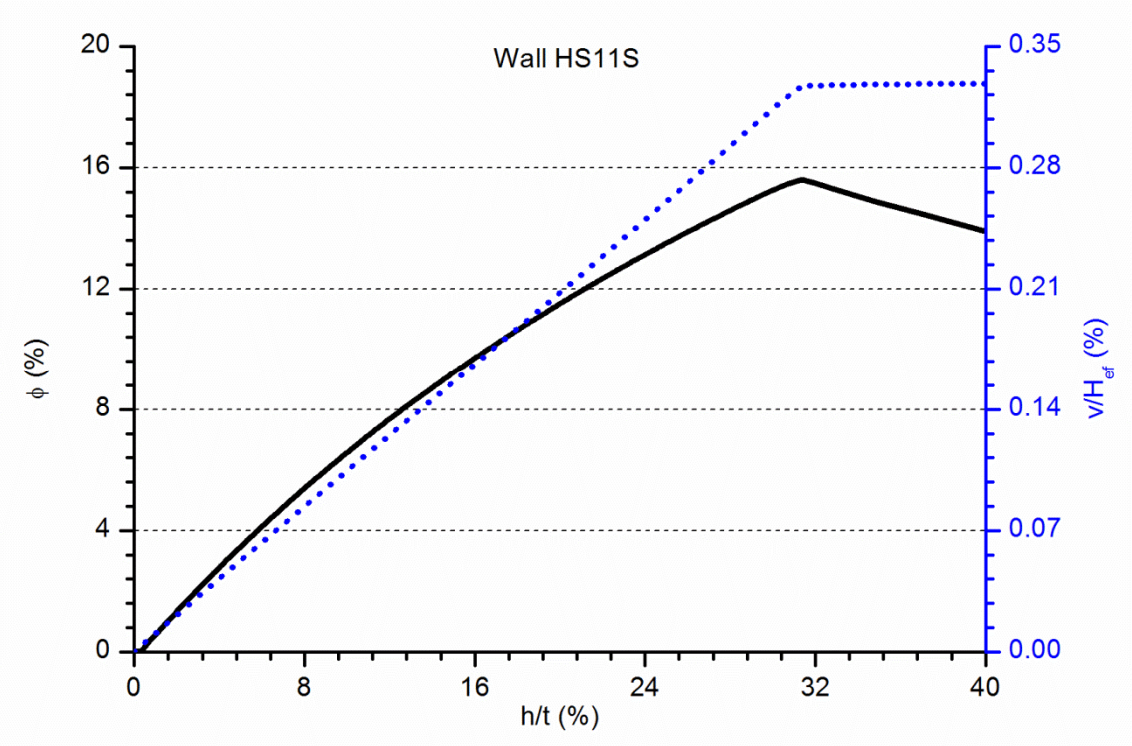


Figure A2. 65 Vertical and lateral calculated response of the wall HS11S

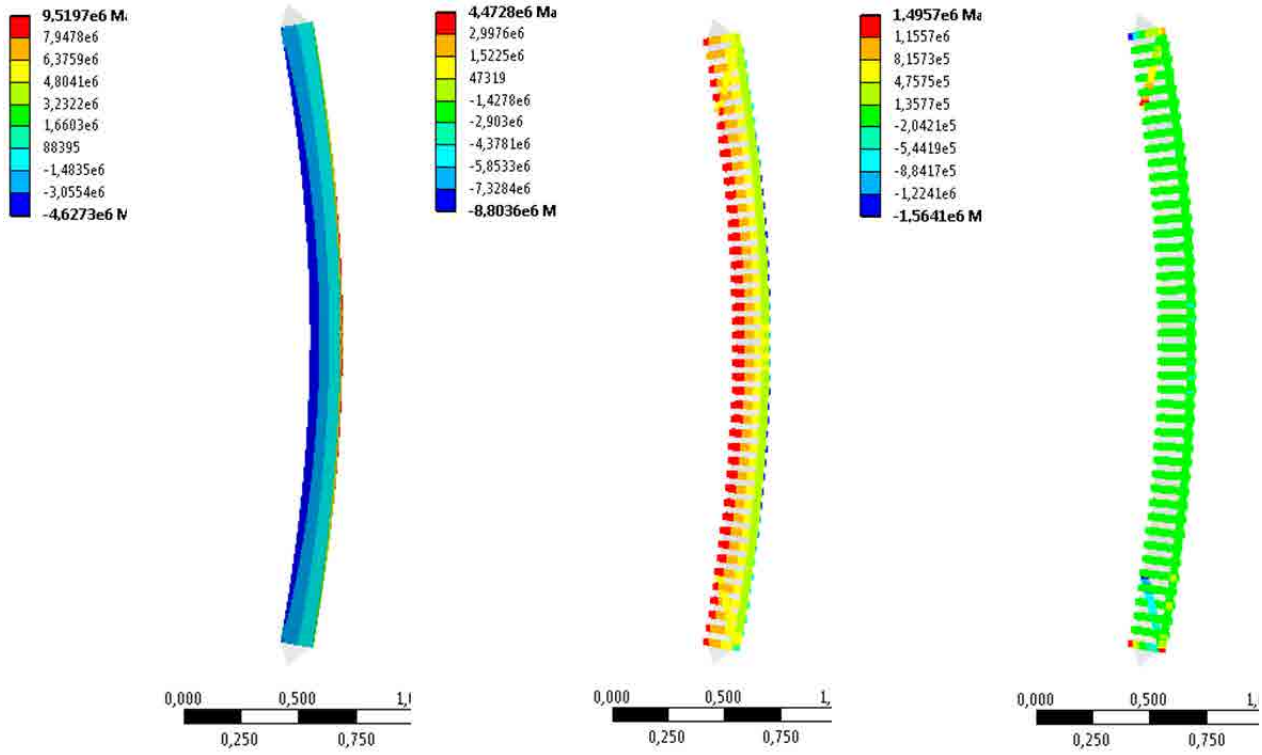


Figure A2. 66 Vertical stress distribution (left), contacts pressure (middle) and contacts shear stress (right) corresponding to the maximum calculated load for wall HS11S. Values in Pa

The left and middle contour plots in Figure A2. 66, which represent the vertical stress and the contacts' pressure respectively, are almost identical to the results of the case HS11. The maximum compressive vertical stress (4.6MPa) is lower than the corresponding strength (10.8MPa) whilst the tensile stress in the TRM punctually reached is maximum value (8.1MPa) in several horizontal joints. In the figure at the right side of Figure A2. 66 it is observed that the maximum shear stress (0.56MPa) is reached in almost half the length of the inclined contacts, so the compressive-shear failure near the wall's endings is a possible failure mode. In conclusion, for case HS11S, the tensile failure of the TRM is the most likely failure mode according with the results, but the masonry failure at the endings is also possible.

## A2.4.5. Wall HS12S

### *A2.4.5.1 Input parameters*

The case HS12S is intended to analyse the effect of placing two fibre grids embedded in one mortar layer on the tensile side of the wall. It also considers the possibility of a compression-shear failure along an inclined crack. Thus, the values of the defining parameters for the masonry are the ones summarised in

Table A2. 14. The strengthening system is characterised by the values in Table A2. 16. The mesh average size is 20mm for masonry and 3mm for TRM.

| *TRM thickness (mm)* | *Density (kg/m$^3$)* | *$f_{cm}$ (MPa)* | *E (MPa)* | *$f_{xt}$ (MPa)* | *$G_f^I$ (N/m)* |
|---|---|---|---|---|---|
| 10 | 1850 | 42.20 | 11000 | 9.0 | 330 |

Table A2. 16. Input data for the TRM strengthening system for wall HS12S

#### *A2.4.5.2 Results*

The load-bearing capacity of wall HS12S is 207.9kN which is slightly higher than the previous case (HS11S) because the tensile strength of the TRM is just a little bigger. Observing the wall's response (see Figure A2. 67) the non-linear relationship between the applied load and the lateral displacement at mid-height (black continuous line) is noticed. In contrast, the proportionality between the vertical descending displacement of the wall's top and the lateral displacement at mid-height is observed up to failure (blue dotted line).

In Figure A2. 68 it is observed that the maximum vertical compressive stress (4.9MPa) is quite lower than the masonry compressive strength whereas the maximum tensile stress in the TRM punctually overpass the TRM tensile strength (9MPa) which suggests the possibility of the horizontal joints opening as a feasible failure mode for this theoretical case. However, the compressive-shear masonry failure near the wall's endings is also a probable failure mode because the shear stresses in the inclined joint reach the material strength (0.56MPa) in approximately half the length of the contact. Thus, both failure modes are possible in case HS12S.

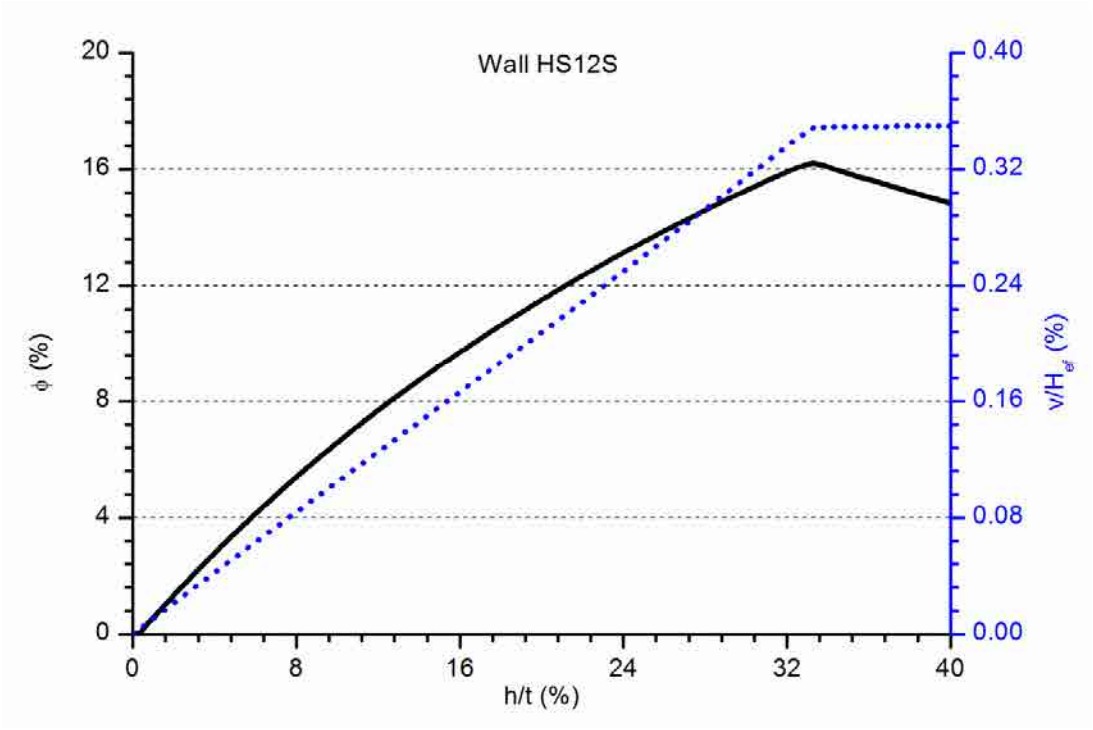


Figure A2. 67 Vertical and lateral calculated response of the wall HS12S

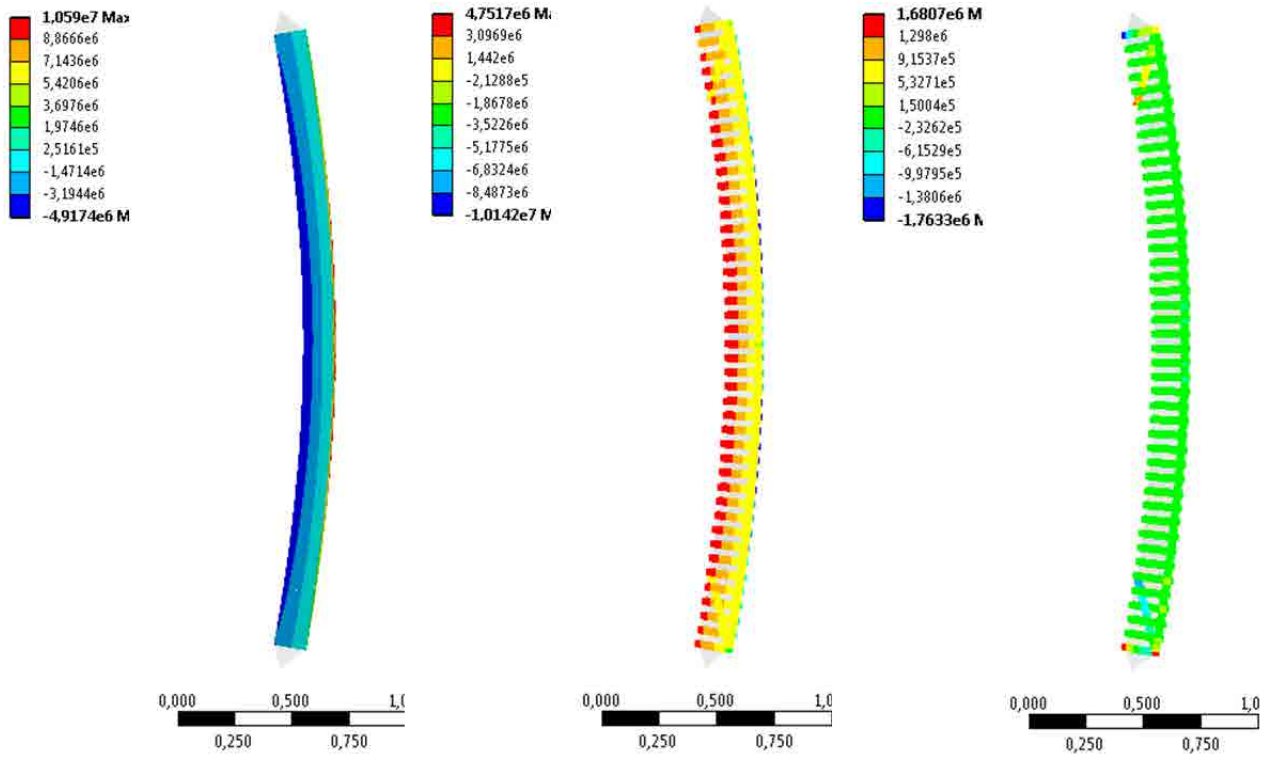


Figure A2. 68 Vertical stress distribution (left), contacts pressure (middle) and contacts shear stress (right) corresponding to the maximum calculated load for wall HS12S. Values in Pa

## A2.4.6. Wall HS14S

### *A2.4.6.1 Input parameters*

The wall HS14S is equivalent to the two previous walls (HS11S and HS12S) but considering a strongest TRM system composed of 4 glass fibre grids embedded into a 20mm layer of Portland-based strengthening mortar. Thus, the masonry is characterised with the values included in Table A2. 14 and the TRM's properties are summarised in Table A2. 17. The mesh average size is 20mm for masonry and 3mm for TRM.

| ***TRM thickness (mm)*** | ***Density (kg/m$^3$)*** | ***$f_{cm}$ (MPa)*** | ***E (MPa)*** | ***$f_{xt}$ (MPa)*** | ***$G_f^I$ (N/m)*** |
|---|---|---|---|---|---|
| 20 | 1850 | 42.20 | 11000 | 9.0 | 330 |

Table A2. 17. Input data for the TRM strengthening system for wall HS14S

### *A2.4.6.2 Results*

The load-bearing capacity of wall HS14S is 257.8kN, which is higher than the previous cases. Qualitatively (see Figure A2. 69) the wall's response is similar to the previous cases, with a non-linear relationship between the applied load and the lateral displacement at mid-height (black continuous line) and a linear relationship between the vertical displacement of the wall's top and the lateral displacement

at mid-height (blue dotted line). In this particular case, the lateral displacement is bigger than for other theoretical walls previously analysed with different strengthening systems.

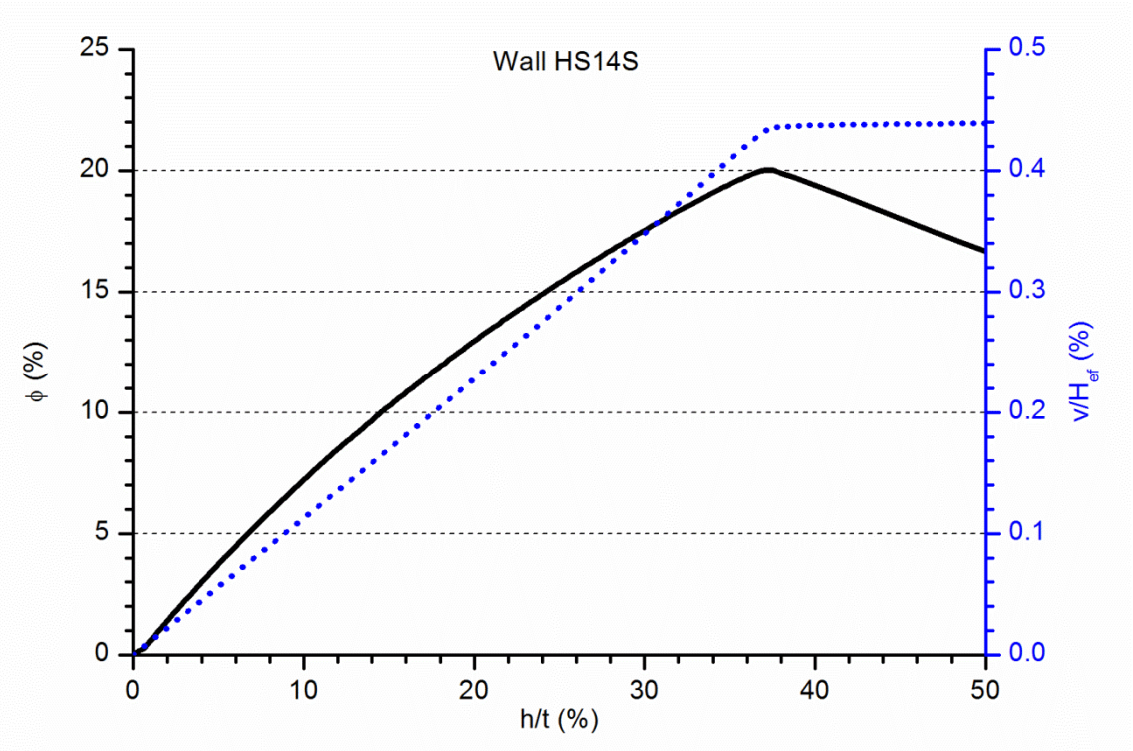


Figure A2. 69 Vertical and lateral calculated response of the wall HS14S

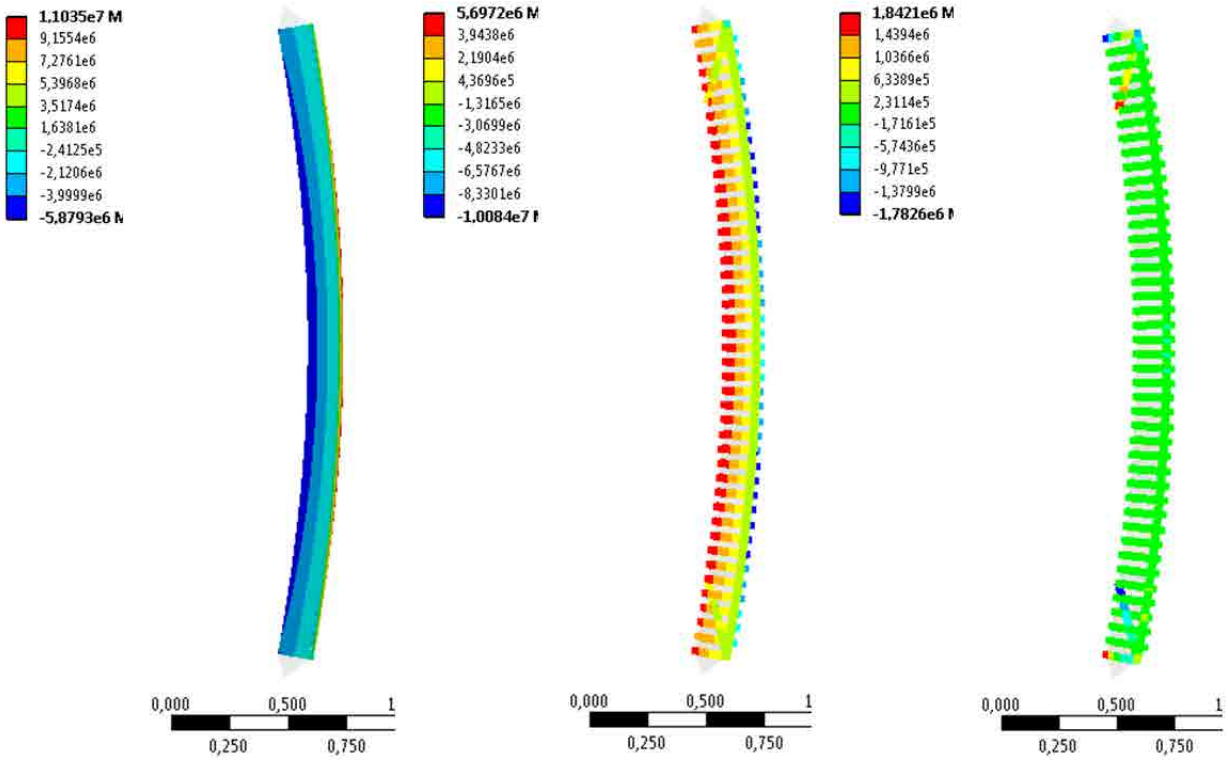


Figure A2. 70 Vertical stress distribution (left), contacts pressure (middle) and contacts shear stress (right) corresponding to the maximum calculated load for wall HS14S. Values in Pa

Regarding the stresses distributions plotted in Figure A2. 70 it is concluded that the masonry crushing at the compression side is not a feasible failure mode as the maximum vertical compressive stress (5.9MPa) is lower than the corresponding strength (10.8MPa). However, from the obtained results, it cannot be said which of the other two considered failure modes is the most likely because the tensile strength of the TRM (9MPa) is reached in several horizontal joints and the shear stresses on the inclined contact defined in the masonry near the fixation points punctually overpass its strength (0.56MPa) in approximately half the contact length.

## A2.4.7. Wall HS21S

### *A2.4.7.1 Input parameters*

This is the first analysed case which considers the possibility of placing the TRM strengthening system in both sides of the wall. The masonry also takes into account the compressive-shear possibility along an inclined crack so the defining properties are presented in Table A2. 14. Each TRM layer is characterised by the values summarised in Table A2. 15. The mesh average size is 20mm for masonry and 3mm for TRM.

### *A2.4.7.2 Results*

The maximum load the wall HS21S might resist according with the FEA results is 725.3kN. The wall's response is quite different from all the previous analysed cases (see Figure A2. 71). The relationship between the applied force and the lateral displacement at mid-height (black continuous line) is plotted with an initial non-linear curve which reaches the maximum load. After the maximum force two linear sections are observed. Firstly, the load descends slowly and after reaching the lateral displacement *h/t>34%* the load decrease at a higher speed. Similarly, the relationship between the vertical descending movement of the top of the wall and the lateral displacement at mid-height is initially non-linear up to the maximum load when this curve turns straight with a lower slope which is again reduced after reaching the *h/t=34%* threshold value.

Observing the Figure A2. 72, it is noticed that the maximum compressive vertical stress in the masonry (3.3MPa) does not reach the strength value (10.8MPa). In contrast, the compressive stress in the TRM reaches its strength values (42.2MPa) in the area around the mid-height. Thus, the crushing of the TRM working in compression is a feasible failure mode. At the same time the tensioned TRM reaches its strength values (8.1MPa) in a large area around the mid-height, so the tensile failure of the TRM is the second possible failure mode. Looking at the image at the right side of the Figure A2. 72 it is noticed that along all the length of the inclined contact the shear stress has reached its maximum strength (0.56MPa) showing that the masonry compressive-shear failure near the wall's ending is the likeliest failure mode for the HS21S case.

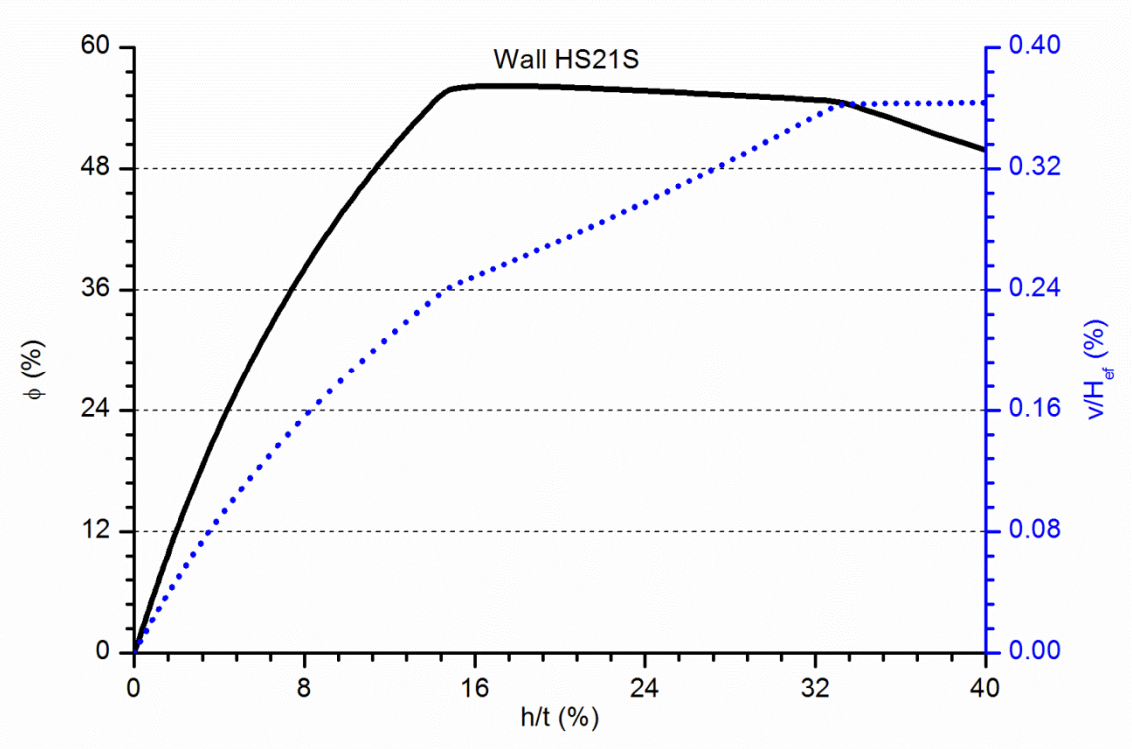


Figure A2. 71 Vertical and lateral calculated response of the wall HS21S

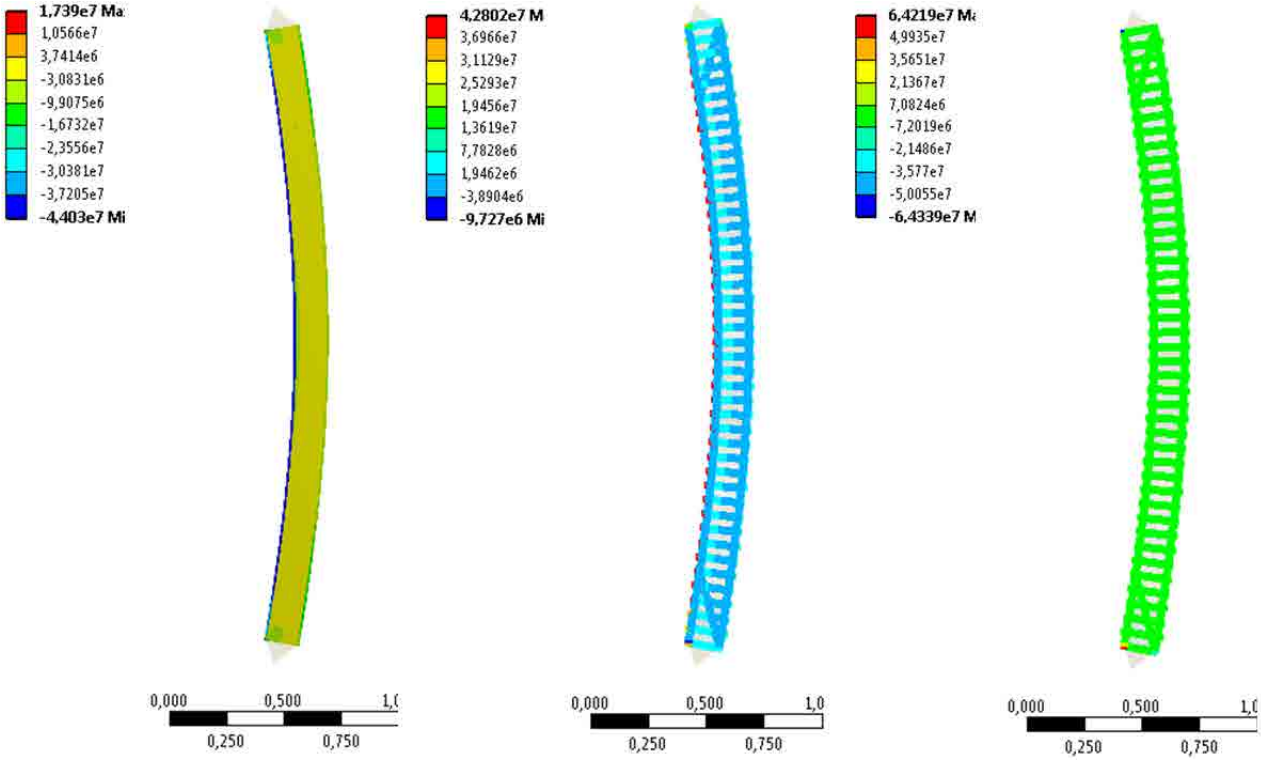


Figure A2. 72 Vertical stress distribution (left), contacts pressure (middle) and contacts shear stress (right) corresponding to the maximum calculated load for wall HS21S. Values in Pa

## A2.4.8. Wall M0

### *A2.4.8.1 Input parameters*

This is the first theoretical wall of the series with a lower slenderness. M0 is the model of an unreinforced masonry wall which does not consider the possibility of compressive-shear failure along an inclined crack. Thus, the masonry properties required by the FEA are the ones presented in Table A2. 13. The average mesh size is 5mm in the masonry.

### *A2.4.8.2 Results*

The load-bearing capacity of the wall M0 calculated with the FEA method is 185.4kN.

The force versus lateral displacement at mid-height relationship plotted in Figure A2. 73 (black continuous line) shows the non-linear response associated with the second order bending effects. This non-linearity is also observable in the blue dotted line which represents the vertical descending movement of the wall's top in relation with the lateral displacement at mid-height. The main difference with the previous unreinforced theoretical wall (H0) is the greater slope of this curve after the maximum load for the case of M0.

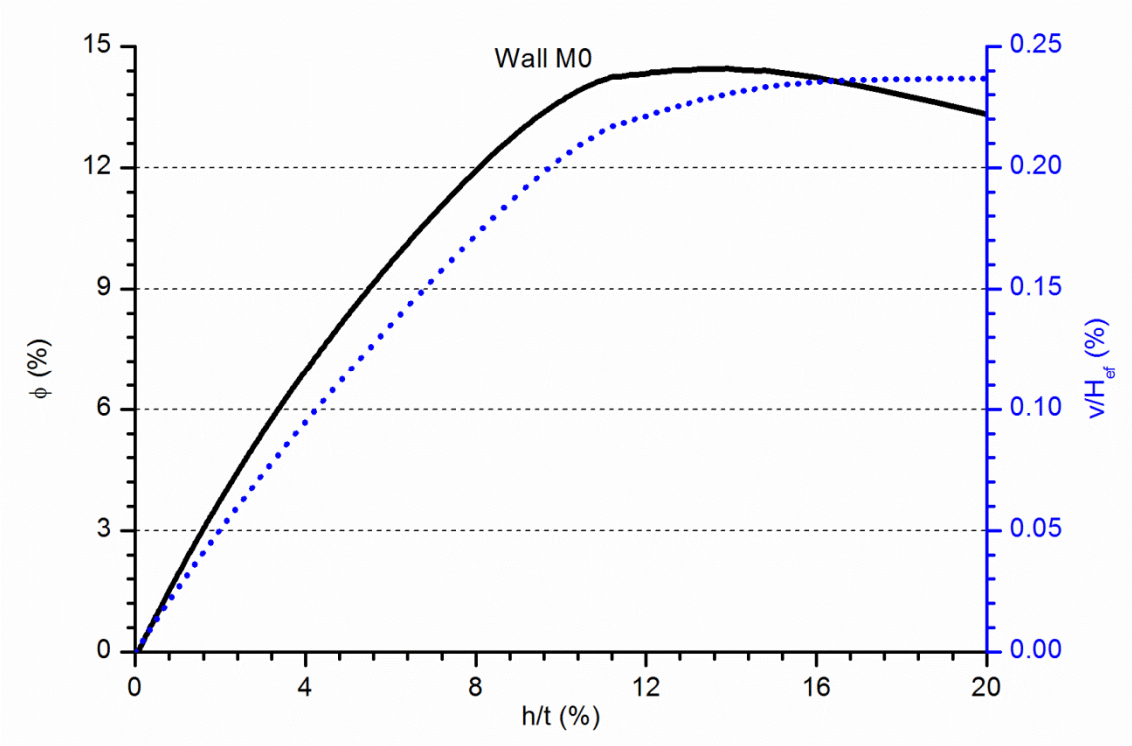


Figure A2. 73 Vertical and lateral calculated response of the wall M0

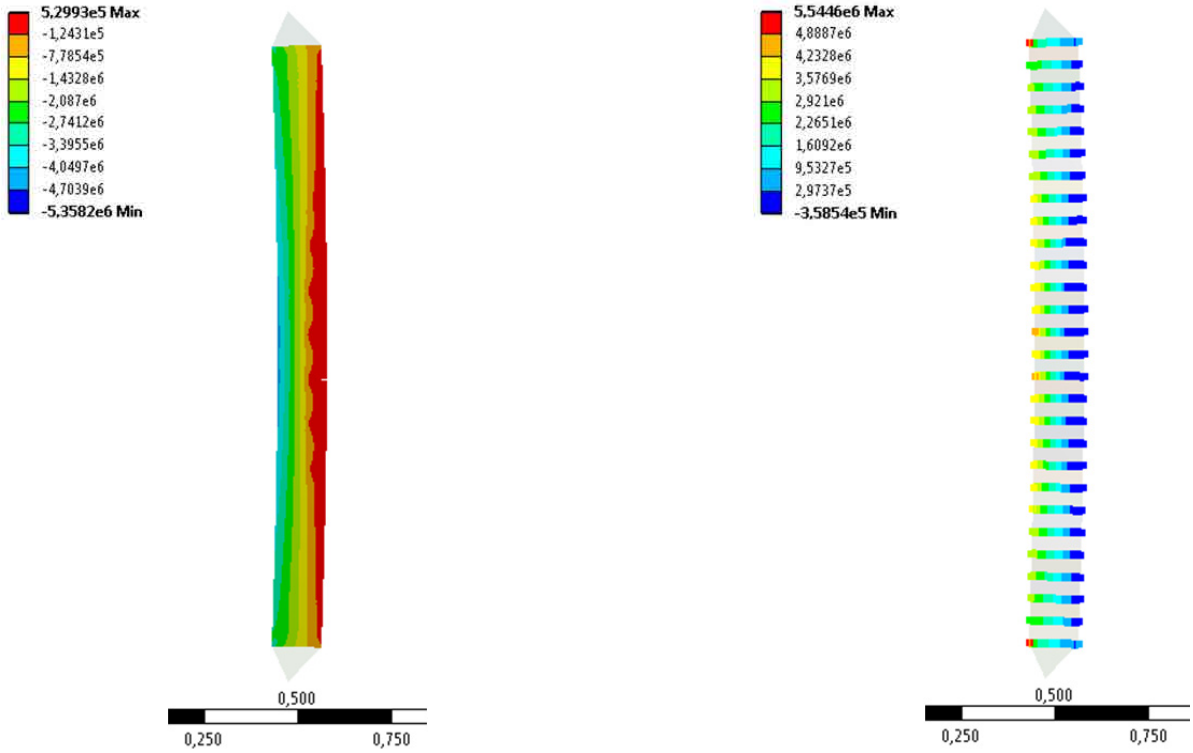


Figure A2. 74 Vertical stress distribution (left) and contact pressure (right) corresponding to the maximum calculated load for wall M0. Values in Pa

In the contour plot placed at the left side of the Figure A2. 74 it is observed that the maximum resulting vertical compressive stress in the masonry (5.4MPa) is lower than the compressive strength of this material (10.8MPa). Thus, the wall M0 failed due to the tensile stress in the horizontal joints between masonry rows which really reached the masonry strength (0.36MPa) in several joints near the mid-height area (see the left image in Figure A2. 74).

## A2.4.9. Wall M0S

### *A2.4.9.1 Input parameters*

This case is equivalent to the previous one but adding the possibility of a compressive-shear failure along an inclined crack near the wall's extremes. Thus, the masonry characteristics used to model this case are showed in Table A2. 14. The average mesh size is 5mm in the masonry.

### *A2.4.9.2 Results*

The wall modelled in case M0S is able to bear a maximum load of 185.4kN according with the FEA results. The wall's response is analogue to the previous case. In Figure A2. 75 it is observed that both curves show a non-linear behaviour up to failure. Thus, the second order bending affects the lateral and vertical displacements of the structure which are not even proportional between them.

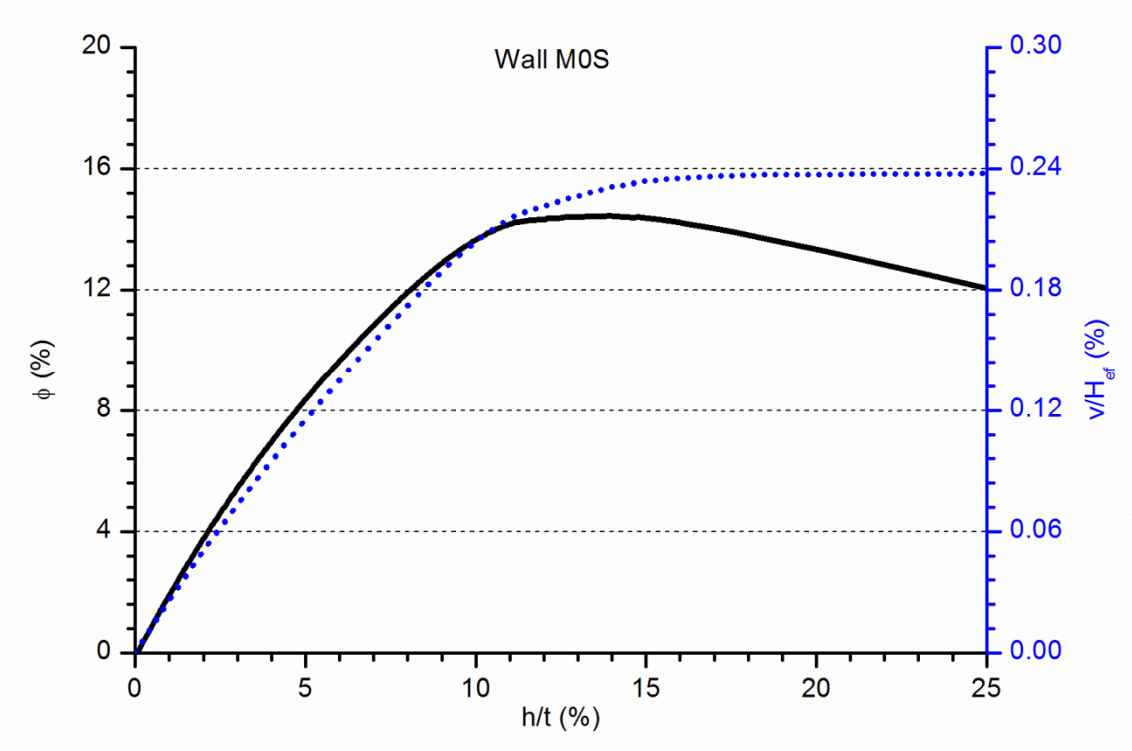


Figure A2. 75 Vertical and lateral calculated response of the wall M0S

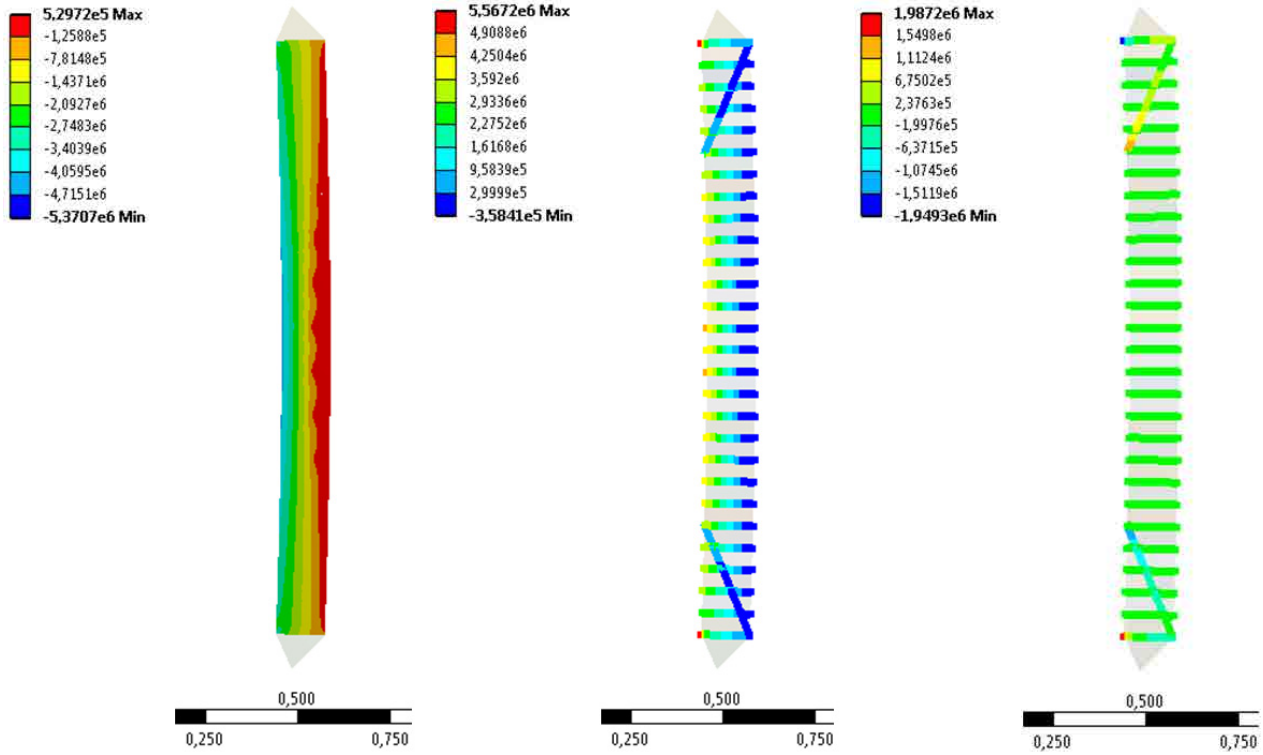


Figure A2. 76 Vertical stress distribution (left), contacts pressure (middle) and contacts shear stress (right) corresponding to the maximum calculated load for wall M0S. Values in Pa

Observing the Figure A2. 76 it is noticed that, similarly to M0 case, the maximum compressive stress on the masonry (5.4MPa) is lower than the corresponding strength so the crushing failure is not supported by the model results. In addition, most of the tangential stresses in the inclined contact (see the image at the right side of the Figure A2. 76) are far lower than the calculated shear strength of masonry (0.56MPa) and this value is only overpassed punctually. Finally, the maximum tensile stress in the contacts between masonry rows is placed at the mid-height area (middle image in Figure A2. 76) and its value (0.36MPa) corresponds with the masonry strength so the tensile opening of a masonry joint is the most likely failure mode according with the FEA results.

## A2.4.10. Wall MS11

### *A2.4.10.1 Input parameters*

This is the first TRM strengthened wall of the series of little slenderness theoretically defined. Its description is identical to the case HS11 only changing the geometry. Thus, the masonry characterisation is summarised in Table A2. 13 and the TRM definition in Table A2. 15. The average mesh size is 5mm in the masonry and 3mm in the TRM.

### *A2.4.10.2 Results*

As previously observed for the walls of the H series, using a TRM strengthening system changes the response of the wall in comparison with the non-strengthened ones. The maximum load-bearing capacity of the wall MS11 is 355.4kN.

Observing the plots in Figure A2. 77, it is noticed that the relationship between the vertical descending displacement of the top of the wall and the lateral displacement of the wall at mid-height is linear up to the maximum applied load (blue dotted line) whereas the force versus lateral movement shows a non-linear plot with a decreasing slope at increasing the load due to the second order bending effects.

By observing the left contour plot in Figure A2. 78 it is worth to mention that the maximum compressive vertical stress (6.9MPa) is lower than the strength of the masonry so the crushing failure mode is not possible according with the FEA results. Observing the plot of the contacts pressures it is noticed that joints around the mid-height have a tensile stress punctually over the tensile strength of the TRM (8.1MPa) what indicates that the TRM tensile failure is the most likely in the case of MS11.

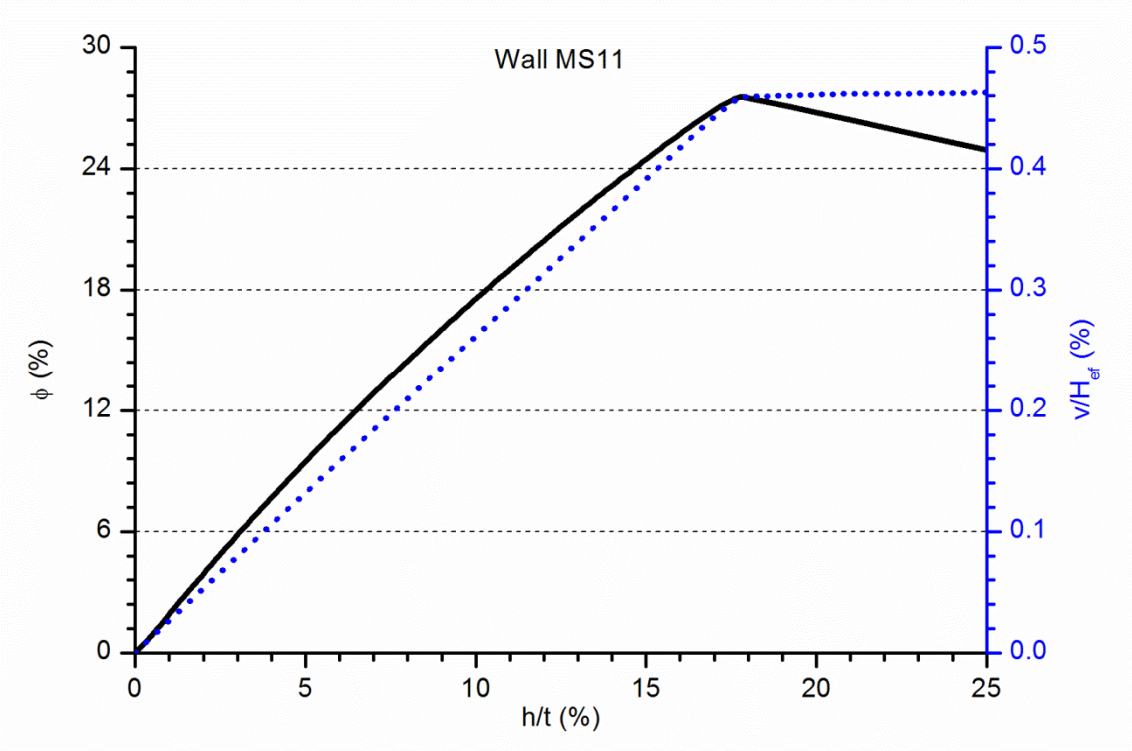


Figure A2. 77 Vertical and lateral calculated response of the wall MS11

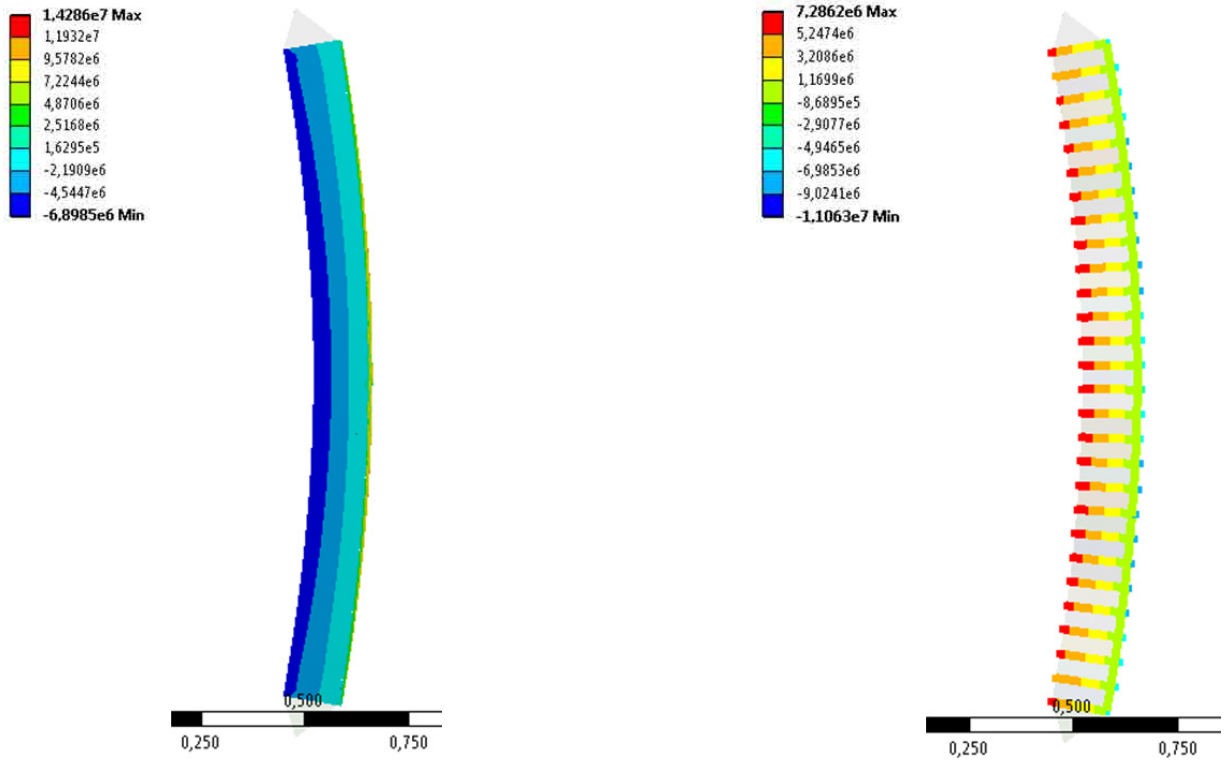


Figure A2. 78 Vertical stress distribution (left) and contact pressure (right) corresponding to the maximum calculated load for wall MS11. Values in Pa

## A2.4.11. Wall MS11S

### *A2.4.11.1 Input parameters*

This wall is identical to the previous one but considering the possibility of a compression-shear failure along an inclined crack near the wall's endings. Thus, the masonry characterisation variables are presented in Table A2. 14. The TRM definition is shown in Table A2. 15. Finally, like in the previous case, for the wall MS11S the average mesh size is 5mm in the masonry and 3mm in the TRM.

### *A2.4.11.2 Results*

As seen in the case of more slender series (HS11 compared with HS11S), the response of the wall MS11S is qualitatively equal to the previously presented for the case MS11. The maximum load bearing capacity of the wall MS11S is 355.4kN.

The linear relationship between the lateral displacement at mid-height and the vertical descending movement of the top of the wall is shown in Figure A2. 79 (blue dotted line). This behaviour is analogue to the one observed for wall MS11. In the same way, the second order bending effects which produce a non-linear relationship between force and lateral displacement at mid-height might be observed in Figure A2. 79 (black continuous line).

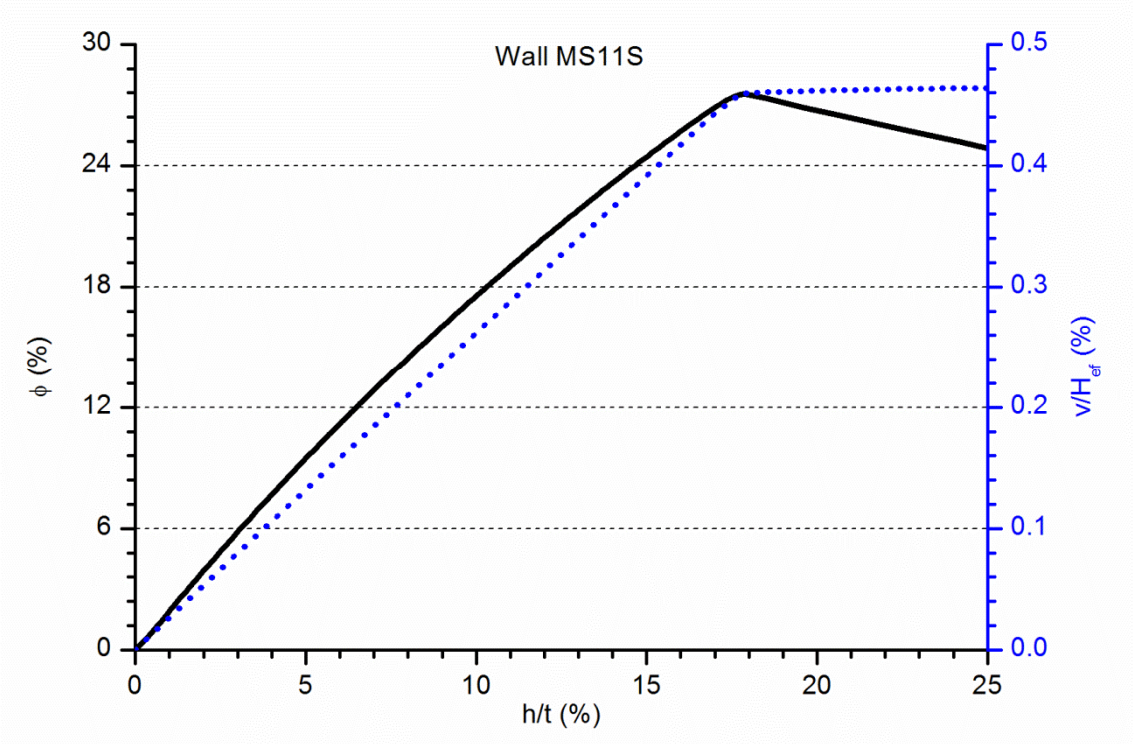


Figure A2. 79 Vertical and lateral calculated response of the wall MS11S

Regarding the stress distribution (Figure A2. 80) it has to be noticed that the maximum vertical compressive stress (6.9MPa) is lower than the masonry strength (10.8MPa) so the masonry crushing is

not the collapse mode of the structure according with the analysis results. Looking at the second image in Figure A2. 80, it is observed that the maximum tensile stress on the TRM is punctually higher than the corresponding strength. Similarly, the tangential stresses on the inclined contacts near the endings of the masonry are over the threshold value of the masonry (0.56MPa) in almost all the length of the contact. Thus, the two failure modes, the TRM tensile failure and the compressive-shear masonry collapse are possible for the wall MS11S according with the results of the simulation.

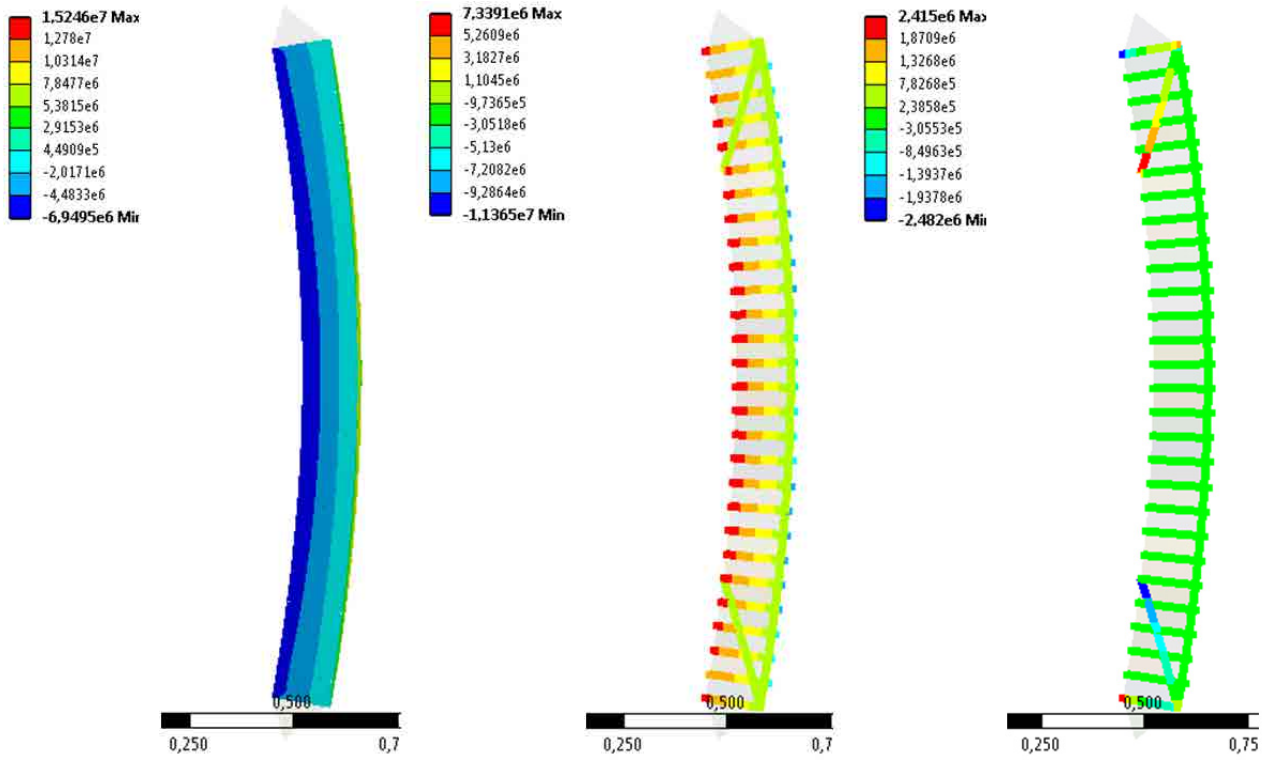


Figure A2. 80 Vertical stress distribution (left), contacts pressure (middle) and contacts shear stress (right) corresponding to the maximum calculated load for wall MS11S. Values in Pa

## A2.4.12. Wall MS12S

### *A2.4.12.1 Input parameters*

For wall MS12S the masonry characterisation is summarised in Table A2. 14 and the TRM definition in Table A2. 16. The average mesh size of the finite elements is 5mm in the masonry and 3mm in the TRM.

### *A2.4.12.2 Results*

The load-bearing capacity of wall MS12S is 370.7kN which is slightly higher than the previous case (MS11S) because the tensile strength of the TRM is bigger due to considering two fibre grids.

Observing the plots in Figure A2. 81 it is noticed that the wall's response is analogue to the previous one. The relationship between the vertical displacement of the wall's top and the lateral displacement at

mid-height is linear up to failure (blue dotted line) whereas the non-linear bending effect are noticeable in the force vs. lateral displacement curve (black continuous line).

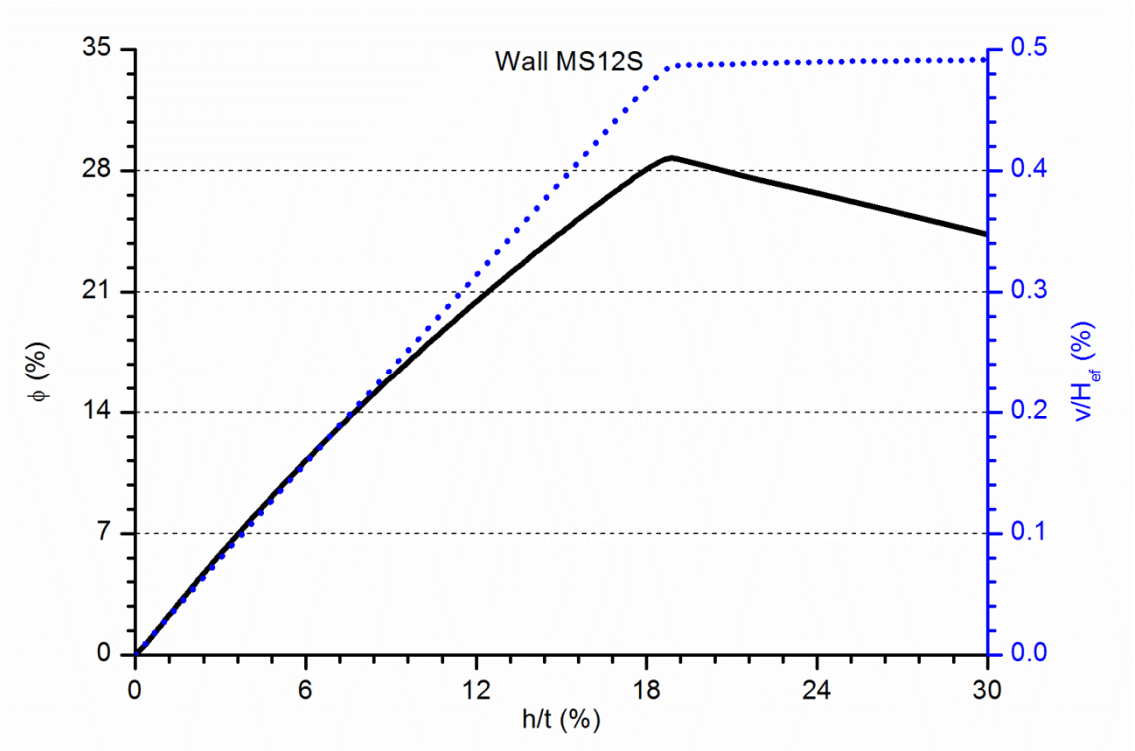


Figure A2. 81 Vertical and lateral calculated response of the wall MS12S

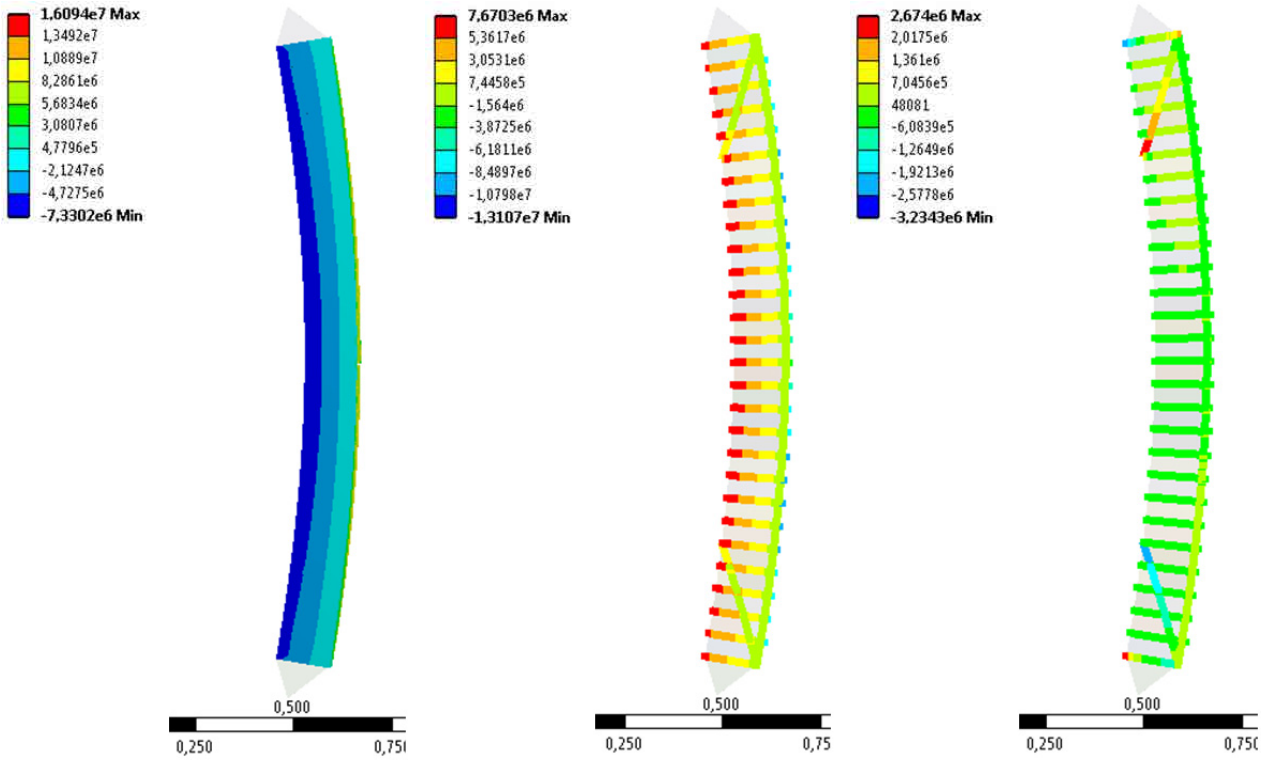


Figure A2. 82 Vertical stress distribution (left), contacts pressure (middle) and contacts shear stress (right) corresponding to the maximum calculated load for wall MS12S. Values in Pa

The most probable failure modes according with the contour plots in Figure A2. 82 are the tensile failure of TRM and the compressive-shear collapse of the masonry near the wall's endings. For the first case, the tensile stress on TRM is punctually higher than its strength (9MPa) near the mid-height sections whereas for the second possible failure mode it has to be highlighted that the tangential stress is greater than the corresponding strength in almost all the defined contact. In contrast, the compressive vertical stress is always below the masonry strength in the compression side of the wall.

## A2.4.13. Wall MS14S

### *A2.4.13.1 Input parameters*

Wall MS14S is characterised like wall HS14S but with a lower slenderness value. Thus, the masonry input variables are summarised in Table A2. 14 and the TRM defining values are gathered in Table A2. 17. The elements average size is 5mm in the masonry regions and 3mm in the TRM's domain like in all previous cases of theoretical walls.

### *A2.4.13.2 Results*

The load-bearing capacity of the wall MS14S is 425.8kN according with the analysis' results. The overall response of the wall MS14S is similar to the previous one but the lateral displacement at mid-height for which the wall reached the maximum load is higher in the MS14S case (over 20% of the wall's thickness, *t*). The simulated behaviour consisted of a linear relationship between the descending displacement of the wall's top and the lateral displacement at mid-height (blue dotted line in Figure A2. 83). This linearity is lost when analysing the force vs. lateral displacement curve (black continuous line in Figure A2. 83) where the second order effects and the increase of the wall's lateral deformation are noticeable.

Contour plots of Figure A2. 84 suggest that the wall WS14S might collapse by reaching the maximum compressive stress of the masonry, by reaching the tensile strength of the TRM or by a compressive-shear failure near the wall's endings. In the left image in Figure A2. 84, it is observed that the maximum vertical compressive stress (13.5MPa) is higher than the corresponding strength (10.8MPa). Similarly, the tensile strength of the TRM is overpassed in all the contacts around the central third of the wall (middle image in Figure A2. 84) and the tangential stress is over the corresponding strength (0.56MPa) along all the inclined contact defined near each wall's ending.

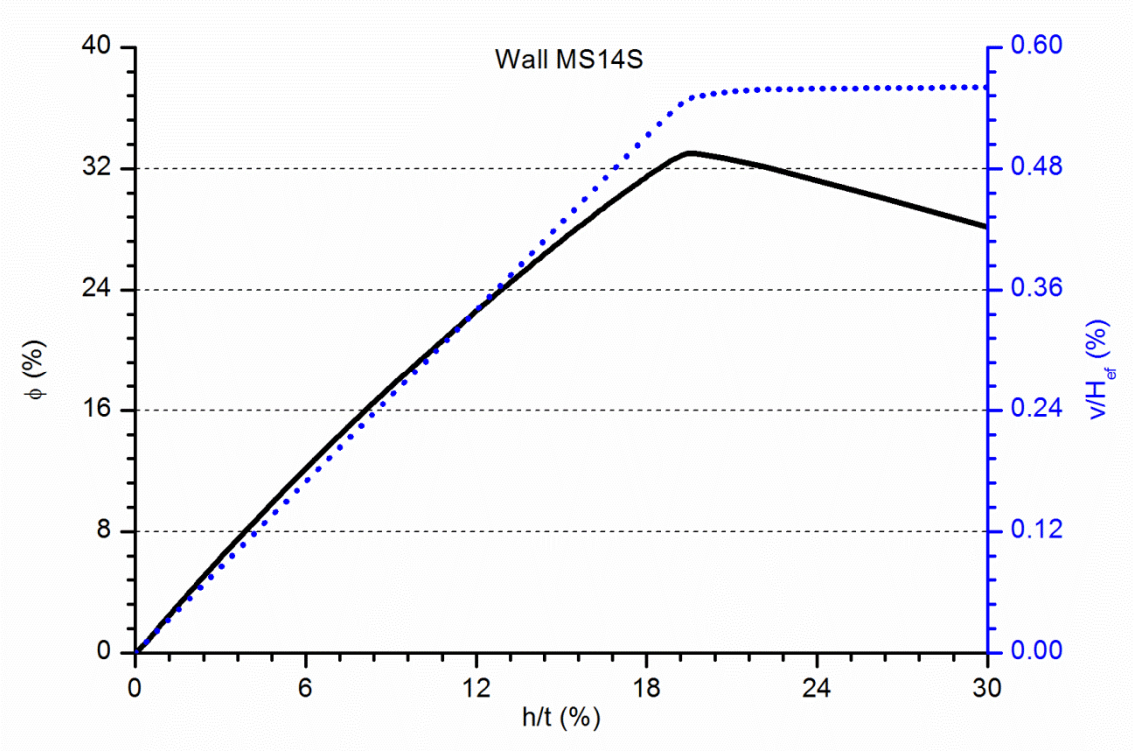


Figure A2. 83 Vertical and lateral calculated response of the wall MS14S

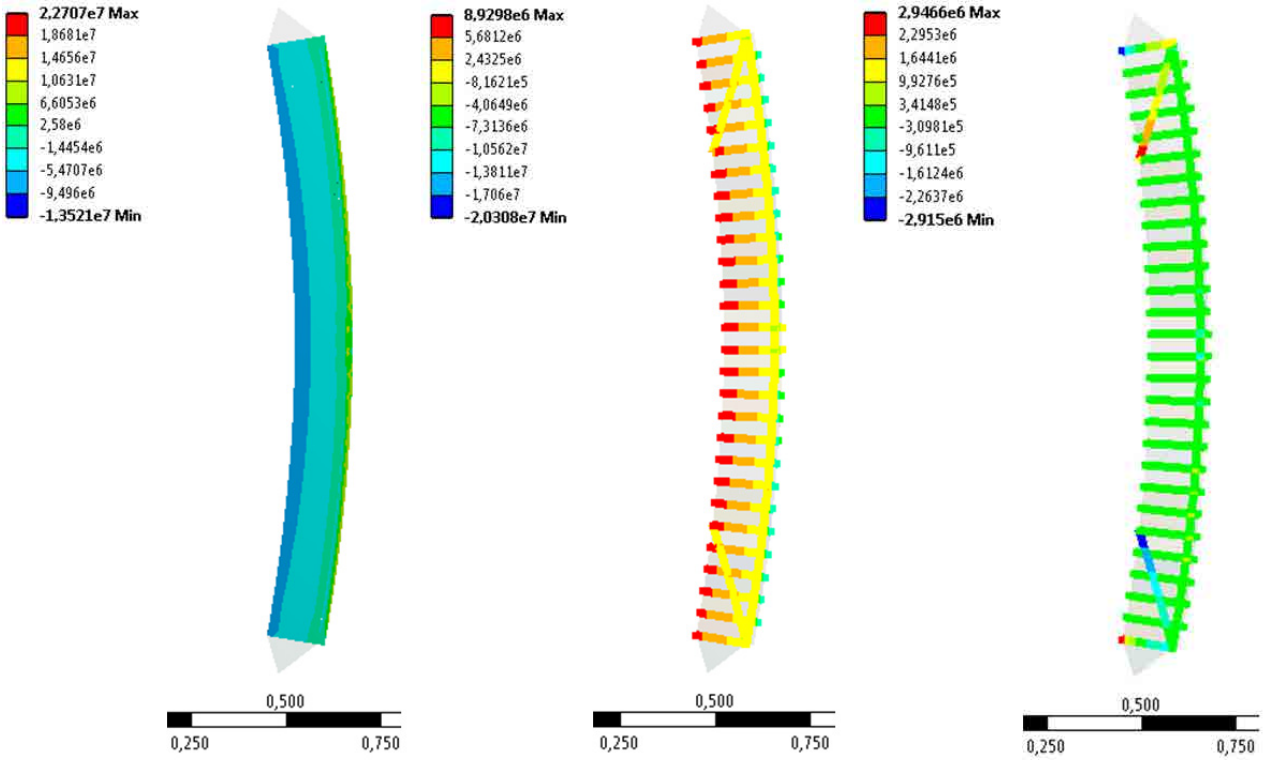


Figure A2. 84 Vertical stress distribution (left), contacts pressure (middle) and contacts shear stress (right) corresponding to the maximum calculated load for wall MS14S. Values in Pa

## A2.4.14. Wall MS21S

### *A2.4.14.1 Input parameters*

This theoretical wall represents the case of a low-slenderness wall strengthened with TRM at both sides. These TRM layers were characterised with the same parameters than wall MS11S, so the values in Table A2. 15 are valid for the present case. The masonry considers the possibility of a compressive-shear failure along an inclined plane near the wall's endings so the characterisation values are summarised in Table A2. 14. The average element size of the FEA mesh is 5mm for the masonry and 3mm for the TRM.

### *A2.4.14.2 Results*

According with the FEA's results, the load-bearing capacity of wall WS21S would be 999.6kN which is the higher among all analysed cases. The mechanical response of wall MS21S is similar to that observed for the wall HS21S. A trilinear plot represents the relationship between the vertical displacement of the wall's top and the lateral displacement at mid-height (blue dotted line in Figure A2. 85). At each curve's change, the slope decrease, so the lateral displacement increases its speed punctually when reaching two different threshold values. The force vs. lateral displacement curve (black continuous line in Figure A2. 85) is also trilinear. The lateral displacement increased proportionally with the applied force up to approximately 80% of the maximum load when the ratio changes and the lateral displacement grows quicker with the applied force. The last plotted branch is also linear although it does not represent any real force-controlled case for which the maximum load would be the last stable point.

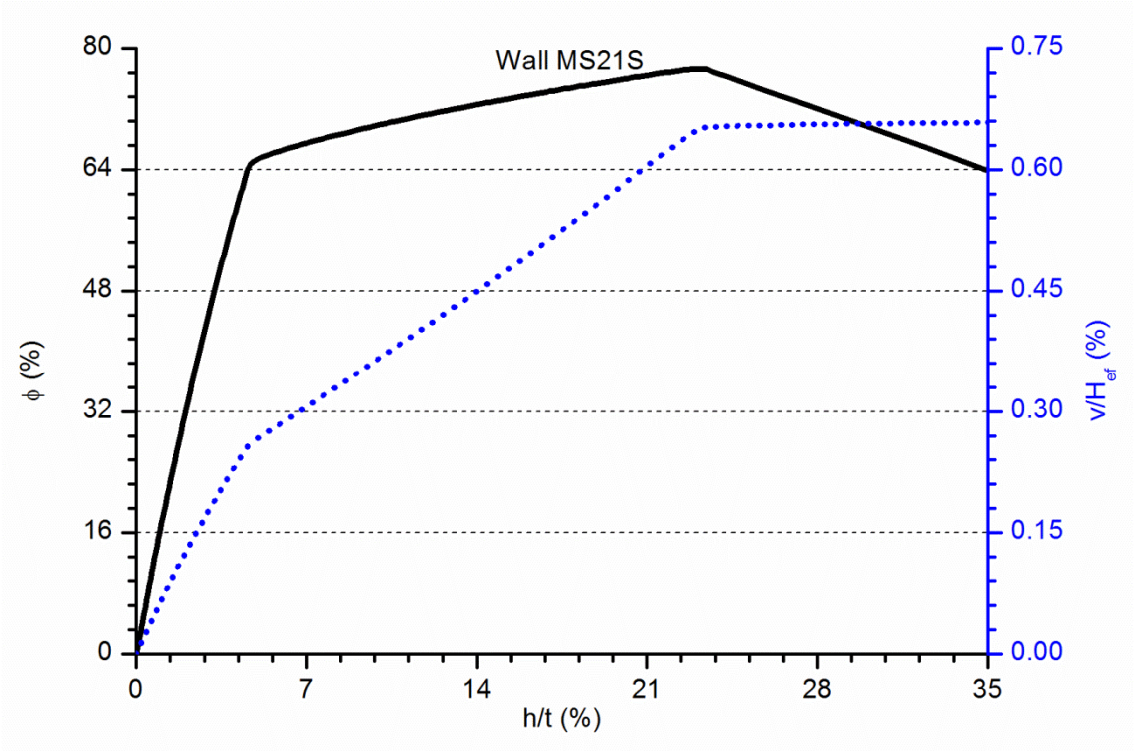


Figure A2. 85 Vertical and lateral calculated response of the wall MS21S

Figure A2. 86 shows the stresses distribution on the wall's section. Looking at the left image it is observed that the masonry would not crush although the TRM's crushing failure is likely because near the mid-height section the maximum vertical stress in TRM overpass its compressive strength (42.2MPa). However, it is not the only possible collapse mode which fits with the obtained results. The tensile failure of the TRM is also likely because the tensile stress on the strengthening sections near the mid-height overpass the corresponding strength (8.1MPa). Finally, the compressive-shear collapse of the masonry near the wall's ending is also a possibility because the tangential stress along the inclined contacts in the masonry is higher than the corresponding strength (0.56MPa) in almost all the contact length.

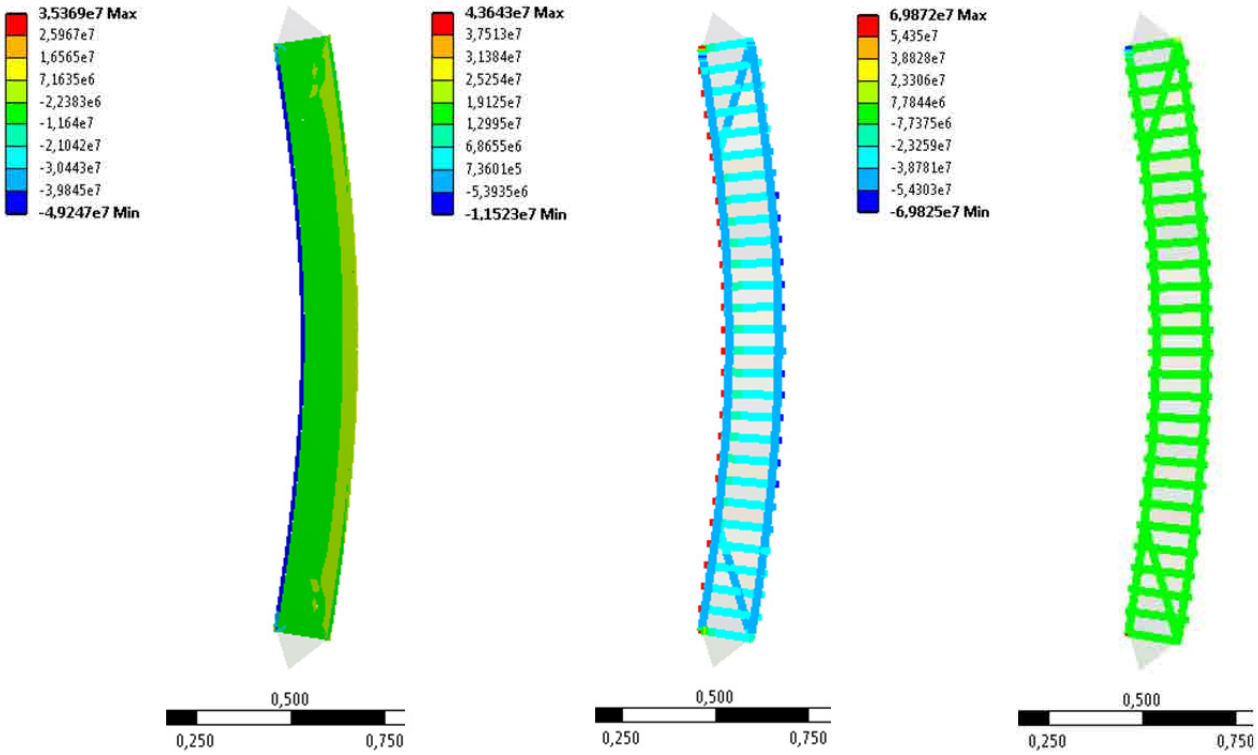


Figure A2. 86 Vertical stress distribution (left), contacts pressure (middle) and contacts shear stress (right) corresponding to the maximum calculated load for wall MS21S. Values in Pa